Improved Inlet Conditions for Terrain CFD

Pedersen, Jesper Grønnegaard; Bechmann, Andreas; Sørensen, Niels N.

Publication date:
2010

Document Version
Publisher's PDF, also known as Version of record

IMPROVED INLET CONDITIONS FOR TERRAIN CFD

8th March 2010

Master thesis by Jesper Grønnegaard Pedersen

Supervisors: Andreas Bechmann & Niels N. Sørensen

Risø, National Laboratory for Sustainable Energy

Technical University of Denmark (DTU)

Abstract

The atmospheric boundary layer flow over different types of terrain is studied through simulations made with the finite volume CFD code of *Ellipsys 2D* and *3D.* The simulations are compared to measurements made at the Høvsøre test site and over the hill of Askervein.
The primary objective of these investigations is to find out, how the wind under neutral atmospheric stratification is affected by changes in the surface roughness.
In both cases of Høvsøre and Askervein, an upstream roughness change is seen to have a significant influence on the observed flow.
General empirical expressions are suggested for describing the flow after a change in the surface roughness. The derivation of these expressions is based on a range of simulations of flows over flat terrain with different types of roughness changes.
The derived expressions show good agreement with simulations and could, as intended, be used to define inlet conditions for flow simulations over terrain, where an upstream roughness change is thought to have an influence. More thorough experimental verification is however, thought necessary to make the expressions sufficiently reliable. The same goes for the simulations-based conclusions regarding the flow over Askervein.

Preface

The present project is carried out as a Master Thesis Project for partial fulfillment (30 ECTS credits) of the Master of Science degree in Engineering at the Technical University of Denmark (DTU).
The project work was done in the period between September 1, 2009 and March 8, 2010 at Risø DTU, National Laboratory for Sustainable Energy under supervision of Andras Bechmann and Niels N. Sørensen.

Nomenclature

CDS	Central difference scheme
CFD	Computational fluid dynamics
HT	Hill top
IBL	Internal boundary layer
QUICK	Quadratic upstream interpolation for convective kinetics scheme
Re	Reynolds number
RS	Reference site
SIMPLE	Semi-implicit method for pressure-linked equations
SUDS	Second order upwind difference scheme
TKE	Turbulent kinetic energy
UDS	Upwind difference scheme

A, A_1, A_2	Parameters of the 'Savelyev/Taylor' IBL height expression
A_{diff}	Constant of the 'diffusion analogy' IBL height expression
A_p, A_{nb}	Coefficients of the discretized governing equations
a, b	Parameters of the 'Elliot approach' IBL height expression
$a_{charnock}$	Constant of the Charnock relation
C	Constant of the 'diffusion analogy' IBL height expression
C1, C2	Constants of the original Elliot IBL height expression
C_1, C_2, C_3, C_4	Parameters used for approximating velocity profiles
c_1, c_2	Parameters used for approximating velocity profiles
C_μ, $C_{\epsilon 1}$, $C_{\epsilon 2}$	Parameters of the $k-\epsilon$ turbulence model
f_1	Parameter of the 'Elliot approach' IBL height expression
g	Gravitational acceleration
I	Turbulence intensity
k	Turbulent kinetic energy
L, l	Characteristic length scales
M	Logarithmical ratio between roughness lengths
n	Exponent of IBL height expression
P	Pressure
p	Mean component of pressure
p'	Fluctuating component of pressure
$P_{available}$	Available power

S	Source term
U,V,W = U_1, U_2, U_3	Velocity components
u, v, w = u_1, u_2, u_3	Mean velocity components[1]
u' ,v' ,w' = u_1', u_2', u_3'	Fluctuating velocity components
u_*	Friction velocity
U_{char}	Characteristic velocity
x, y, z = x_1, x_2, x_3	Cartesian coordinates
y^+	Dimensionless height of a near wall grid point
y_p	Height of near wall grid point
z_0	Roughness length
z_1, z_2	Length scales used in the 'Elliot approach' IBL height expression
z_{min}	Height of near wall grid point
ϵ	Rate of dissipation of turbulent kinetic energy
ν	Kinematic viscosity
ρ	Density
ϑ	Velocity scale
μ_t	Eddy viscosity
κ	Von Karman constant
σ_κ, σ_ϵ	Parameters of the $k-\epsilon$ turbulence model
ϕ	A flow quantity
τ_0	Wind shear at ground level
$\Delta z_{\min}$	Near wall cell height
μ	Molecular viscosity
δ	IBL height
$\delta_{velocity}$	Velocity based IBL height
δ_{TKE}	TKE based IBL height
α	Parameter of IBL height expressions
σ_w	Vertical diffusion intensity
ΔS	Speed-up
$\overline{(\ )}$	Mean value

[1] u_1 and u_2 are also used for the velocity in the x-direction upstream and downstream of a roughness change respectively

Contents

1. Introduction

When planning a wind farm or designing tall buildings, it is important to have some knowledge of the wind conditions at the planned site of erection. The potential wind power available to a wind turbine increases with the wind speed cubed, and the potential wind loads on a structure with the wind speed squared. On top of this comes the potential fatigue loads, caused by the turbulent fluctuations in the wind.

Knowledge of the potential wind resources and wind loads at a specific site can be and is often obtained through field experiments. It is, however, a difficult and time consuming task to get a full understanding of the wind conditions through such experiments.
For this reason, it is common practice to use computer simulations of the wind to replace or supplement measured data.

Today an increasing number of wind farms are erected at sites of complex terrain (e.g. in areas with hills or mountains). In order to make reliable wind predictions in such terrain, there is a demand from the wind energy community for continuous development of non-linear computational fluid dynamics (CFD) models. An aim of this project is to improve the inlet conditions used in such models.

The traditional way of specifying the inlet conditions for a wind simulation, is to assume what will be referred to as logarithmic conditions. That is, the mean velocity is assumed to be purely horizontal, and the mean wind shear to be dependent only on the height above ground level, the wind shear at ground level and the density of the air. This leads to a velocity profile that increases logarithmically with the height above ground level. The turbulent kinetic energy (TKE) associated with such a velocity profile remains constant with height, while the rate of dissipation of TKE is assumed to be inversely proportional to the height above ground level.

At sites, where the incoming flow is undisturbed and in equilibrium with the underlying surface, logarithmic conditions can be a good assumption – at least up to the height at which the Coriolis effect becomes significant.
At many sites however, the flow cannot be considered to be undisturbed. It will typically carry some influence of upstream changes in e.g. terrain level, temperature, humidity or surface roughness. Furthermore neutral atmospheric stratification is required for the assumption of logarithmic conditions to be valid.

To simulate the wind in cases, where the incoming flow is not logarithmic, it can be necessary to expand the computational domain to include the upstream source of disturbance to get reliable results. Alternatively, a precursor simulation can be run to get profiles of the disturbed flow, which then can be used as inlet conditions for the original simulation of interest.
These options are, however, often not very attractive due to the increased computational time and modeling effort required. A much more convenient option would be, to have analytically or empirically determined expressions describing the disturbed flow, and then simply use these to define the inlet conditions.

The aim of this project is to find expressions of this kind, describing the flow after a change in the surface roughness, and to get an understating of how the flow over complex terrain is influenced by upstream roughness changes. Computer simulations will provide the background for the investigations to be made.

The present report consists of a short description of the numerical model used for the simulations. This is followed by a study of some test cases regarding the flow over flat terrain with a uniform surface roughness. Then the effect of introducing a roughness change to the flat terrain is studied, and finally the effects of an upstream roughness change on the flow over non-flat terrain is investigated. The flow over Askervein Hill is considered for this purpose. Neutral atmospheric stratification is assumed throughout.

2. The numerical model

2.1 Introduction

The CFD simulations presented in this report are made with the *Ellipsys 2D* and *3D* finite volume codes (see (Michelsen, 1992), (Michelsen, 1994) and (Sørensen, 1995)) using the $k-\epsilon$ turbulence model. A short and quite general description of the methods used in the code will be given here. More detailed descriptions can be found in e.g. (Sørensen, 1995) or (Versteeg & Malalasekera, 1995). Most of the following is based on these two references.

2.2 Description of the model

The basic concept of the finite volume method is to divide the computational domain into a grid of control volumes or cells. The governing equations of the flow are satisfied in each control volume and thereby in the entire computational domain.

The governing equations, in this case, are the continuity equation and the momentum equations in the x-, y- and z-directions (also referred to as the x_1-, x_2-, x_3-directions). The flow is assumed to be incompressible and isothermal. The Coriolis effect is not taken in to account and a steady state solution is sought. To account for the influence of turbulence the velocity components $(U,V,W)=(U_1,U_2,U_3)$ and the pressure *P* are split up in to mean parts u_i and p and fluctuation parts u_i' and p'. The Reynolds averaged versions of the continuity and Navier-Stokes equations ((1) and (2)) are used.

$$\frac{\partial u_i}{\partial x_i}=0 \tag{1}$$

$$\frac{\partial u_i}{\partial t}+\frac{\partial u_j u_i}{\partial x_j}=-\frac{1}{\rho}\frac{\partial p}{\partial x_i}+\nu\frac{\partial^2 u_i}{\partial x_j \partial x_j}-\frac{\partial \overline{u_i' u_j'}}{\partial x_j} \tag{2}$$

ν is the kinematic viscosity of the air and ρ the density.

The time derivative is omitted when doing steady state simulations.

With the $k-\epsilon$ turbulence model, the so called turbulent stresses, that appear in the Reynolds equations are assumed to be proportional to the mean velocity gradients (i.e. the Boussinesq approximation):

$$-\rho\overline{u_i' u_j'}=\mu_t\left(\frac{\partial u_i}{\partial x_j}+\frac{\partial u_j}{\partial x_i}\right) \tag{3}$$

The proportionality factor μ_t in equation (3) is called the eddy viscosity and is in the $k-\epsilon$ turbulence model calculated from the TKE k and the rate of dissipation of turbulent kinetic energy ϵ (from now on simply referred to as dissipation).

These two parameters are used to define a velocity-scale and a length-scale to represent the largest turbulent eddies of the flow:

$$\vartheta=k^{\frac{1}{2}} \quad \text{and} \quad l=\frac{k^{\frac{3}{2}}}{\epsilon} \tag{4}$$

Since it is these dominant eddies that interact with and extracts energy from the mean flow, their velocity and length scales can be used to describe the influence of turbulence on the mean flow[2]. Multiplying them gives an equation for the eddy viscosity:

$$\mu_t = \frac{\rho C_\mu k^2}{\epsilon} \tag{5}$$

C_μ is a dimensionless constant.

k and ϵ themselves are estimated through modeled equations[3]:

$$\frac{\partial(\rho k)}{\partial t} + \frac{\partial(\rho u_j k)}{\partial x_j} - \frac{\partial}{\partial x_j}\left(\left(\mu + \frac{\mu_t}{\sigma_k}\right)\frac{\partial(k)}{\partial x_j}\right) = \mu_t \frac{\partial u_i}{\partial x_j}\left(\frac{\partial u_i}{\partial x_j} + \frac{\partial u_j}{\partial x_i}\right) - \rho\epsilon \tag{6}$$

$$\frac{\partial(\rho\epsilon)}{\partial t} + \frac{\partial(\rho u_j \epsilon)}{\partial x_j} - \frac{\partial}{\partial x_j}\left(\left(\mu + \frac{\mu_t}{\sigma_\epsilon}\right)\frac{\partial(\epsilon)}{\partial x_j}\right) = \frac{C_{\epsilon 1}\epsilon}{k}\mu_t \frac{\partial u_i}{\partial x_j}\left(\frac{\partial u_i}{\partial x_j} + \frac{\partial u_j}{\partial x_i}\right) - \frac{\rho C_{\epsilon 2}\epsilon^2}{k} \tag{7}$$

The model constants in equations (6) and (7) have been determined empirically. Standard values for atmospheric boundary layer flows are given in Table 1 below[4]. These values are used throughout this project unless other is stated.

κ	C_μ	σ_k	σ_ϵ	$C_{\epsilon 1}$	$C_{\epsilon 2}$
0.4	0.03	1.00	1.30	1.21	1.92

Table 1: Standard values used in the $k-\epsilon$ turbulence model for atmospheric boundary layer flows

The momentum equations and the equations for k and ϵ are integrated over each control volume to get a set of discretized equations, which can be put into the form:

$$A_P \phi_P + \sum A_{nb}\phi_{nb} = S \tag{8}$$

ϕ_P is the cell center value of a flow quantity in a given cell and A_P the associated coefficient containing diffusive and convective fluxes.
ϕ_{nb} represents the cell center value in a neighboring cell and A_{nb} its coefficient. *S* is a source including for instance the pressure term in the momentum equations

Doing the integration brings up a need to approximate cell face values of velocities and scalar quantities as well as their gradients from cell center values.
In general this can be done using the central differencing scheme (CDS) and linear interpolation. In short the CDS approximates a cell face gradient by use of the two neighboring cell center values of the variable to be differentiated.
For the convective terms, however, it is necessary to use a different scheme to ensure transportiveness and a bounded solution.

[2] (Versteeg & Malalasekera, 1995) page 42
[3] (Sørensen, ., 1995) page 12
[4] (Sørensen, ., 1995) page 13

Transportiveness is a measure, of how well the scheme reflects the Peclet number of the flow (the ratio between convection and diffusion) and the direction of the flow. The CDS does not take either the Peclet number or the flow direction into consideration. Upstream and downstream influences are treated with equal weight in all cases, and the scheme is not suitable for describing the convective terms in a convective dominated flow.
In a bounded solution, the internal nodal values of a flow quantity should, in the absence of sources, be bounded by its boundary values. With no sources, this can be ensured by fulfilling the criterion below (equation (9)) and making sure, that all coefficients of the discretized equations have the same sign[5].

$$\frac{\sum|A_{nb}|}{|A_P|}\begin{cases}\leq 1 & \text{at all nodes}\\ < 1 & \text{at one node at least}\end{cases} \tag{9}$$

The details of these requirements will not be discussed further here.

In the simulations presented in this report, the equations are solved on four grid levels with increasing refinement for fast convergence. On the first grid level the upwind difference scheme (UDS) is used for the convective terms, on the second level the second order UDS (SUDS) is used, and finally the quadratic upwind scheme QUICK is used for the last two grid levels, until the residuals reach a level of 10^{-5}.

The discretized equations are solved by use of the SIMPLE algorithm. The basic nature of the algorithm is described below.
In the case of the momentum equations the algorithm is initiated using guessed values for pressure and velocity. These values go into the source term and coefficients of equation (8), and from this a new velocity can be calculated. This new velocity is considered to be the correct velocity minus a correction term:

$$u = u_{correct} - u_{correction} \tag{10}$$

The same idea is used in relation to the pressure:

$$p = p_{correct} - p_{correction} \tag{11}$$

By subtracting equation (8) with *u* and *p* from equation (8) with $u_{correct}$ and $p_{correct}$ an expression for the velocity correction term can be found. This expression is simplified by omitting the influence of the correction terms in the neighboring cells.
By substitution of the expression for the corrected velocity into the continuity equation, an expression for the pressure correction is found. Adding the pressure correction to the initial pressure guess *p* gives the correct pressure, which in turn can be used to determine the correct velocity.
The corrected pressure and velocity can then be used as initial values in the next iteration step. This procedure is continued, until the residuals are sufficiently low.

2.3 Closure

This chapter has dealt with the basic concepts of the *Ellipsys 2D/3D* code used in this project. Subjects such as the finite volume method, the $k-\epsilon$ turbulence model, differencing schemes and the SIMPLE algorithm have been briefly touched. More detailed descriptions are not considered to be within the scope of this project.

[5] (Versteeg & Malalasekera, 1995) page 112

Finally it should be noted, that the *Ellipsys* code uses curvilinear coordinates instead of the Cartesian used above to facilitate the simulation of flow around complex geometries or over complex terrain.

3. The flow over flat terrain with uniform roughness

3.1 Introduction

To test and investigate the properties of the numerical model used throughout this project, a few simple two dimensional test cases regarding the flow over flat terrain with uniform surface roughness are simulated.
The aim of doing these test cases is to see whether the velocity and TKE develop as expected through the computational domain and to examine the grid dependency of the solution.

The roughness of a given surface is characterized by its roughness length z_0. In this chapter simulations with roughness lengths of 0.0001 m and 0.5 m are considered.
These are the most extreme values used throughout this project. According to Figure 10.5 in (Arya, 2001) they correspond to the roughness lengths of "calm open sea" and "fairly level wooded country" respectively, i.e. a quite smooth surface and a very rough surface.
Concerning wooded country it should be noted, that the simulations made here, does not actually take the effect of trees and their foliage into account. One would need a special numerical model to do this. All simulations presented in this report are made with the standard model described in the previous chapter.

The reason for looking at these two extreme roughness lengths is primarily to see how changing this parameter influences the development of the simulated flow.
Doing these uniform roughness simulations also provide valuable information regarding the level of numerical error to be expected with the used model and grid resolution. This information will help to interpret the results of the roughness change simulations presented later in this report.

3.2 Setup of the simulations

A sketch of the computational domain used for the following test cases is shown in Figure 1. It consists of a rectangle of 20x5 km with inlet conditions along the left and top boundaries, outlet condition on the right boundary and a no-slip wall condition on the bottom boundary.

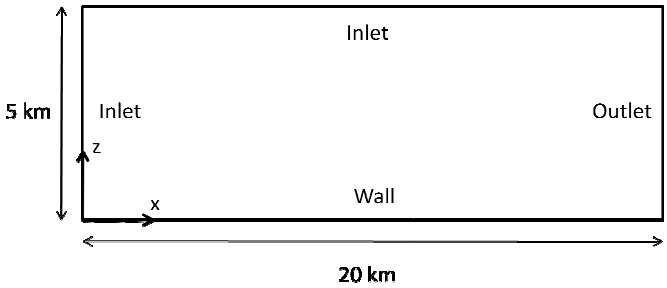

Figure 1: Sketch of the computational domain used for the simulations over flat terrain

A Cartesian coordinate system with *x* in the main flow direction from left to right and *z* in the vertical direction from the bottom to the top is used to describe the flow. In the model $z = 0$ represents ground level plus the roughness length z_0.

As inlet conditions a logarithmic profile is prescribed for the velocity in the x-direction and zero velocity in the z-direction:

$$u = \frac{u_*}{\kappa} \ln \frac{z + z_0}{z_0} \quad \text{and} \quad w = 0 \tag{12}$$

$\kappa = 0.4$ is the von Karman constant.

u_* is the friction velocity.

The profile is based on the assumption, that the mean wind shear $\frac{\partial u}{\partial z}$ is dependent only on the height above ground level, the wind shear at ground level τ_0 and the density of the air ρ. Defining the friction velocity as $u_* = \sqrt{\frac{\tau_0}{\rho}}$ leads through dimensional analysis to:

$$\frac{\partial u}{\partial z} = \frac{u_*}{\kappa(z + z_0)} \tag{13}$$

Integration of equation (13) leads to equation (12) with the constant of integration determined to get zero velocity at $z = 0$. The value of the Von Karman constant which appears as a proportionality factor in equation (13) has been determined empirically.
The inlet velocity profile is associated with a turbulence profile, which is constant with height. The TKE is found as:

$$\mathrm{k} = \frac{u_*^2}{\sqrt{c_\mu}} \tag{14}$$

For the considered test cases, the inlet friction velocity is set together with the desired roughness length to get a wind speed of 10 m/s at a height of 10 m above ground level.

3.3 Results

With a uniform roughness length throughout the domain equal to the one used to specify the inlet conditions, the flow is assumed to be in equilibrium. No changes of either the velocity or the TKE profile should occur. As shown in Figure 2, Figure 3 and Figure 4 this is more or less the case when using a suitable grid.
An investigation regarding the dependency of the solution on the grid layout follows below. It is divided in two parts. First the influence of changing the height of the near wall cells is studied and then the dependency on the number of cells in the domain is investigated.

Figure 2 shows the simulated velocity profiles at x = 15000 m for both roughness cases along with their respective inlet profiles. The profiles are normalized with the local friction velocity. The simulations are made with a grid of 256x256 cells and a near wall cell height of $\Delta z_{\min} = 0.052$ m.
It is difficult to see any differences at all between the inlet and the downstream velocities. In Figure 3 where the scale of the vertical axis is logarithmic, some small deviations from the otherwise completely straight line is seen very close to the ground in the case of $z_0 = 0.0001$ m.

Regarding the turbulent kinetic energy shown in Figure 4 there is also very little difference between the inlet profiles and simulated profiles at x = 15000 m. The only visible deviation is close to the ground in the case of $z_0 = 0.5$ m.

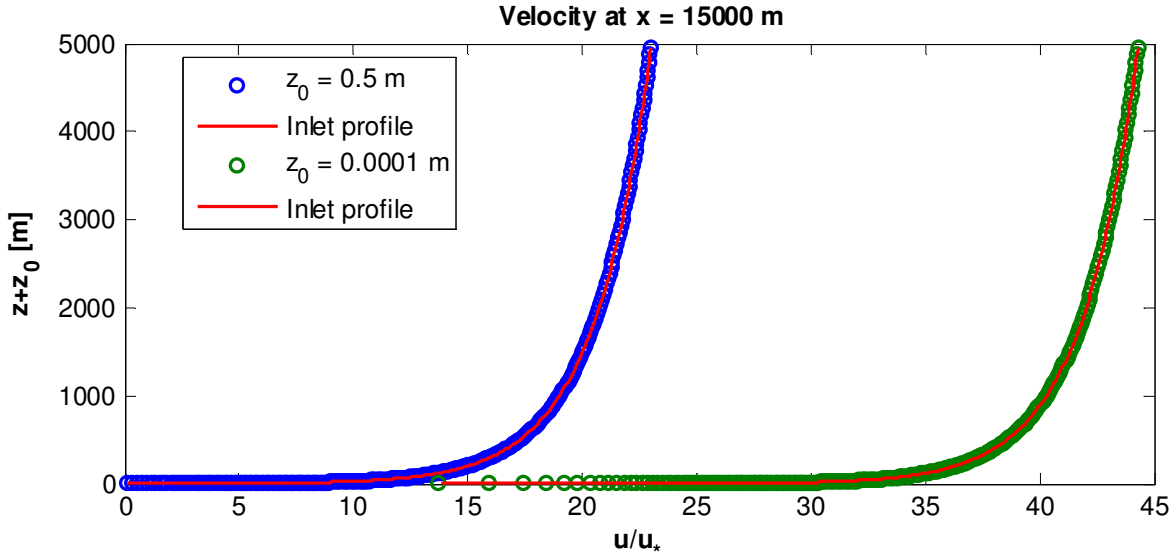

Figure 2: Simulated velocity profiles at x=15000 m and inlet profiles – normalized with the corresponding friction velocities

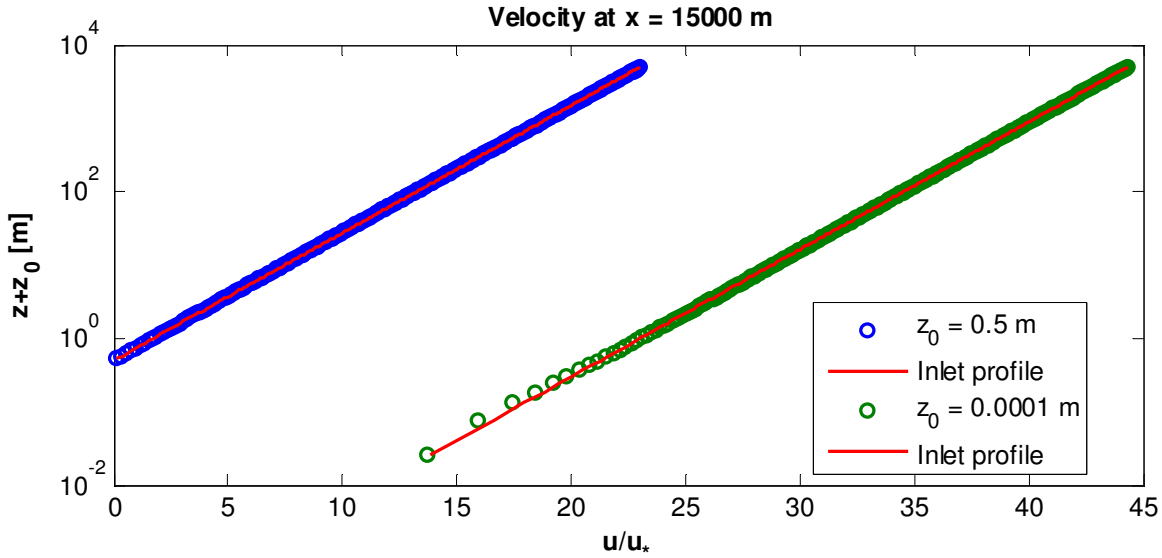

Figure 3: Logarithmic scale plot of simulated velocity profiles at x=15000 m and inlet profiles – normalized with the corresponding friction velocities.

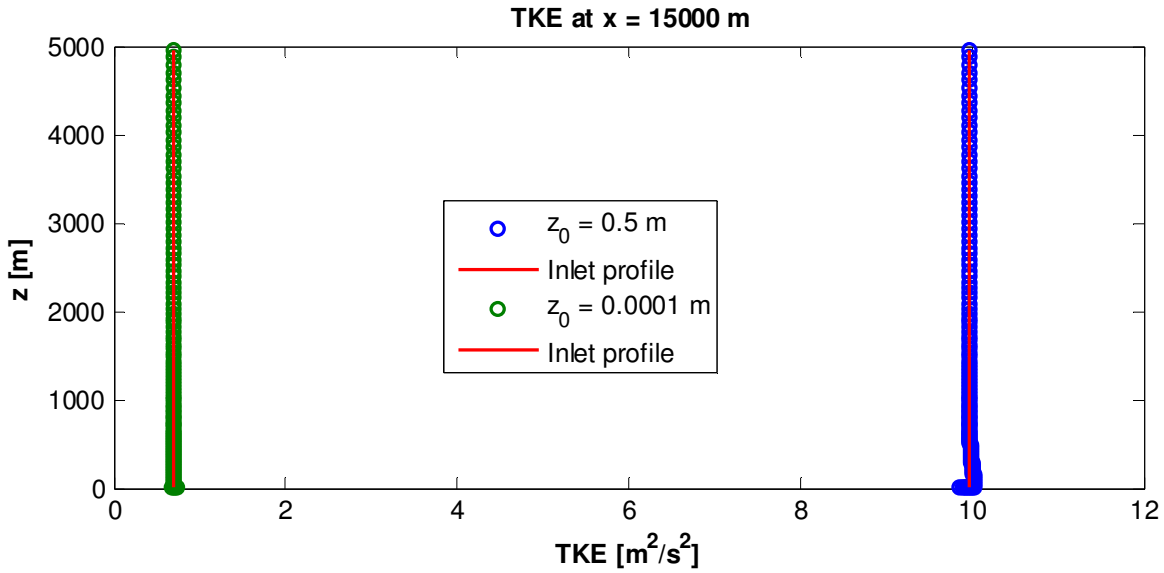

Figure 4: Simulated TKE profiles at x=15000 m and inlet profiles

3.3.1 Solution dependency on cell height

As seen in Figure 2 the gradient of the logarithmic velocity profile increases towards the wall. To capture this, the height of the grid cells is decreased towards the wall. A tangent hyperbolic stretch function is used. The length of the cells is kept constant.

Figure 5 shows the discrepancy between the inlet velocity profile and the simulated profile at a position 15000 m downstream of the inlet as a function of the height of the first grid point above the wall, $z_{\min}$ (corresponding to half the near wall cell height $\Delta z_{\min}$).
The plotted error is an average of the errors at heights of 1, 10, 50 and 100 m. The heights included in this average value is assumed to represent the most interesting spectrum with respect to prediction of wind loads and of wind energy resources. The reason for not simply including every point between 1 m and 100 m in the average, is to avoid the result being dominated by near wall errors due to the increasing concentration of points towards the wall.

The error at a given height is defined as:

$$\mathrm{Error}(z) = \frac{u_{\mathrm{inlet}}(z) - u(z)}{u_{\mathrm{inlet}}(z)}$$

The blue line in Figure 5 represents simulations with a roughness length of 0.5 m and the green line represents simulations with a roughness length of 0.0001 m. In all cases a grid of 256x256 cells is used.

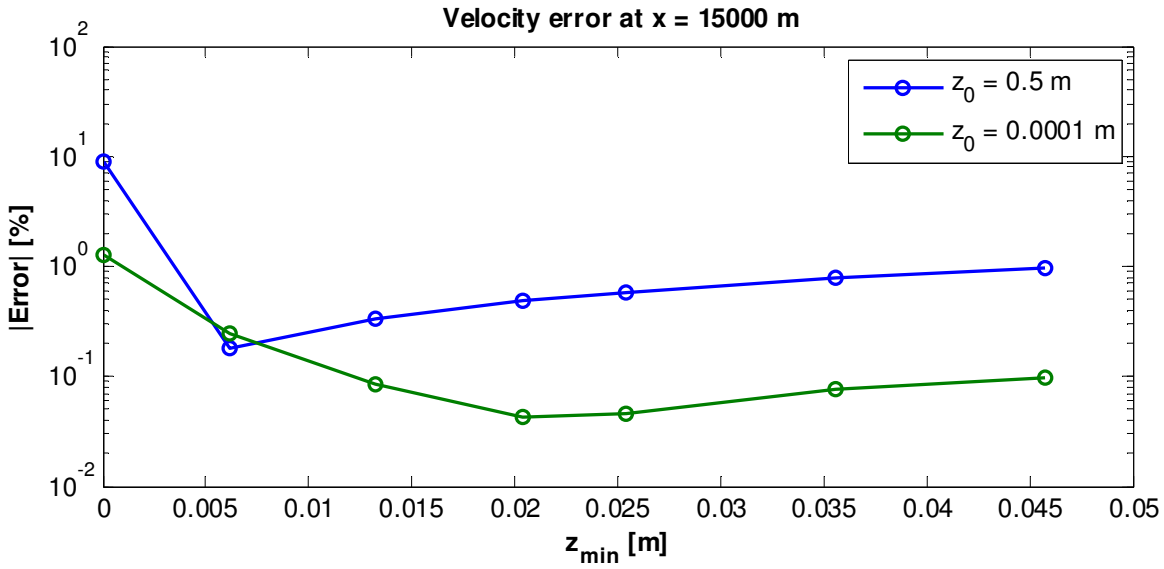

Figure 5: Error between inlet velocity and the simulated velocity at a position 15000 m downstream of the inlet plotted as a function of the height of the first grid point above the wall. The plotted error is an average of the errors at heights of 1, 10, 50 and 100 m.

For both the low and the high roughness length the highest error (approximately 1% and 10% respectively) occurs with the smallest near wall cell height ($\Delta z_{\min} = 2 \cdot z_{\min} = 2 \cdot 10^{-5}$ m). Increasing the height reduces the error to a certain level after which it increases again. More or less the same tendency is observed for the corresponding TKE error shown in Figure 6. The maximum error is however a bit higher (approximately 4% and 20%).

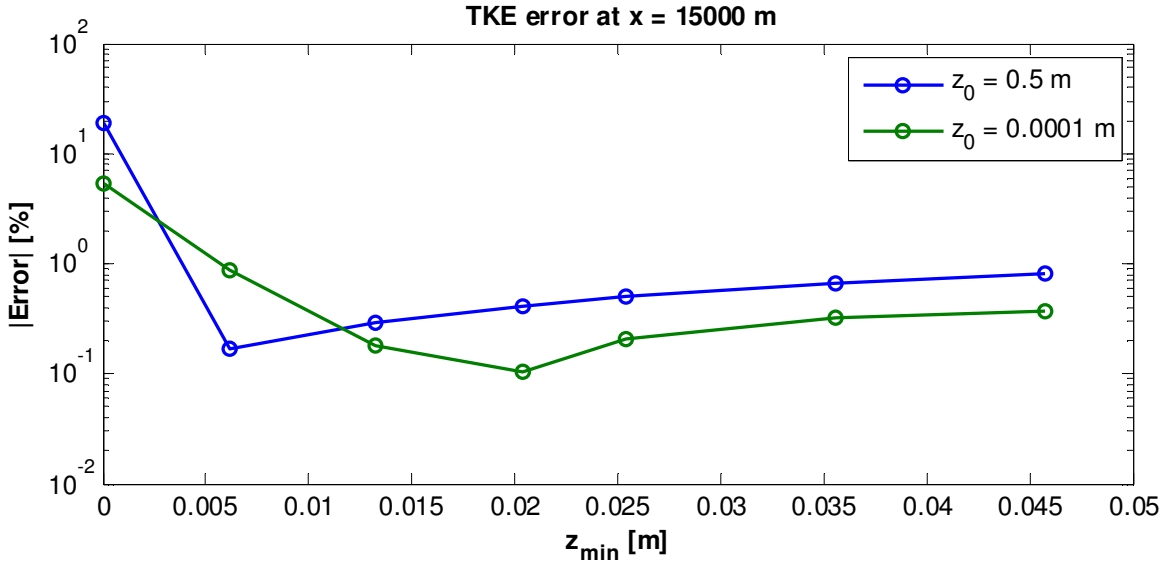

Figure 6: Error between inlet TKE and the simulated TKE at a position 15000 m downstream of the inlet plotted as a function of the height of the first grid point above the wall. The plotted error is an average of the errors at heights of 1, 10, 50 and 100 m.

As the height of the first cell is reduced, the resolution higher in the domain is decreased due to the stretch function. This could explain the observed increase of the error. However, looking at a simulation with 1024 cells in the vertical direction instead of 256 suggests that resolution is not the problem (see Figure 7).
The resolution of the 256x1024 grid with $z_{\min} = 10^{-5}$ m is at all heights better than the resolution of e.g. the 256x256 grid with $z_{\min} = 0.046$ m, but the observed error is still much bigger. In fact it also exceeds

the error obtained with the 256x256 grid with $z_{\min} = 10^{-5}$ m.
Figure 7 and Figure 8 shows the velocity and TKE errors respectively as functions of the height at *x* = 15000 m. Only the high roughness simulations are presented since the error in these in general are found to be the higher than those of the low roughness simulations.

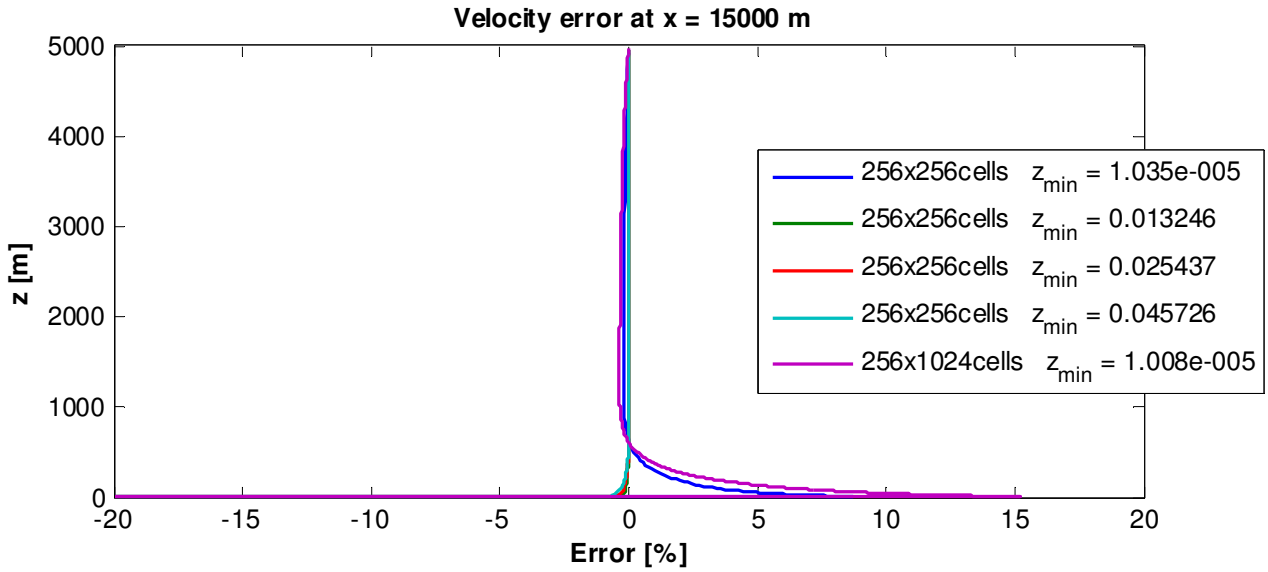

Figure 7: Error between inlet velocity and simulated velocity at a position 15000 m downstream of the inlet. Only the case with a roughness length of 0.5 m is shown.

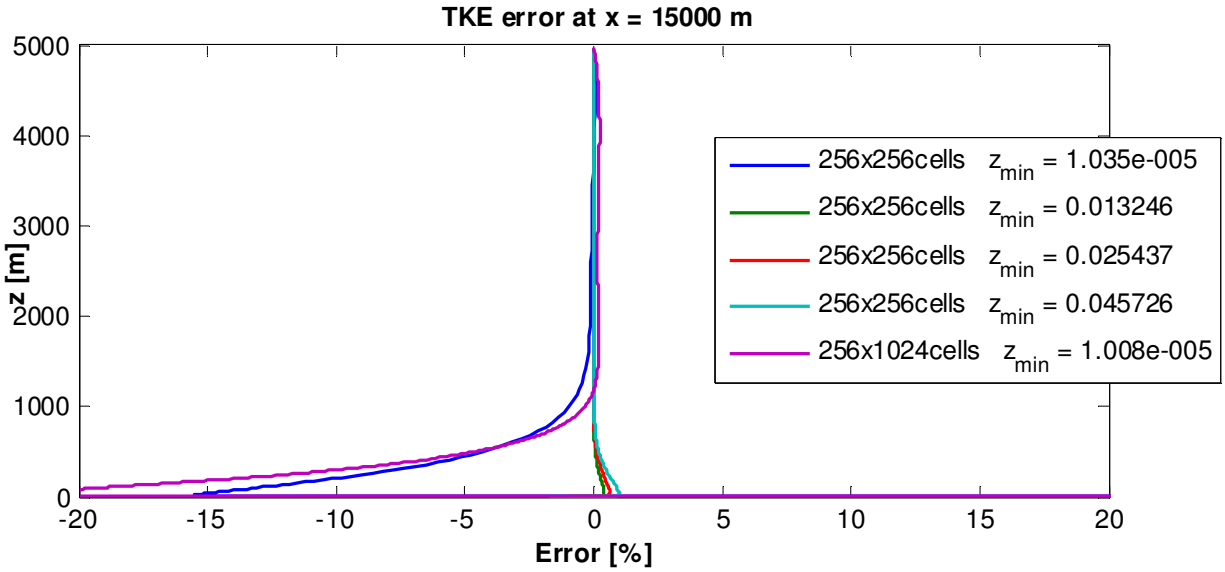

Figure 8: Error between inlet TKE and simulated TKE at a position 15000 m downstream of the inlet. Only the case with a roughness length of 0.5 m is shown.

The high errors (up to around 300% and -70% at the lowest grid point for TKE and velocity respectively) of the simulations with the smallest $z_{\min}$ are suspected to be caused by the very high aspect ratio of the cells closest to the wall. With 256x256 cells and $z_{\min} = 10^{-5}$ m the maximum aspect ratio goes up to about $3.9 \cdot 10^{6}$.

The roughness lengths of 0.0001 m and 0.5 m are the minimum and maximum values to be used throughout this report. Going back to Figure 5 and Figure 6 a value of $z_{\min}$ around 0.026 m seems like good

general choice for simulations of the flow over flat terrain. It is low enough to give good accuracy and high enough to avoid aspect ratio problems.
With a near wall cell height of $\Delta z_{\min} = 2 \cdot 0.026\ \mathrm{m}$ and a grid of 256x256 cells the maximum cell aspect ratio is around 1500. The velocity and TKE errors plotted in Figure 5 and Figure 6 are approximately 0.06% and 0.2 % in the case of the low roughness length and about 0.8% in the case of the high roughness length. These errors are considered as being quite low. As a general recommendation aspects ratios higher than 1500 should be avoided when simulating flow over flat terrain. For the flow over more complex terrain the critical limit is assumed to be somewhat lower.

The inlet profiles of constant TKE used in the presented simulations follows from traditional boundary layer theory (see e.g. (Versteeg & Malalasekera, 1995)).
A turbulent boundary layer is typically divided into an inner region of about 10% or 20% of the full boundary layer and an outer region covering the rest. The inner region, which is characterized by a constant level of shear stress, includes a sub layer very close to the wall. In this sub layer viscous stresses dominate over turbulent stresses, and the velocity increases linearly with height.
In the used turbulence model a high Reynolds number is assumed, and some terms are neglected in the equations for *k* and ϵ. Thus, it is necessary to stay clear of the viscous dominated sub layer when defining the computational grid. This way the problem of resolving the very high velocity gradient near the wall is also avoided. Instead of simulating the flow near the wall, it is modeled by the so called logarithmic wall law. This means e.g. that for rough walls, as used throughout this project, the velocity at the near wall grid points are determined as by equation (12).
The parameter $y^+ = \frac{y_p u_*}{\nu}$ is normally used to determine whether the height of the near wall grid point y_p is above or below the height of the viscous sub layer. (Versteeg & Malalasekera, 1995) recommends a value of $y^+ > 30$ to stay clear of this layer.
In the simulations presented above with a near wall cell height of 0.052 m values of $y^+ = \frac{(z_0 + z_{\min})u_*}{\nu}$ are found to be around 46000 and 600 for the two roughness cases, $z_0 = [0.5\ \mathrm{m}, 0.0001\ \mathrm{m}]$. Thus, it should be safe to assume that no attempt to simulate the viscous sub layer is made.
The air density of the presented simulations is set to $\rho = 1.225 \frac{\mathrm{kg}}{\mathrm{m}^3}$ and the molecular viscosity to $\mu = 1.85 \cdot 10^{-5}\ \frac{N \cdot s}{m^2}$.

3.3.2 Solution dependency on grid resolution

For a look at the dependency on the number cells in the vertical direction, the velocity error averaged at heights of 1, 10, 50 and 100 m as a function of *x* for four different grid resolutions is plotted in Figure 9. Again only the errors of the high roughness simulations are plotted.
The solution seems to be more or less grid independent when using 256 cells or more. A near wall cell height of 0.052 m is used.

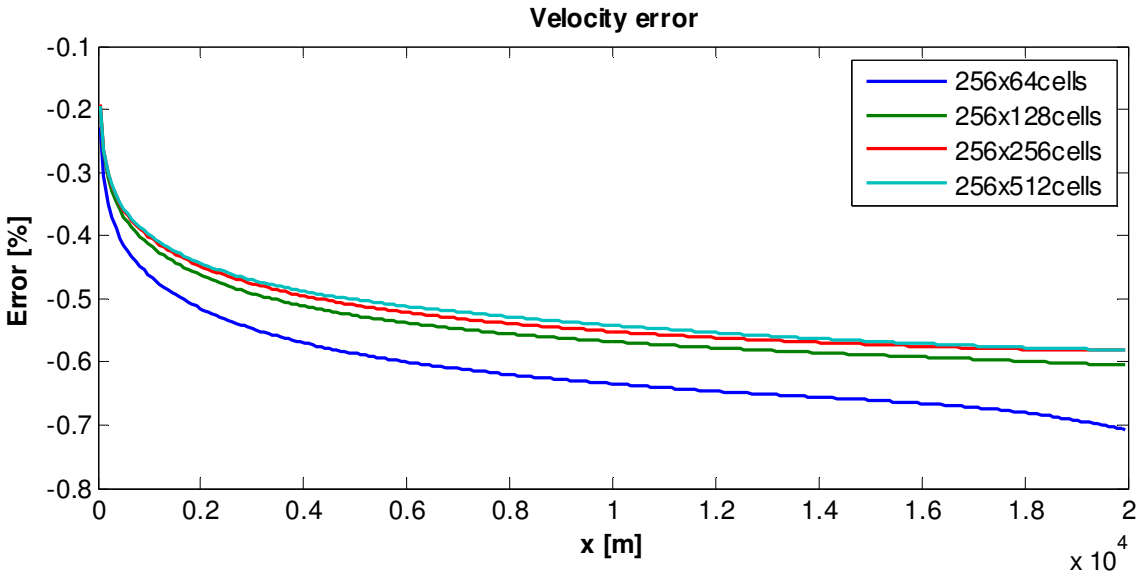

Figure 9: Error between inlet velocity and simulated velocity averaged at heights of 1, 10, 50 and 100 m. z_0 = 0.5 m and z_{min} = 0.026 m.

The tendency for the TKE error shown in Figure 10 is not as clear as for the velocity error. The error actually increases a bit with the number of cells. But in all cases the error is quite small and a grid with 256 cells is assumed to be adequate.

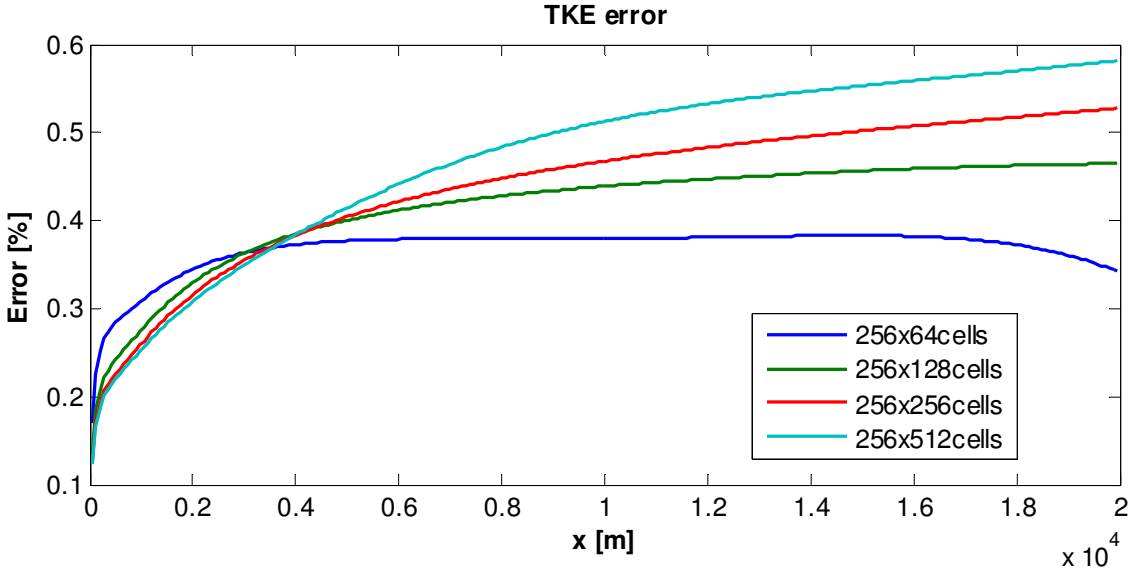

Figure 10: Error between inlet TKE and simulated TKE averaged at heights of 1, 10, 50 and 100 m. z_0 = 0.5 m and z_{min} = 0.026 m.

Regarding the number of cells in the horizontal direction 256 or even 128 seems to be enough. Figure 11 and Figure 12 show the velocity error and TKE error for different grid resolutions .

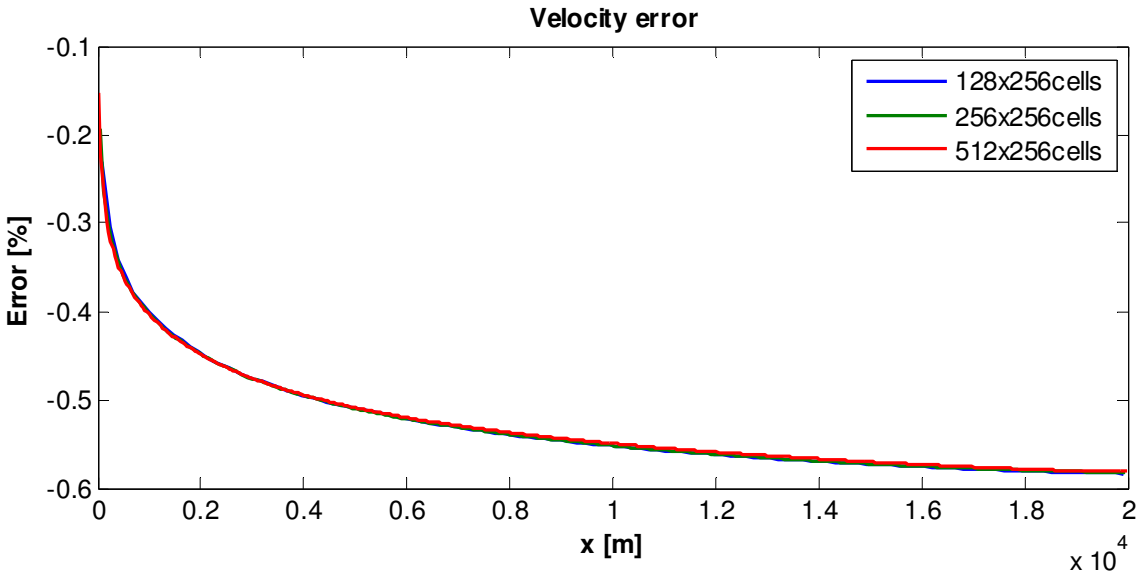

Figure 11: Error between inlet velocity and simulated velocity averaged at heights of 1, 10, 50 and 100 m. z_0 = 0.5 m and z_{min} = 0.026 m.

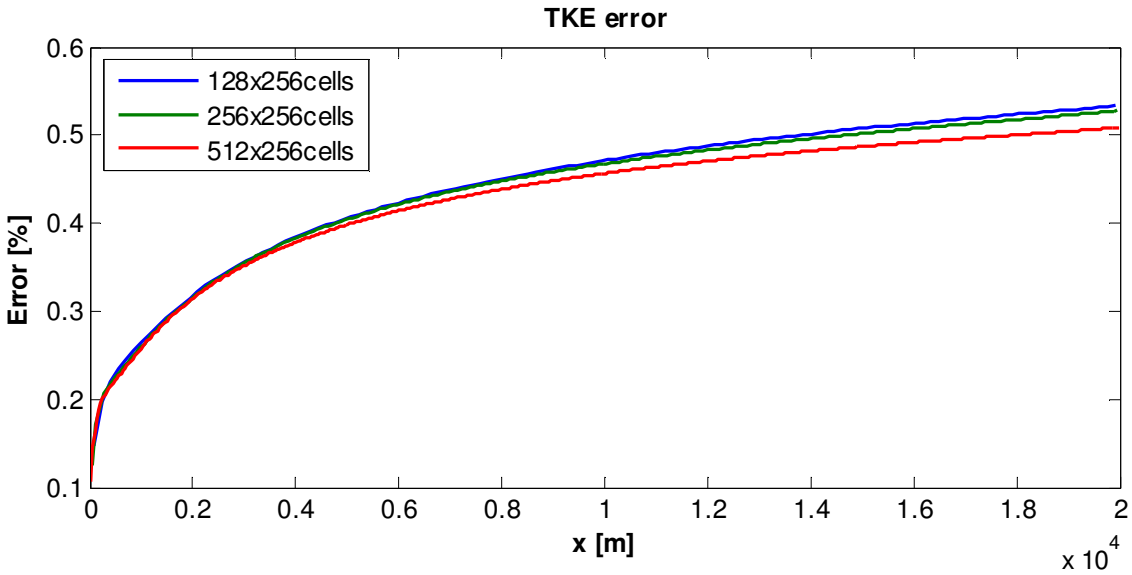

Figure 12: Error between inlet TKE and simulated TKE averaged at heights of 1, 10, 50 and 100 m. z_0 = 0.5 m and z_{min} = 0.026 m.

3.4 Closure

The numerical model has been tested for flows over flat terrain with uniform roughness. The prescribed logarithmic velocity profile and the constant TKE profile was expected to remain unchanged when moving downstream of the inlet. This has been shown to be more or less true depending on the number of grid points in the domain and the height of the cells closest to the wall.

A near wall cell height of about 0.052 m and a grid of 256x256 cells has been found to be adequate for this type of simulation with roughness lengths of both 0.5 and 0.0001 m.

The errors of the high roughness simulation on such a grid turned out to be higher than those of the low roughness simulation. They remain, however, below approximately 1%. Thus, with prober meshing this is the maximum error of both TKE and velocity to be expected in simulations of flow over flat terrain with a uniform roughness length between 0.5 and 0.0001 m.

An increase of the TKE error was observed when increasing the grid resolution. This might be due to some

inaccuracy in the turbulence model; for instance in the choice of modeling constants. It has also been found that decreasing the height of the near wall cells too much and thereby increasing the cell aspect ratio, could significantly decrease the accuracy of the solution. With the numerical model used here aspects ratios higher than 1500 should be avoided when simulating flow over flat terrain.

4. The flow over flat terrain with a single roughness change

4.1 Introduction

So far simulations of the quite uneventful flow over flat terrain with an uniform surface roughness has been studied. This has been done mainly to get an idea of the accuracy of the numerical model.

The focus of this chapter is on the flow over flat terrain with a single change in roughness length from z_{01} to z_{02}.

The effects of such a change on the flow in the atmospheric boundary layer has been studied at least since the 1950s (e.g. (Elliot, 1958)), and over the years many different approaches have been proposed to describe these effects. (Garratt, 1990) provides a review of the research in the field up until around 1990. More recently (Savelyev & Taylor, 2005) presents some new ideas while also discussing earlier work.

A main issue has been to describe the development of a so called internal boundary layer. The basic idea is, that when passing a change in the surface roughness, the flow will either slow down and become more turbulent or speed up and become less turbulent. The behavior depends on whether the change is from a low to a high surface roughness or from a high to a low surface roughness.

Immediately after the change only the lowest part of the flow is affected. Looking further downstream still larger parts of the flow feels the effect of the roughness change. This growing layer in which the flow is modified is referred to as the internal boundary layer or the IBL.

In the following, the height of the IBL (δ) and the vertical profiles of velocity, TKE and dissipation downstream of different roughness changes are examined through a range of simulations. The examined parameters are compared to analytical and empirical expressions.

The aim is to find some general expressions, that can be used to define inlet profiles for simulations over terrain where an upstream roughness change is suspected to have an influence. With such expressions the efforts of including the roughness change in the computational domain or of doing a precursor simulation to generate the inlet profiles could be saved.

The actual effect of using inlet profiles modified by a roughness change instead of standard logarithmic inlet profiles is studied later in this report (in the chapters of 'Askervein – 2D simulation' and 'Askervein – 3D simulation').

Both changes from smooth to rough surfaces and from rough to smooth surfaces are studied. Simulations with upstream roughness lengths of $z_{01} = 0.0001\,\mathrm{m}$, $z_{01} = 0.001\,\mathrm{m}$ and $z_{01} = 0.01\,\mathrm{m}$ are considered in the category of smooth-to-rough surface changes and simulations with $z_{01} = 0.5\,\mathrm{m}$, $z_{01} = 0.05\,\mathrm{m}$ and $z_{01} = 0.005\,\mathrm{m}$ in the category of rough-to-smooth surface changes. The inlet profiles of velocity and TKE for all simulations are, as described earlier, logarithmic and constant respectively and are in equilibrium with z_{01}. Table 2 gives an overview of all the performed simulations.

Smooth to rough		
z_{01} [m]	z_{02} [m]	$\frac{z_{02}}{z_{01}}$
0.0001	0.5	5000
	0.045	450
	0.02	200
	0.009	90
	0.004	40
	0.002	20
	0.001	10
	0.0004	4
0.001	0.45	450
	0.2	200
	0.09	90
	0.04	40
	0.02	20
	0.01	10
	0.004	4
0.01	0.4	40
	0.2	20
	0.08	10
	0.04	4

Rough to smooth		
z_{01} [m]	z_{02} [m]	$\frac{z_{02}}{z_{01}}$
0.5	0.0001	0.0002
	0.002	0.004
	0.004	0.008
	0.009	0.018
	0.02	0.04
	0.045	0.09
	0.1	0.2
0.05	0.0002	0.004
	0.0004	0.008
	0.0009	0.018
	0.002	0.04
	0.0045	0.09
	0.01	0.2
0.005	0.0002	0.04
	0.00045	0.09
	0.001	0.2

Table 2: Overview of the roughness change simulations used throughout the project.

4.2 Computational domain

The computational domain used for the simulations is more or less identical to the one described in the previous chapter (see Figure 1). The only difference is the roughness length associated with the wall boundary. It changes from z_{01} to z_{02} at the grid point located at $x = 0$. The inlet is placed at $x = -5000$ m.

The grid is generated as suggested in the conclusion of the previous chapter with 256x256 cells and a near wall cell height of approximately 0.052 m. According to the results of Figure 13, Figure 14, Figure 15 and Figure 16 this should be adequate. In these, the profiles of TKE and velocity at $x = 5000$ m are plotted for simulations with changes in roughness lengths from 0.0001 m to 0.5 m and from 0.5 m to 0.0001 m. Four different resolutions of the grid in the vertical direction are presented. Figure 13 and Figure 14 shows the smooth-to-rough case and Figure 15 and Figure 16 the rough-to-smooth case.

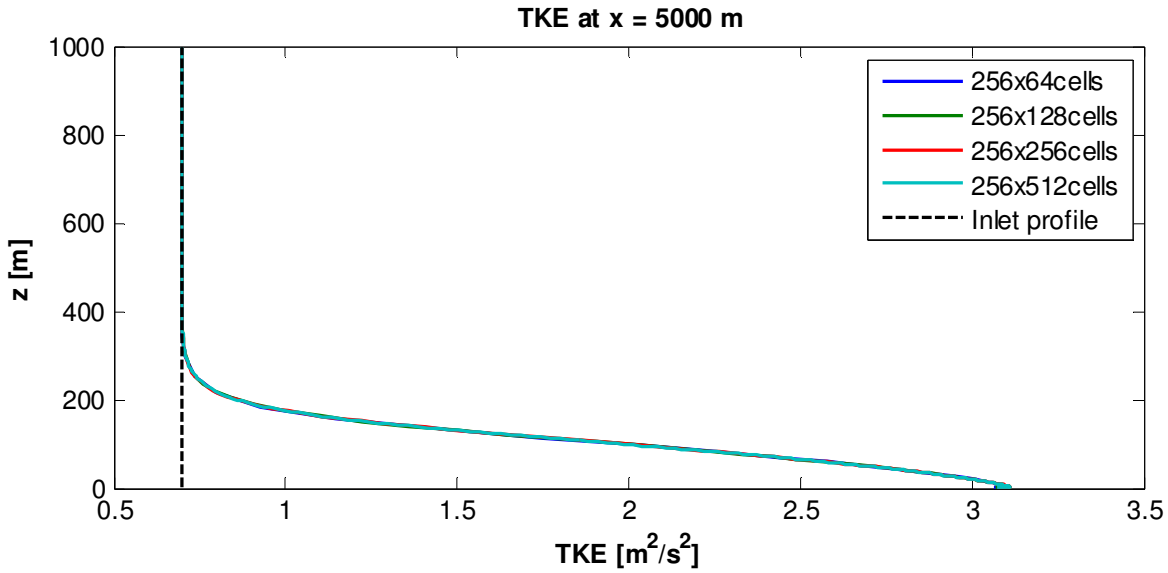

Figure 13: TKE profiles at x = 5000 m after a change in roughness length from 0.0001 m to 0.5 m at x =0.

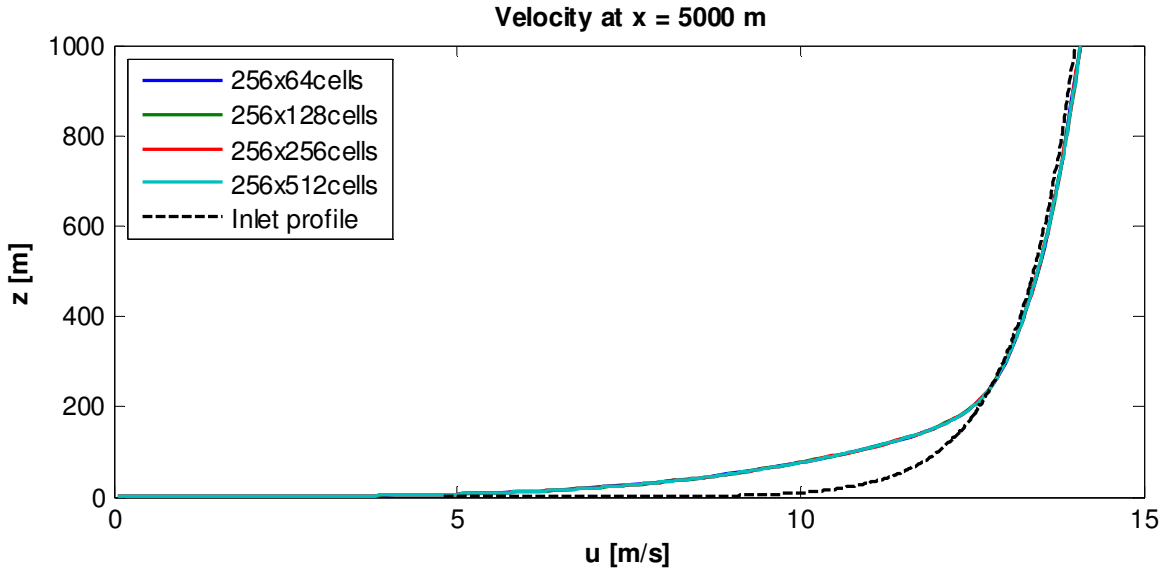

Figure 14: Velocity profiles at x = 5000 m after a change in roughness length from 0.0001 m to 0.5 m at x =0.

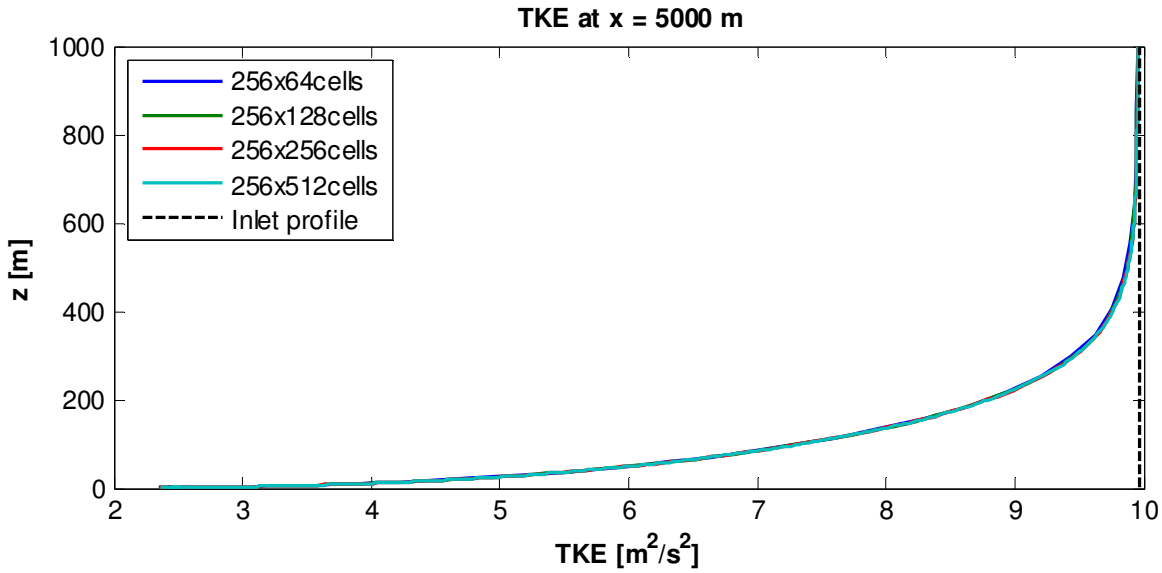

Figure 15: TKE profiles at x = 5000 m after a change in roughness length from 0.5 m to 0.0001 m at x =0.

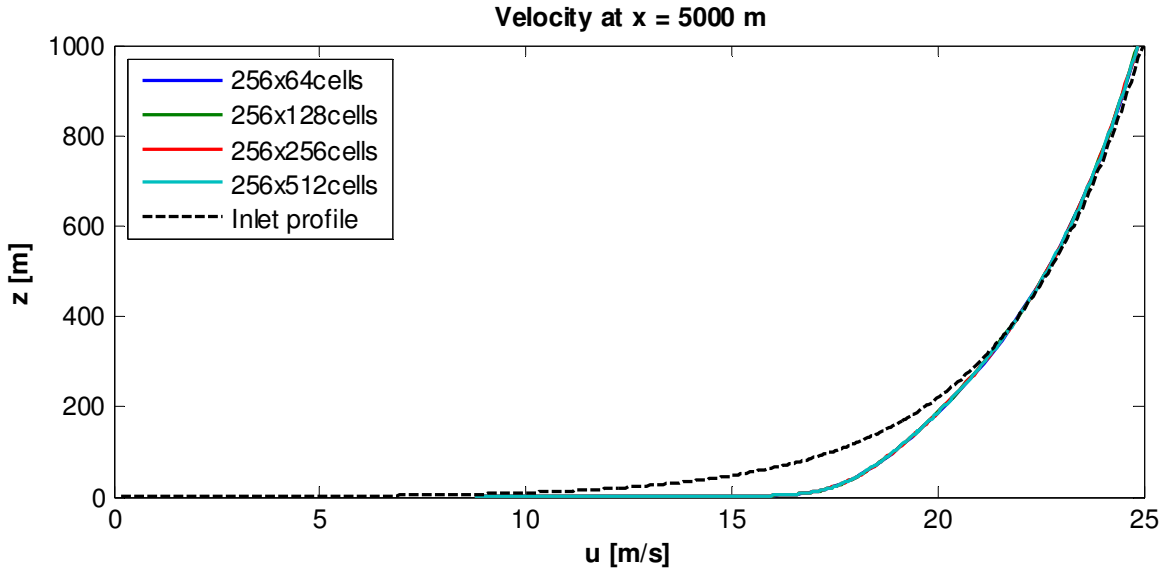

Figure 16: Velocity profiles at x = 5000 m after a change in roughness length from 0.5 m to 0.0001 m at x =0.

In both cases the results seem to be independent of the grid resolution. The 256x64 cells grid would actually most likely be sufficient, but since the computational time is quite low for these simple 2D cases the 256x256 cells grid is chosen.

4.3 IBL heights

The height of the IBL can be defined in different ways. In this report, definitions based on velocity and TKE are considered.

Profiles downstream of the roughness change are compared to the inlet profiles. The height at which a downstream profile starts to differ more than some percentage from the inlet profile, is defined as the height of the IBL. The search of this height is carried out from the top of the domain towards the bottom.

Examples of the two definitions δ_{TKE} and $\delta_{velocity}$ are shown below. In both cases a difference higher than 2 % between inlet profile and downstream profile is used as the limit to define the IBL height. That is:

$$\frac{u_{inlet}(x, \delta_{velocity}) - u(x, \delta_{velocity})}{u_{inlet}(x, \delta_{velocity})} = \mathrm{IBL}_{\mathrm{limit}} = 0.02 \quad (15)$$

Or:

$$\frac{k_{inlet}(x, \delta_{TKE}) - k(x, \delta_{TKE})}{k_{inlet}(x, \delta_{TKE})} = \mathrm{IBL}_{\mathrm{limit}} = 0.02 \quad (16)$$

Unless anything else is stated 2% is used in the following as the IBL limit. Essentially an IBL limit of 0 % would be more correct, but due to the presence of numerical errors, this would most likely result in poor estimates of the IBL height.

Figure 17 and Figure 18 show the development of δ_{TKE} and $\delta_{velocity}$ as the roughness length goes from 0.5 m to 0.0001 m.

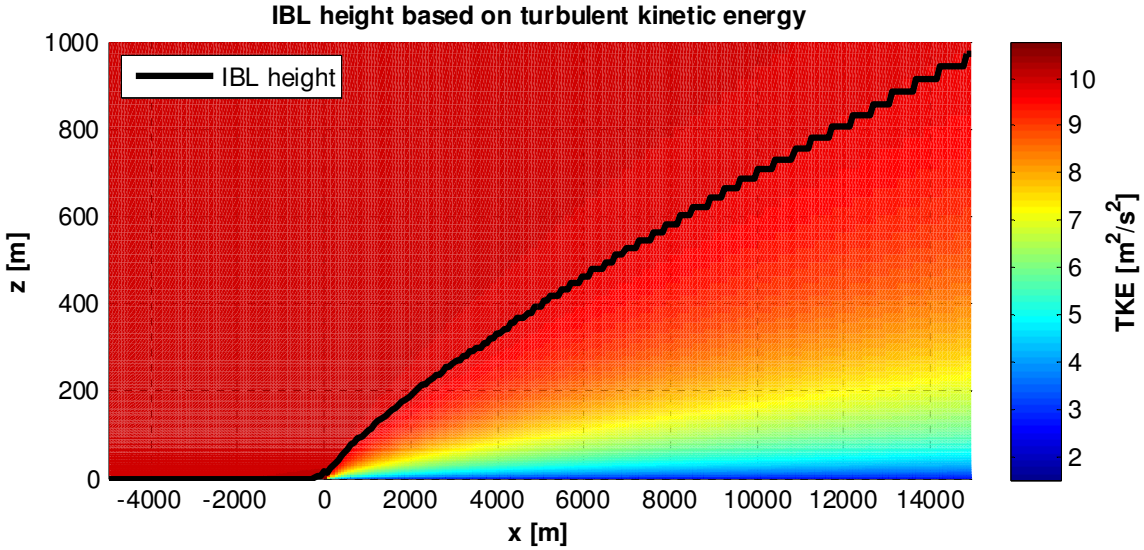

Figure 17: The TKE based IBL height due to a change in roughness length from 0.5 m to 0.0001 m at x = 0.

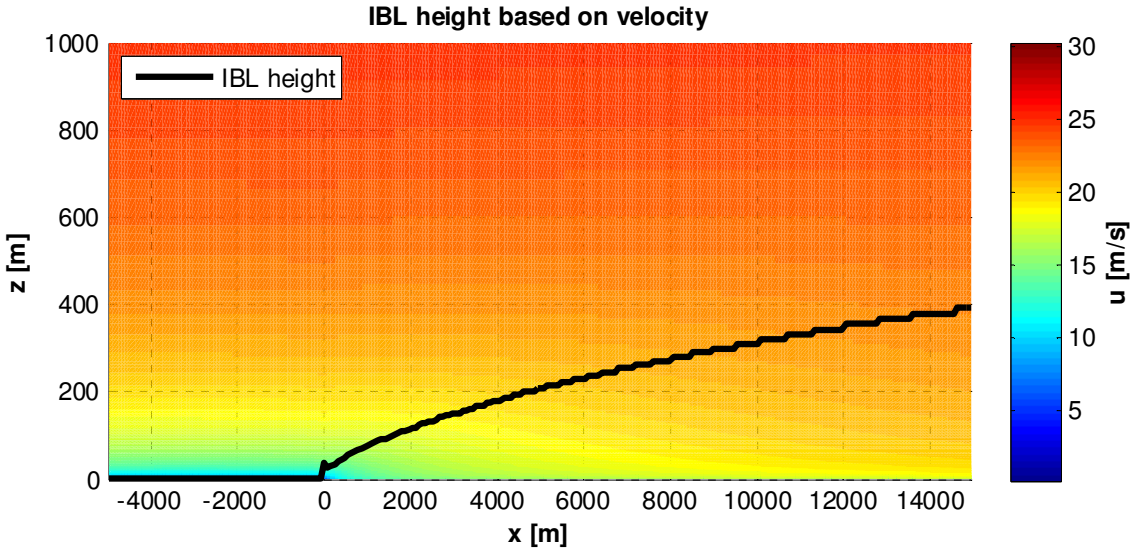

Figure 18: The velocity based IBL height due to a change in roughness length from 0.5 m to 0.0001 m at x = 0.

In both cases the internal boundary layer starts to grow quite smoothly after the roughness change. The step like appearance is caused by the limited grid resolution in the vertical direction. Very near the change a small peak is observed in each case. These are assumed to be related to the high curvature of the streamlines in this area. Highly curved streamlines are associated with high pressure gradients which in turn could cause the observed peaks. Figure 19 shows the streamlines in the lowest part of the computational domain.

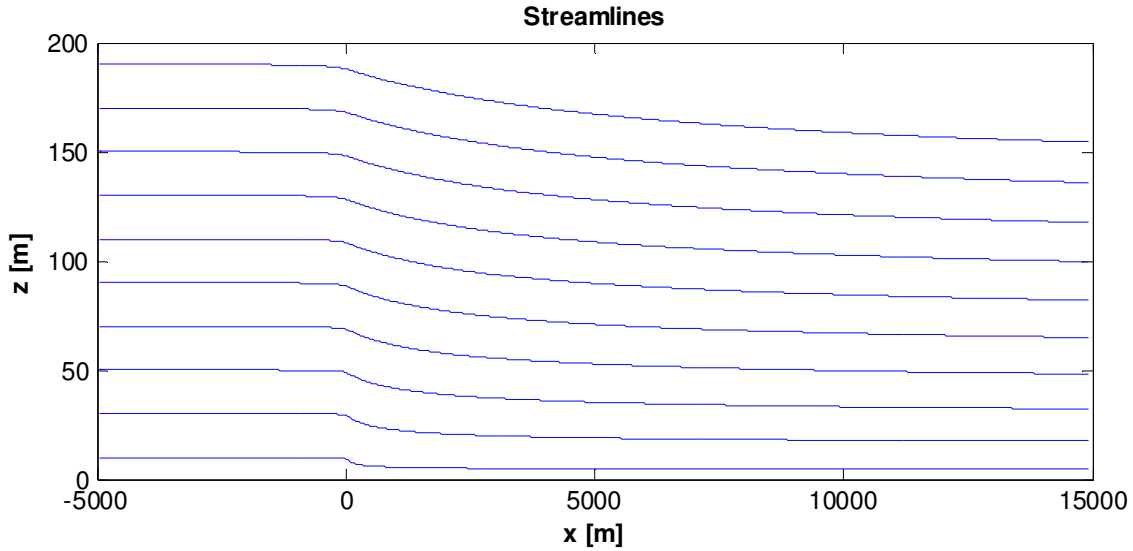

Figure 19: Simulated streamlines over a change in roughness length from 0.5 m to 0.0001 m at x = 0.

As seen in Figure 17 and Figure 18 the TKE based IBL height is in general found to be higher than the velocity based IBL height. The ratio between the two heights varies with both the fetch length *x* and the roughness lengths involved. Choosing different values for the limits defining the two IBL heights can bring them closer together, but it seems impossible to find general values that will apply in all cases.
In the following δ refers to $\delta_{velocity}$ if nothing else stated as this seems to be the traditional definition.

4.3.1 Review of earlier work

Several expressions for predicting the growth of the IBL can be found in the literature. Table 1 in (Savelyev & Taylor, 2005) gives an overview of the expressions suggested so far for the IBL height at short fetch lengths. A whole branch of the expressions seems to be based on an assumption of:

$$\delta \propto x^n \tag{17}$$

Examples of these include the earliest of all the formulae, suggested by (Elliot, 1958):

$$\delta = z_{02} \cdot (C1 + C2 \cdot M) \cdot \left(\frac{x}{z_{02}}\right)^{0.8} \tag{18}$$

x is the fetch length, i.e. the distance downstream of the roughness change.

C1 and *C2* are constants with values of 0.75 and -0.03 respectively and $\mathrm{M} = \ln\frac{z_{02}}{z_{01}}$.

A similar but simpler expression, in which only the downstream roughness length is taken into account, is given by (Arya, 2001):

$$\delta = z_{02} \cdot \alpha \cdot \left(\frac{x}{z_{02}}\right)^{0.8} \tag{19}$$

α is an empirical constant between 0.35 and 0.75.

Another branch of IBL height expressions is supposedly based on the 'diffusion analogy' proposed by Miyake in 1965. As explained in (Savelyev & Taylor, 2005), the idea is that the influence on the flow of a change in the surface conditions will diffuse upwards in the same way as a passive contaminant e.g. a smoke plume would. With a vertical diffusion intensity found as $\sigma_w = (\overline{w'w'})^{1/2}$ the basis of these expressions is given by:

$$u(\delta)\frac{d\delta}{dx} = A_{diff} \cdot \sigma_w \tag{20}$$

With some further assumptions equation (20) can be integrated to get the IBL height.
In a model of Panofsky and Dutton (see e.g. (Garratt, 1990), (Savelyev & Taylor, 2005) or (Kaimal & Finnigan, 1994)) it is assumed that $\sigma_w = Cu_*$ and that $A_{diff} = 1$. The velocity within the IBL is used to determine $u(\delta)$, and this velocity is assumed to have a logarithmic profile in equilibrium with the roughness length downstream of the roughness change:

$$u_2(z) = \frac{u_{*2}}{\kappa}\ln\frac{z}{z_{02}} \tag{21}$$

With this assumption the friction velocity u_{*2} can be defined through the equality of the velocities inside and outside the IBL at the top of the IBL:

$$\begin{gathered} u_1(\delta) = u_2(\delta) \quad => \\ \frac{u_{*1}}{\kappa}\ln\frac{\delta}{z_{01}} = \frac{u_{*2}}{\kappa}\ln\frac{\delta}{z_{02}} \quad => \\ u_{*2} = u_{*1}\frac{\ln\frac{\delta}{z_{01}}}{\ln\frac{\delta}{z_{02}}} \end{gathered} \tag{22}$$

Panofsky and Dutton integrated equation (20) to get:

$$C \cdot \kappa = \frac{\delta}{x}\left(\ln\left(\frac{\delta}{z_{02}}\right) - 1\right) + 1 \tag{23}$$

In the original model $C = 1.25$ is used.

Equation (23) appears to be more theoretically based than (18) and (19), but it suffers from being implicit with respect to δ. This makes it more difficult to solve, and it also only depends on the downstream roughness length.

The models of Elliot and Panofsky/Dutton were compared to atmospheric data in (Walmsley, 1989). In the comparison was also a formula by Jackson based on the same ideas as the Panofsky/Dutton formula. The atmospheric data was taken from different experiments with values of $\frac{z_{02}}{z_{01}}$ ranging between 0.0023 and 125. It consists mainly of measurements at very short fetch lenghts ($x < 10$ m). The longest fetch length in the data set is 160 m. Walmsley concluded that of the three formulae, the one by Panofsky and Dutton gave the best overall agreement with the data set. The formula by Elliott was seen to generally overestimate the IBL height.

The data collected by Walmsley was used again in 2005 by Savelyev and Taylor to find yet another formula based on equation (20). In (Savelyev & Taylor, 2005) they suggested adding an extra term to the equation to include the effect of the vertical velocity component appearing at the roughness change. The appearance of this velocity component is necessary to fulfill the continuity equation. It can be seen in Figure 19 as deflection of the streamlines.
In the added term $A_2 W(\delta)$, the vertical velocity component $W(\delta)$ was determined by approximating the horizontal velocity gradient and integrating the continuity equation over the depth of the IBL. This procedure resulted in equation (24):

$$\frac{d\delta}{dx} = \left(C\kappa A_1 + A_2 \frac{\delta}{x} M\right)\left(\ln \frac{\delta}{z_{01}}\right)^{-1} \qquad (24)$$

By fitting the function to experimental data presented in (Walmsley, 1989) and using $C = 1.25$ Savelyev and Taylor determined:

$$A_1 = 1$$
$$A_2 = 0.5$$

Equation (24) with these constants was compared to an experiment not a part of the (Walmsley, 1989) data set. Only a single data point at a distance of 90 m from a transition between the sea and a sand beach was considered. The roughness length was estimated to change from $3 \cdot 10^{-6}$ m to $3 \cdot 10^{-2}$ m. At this point equation (24) predicts an IBL height of 5.9 m which is 18 % below the measured height. In comparison the Elliot and the Panofsky-Dutton formulae overestimate the height by 19 % and 32 % respectively.
The flow over a similar roughness change simulated in *Ellipsys* gives an IBL height of approximately 4 m. This is 44 % below the measured height.
These numbers are presented just to give an idea of the uncertainties regarding predictions of the IBL height. It would not be fair to judge the different models on a single data point of a single experiment. Furthermore the ratio between the roughness lengths of the experiment must be said to be quite high $\left(\frac{z_{02}}{z_{01}} = 10000\right)$.

Equations (18), (19), (23) and (24) with the original proposed constants are in Figure 20 compared to the results of a simulation with a change in roughness length from 0.0001 m to 0.5 m.
Quite substantial deviations are observed at practically all fetch lengths, which is not satisfying. Note that all models including the numerical are designed for short fetch lengths - e.g. the numerical model does not take the Coriolis force into account, and in this sense it is only valid in the lowest part of the atmospheric

boundary layer, where this force can actually be neglected. At long fetch lengths the IBL will outgrow this part.

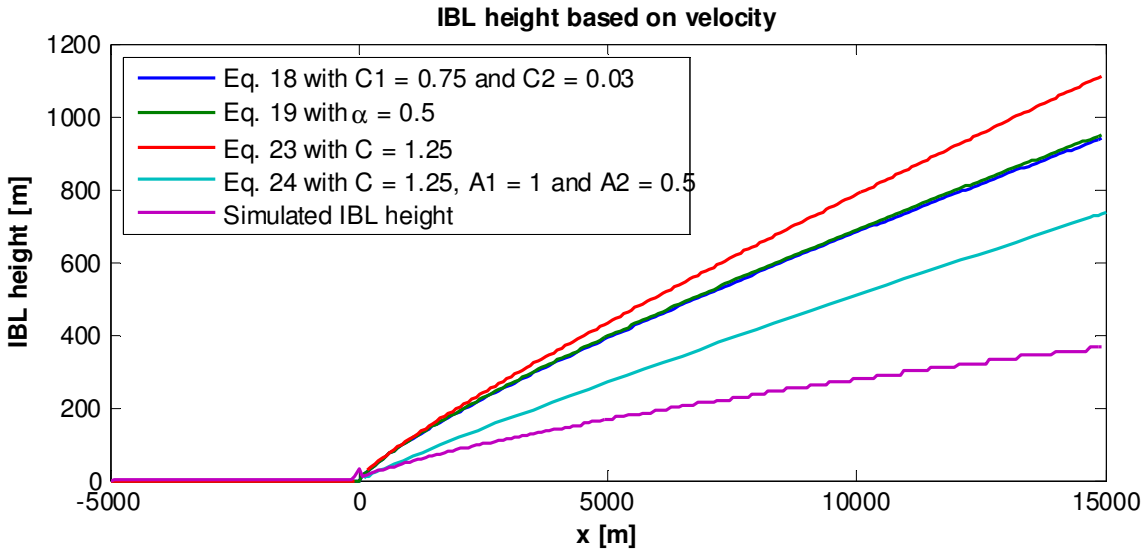

Figure 20: Comparison of the simulated and predicted IBL heights. The used constants are those originally proposed for each expression

It is difficult to say which model is the best. The formula of Savelyev and Taylor (equation (24)) is based on both experimental results and theoretical derivations. This makes it appear more reliable than the three other formulae. Furthermore, it is the one that shows best agreement with the simulation in the particular case. For short fetch lengths ($x < 500$ m) they are actually quite close. The deviation between the results of equation (24) and the simulated height might be related to the high value of $z_{02} = 0.5$ m used in this case. The highest value of z_{02} in the (Walmsley, 1989) data set, on which equation (24) is based, is 0.0122 m.

The definition of the simulated IBL height could obviously also be a source of error. In the presented case the IBL height is defined by an IBL limit of 2%. Choosing a limit closer to zero would most likely give a higher IBL. However, as mentioned earlier, this is not practically possible due to the presence of numerical errors in the simulation. For comparison, increasing the limit from 2% to e.g. 4% reduces the IBL height with approximately 14 % at $x = 15000$ m in the present case.

4.3.2 Search for a new expression

In Figure 21 it is shown that with some adjustment of the constants each of the expressions (equation (18), (19), (23) and (24)) can be fitted quite well to the specific simulation with a change in roughness length from 0.0001 m to 0.5 m.

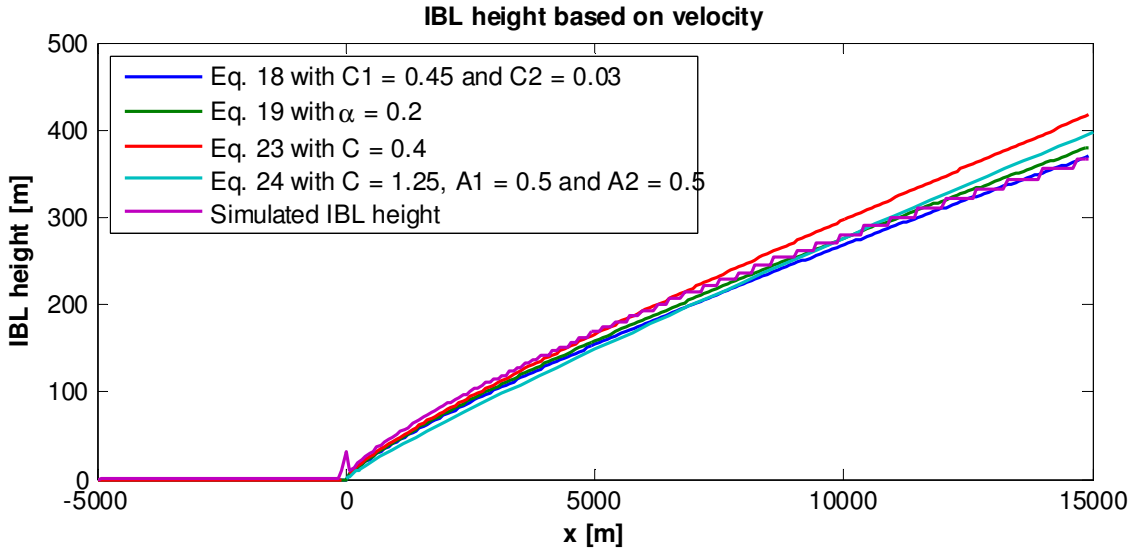

Figure 21: Comparison of the simulated and predicted IBL heights. The used constants are modified to make the predicted heights match the simulated.

An aim of this project is, however, to obtain a more general description of how the flow is affected downstream of a roughness change. In the following an attempt is made to find a general expression for the IBL height that will fit the range of simulations shown in Table 2[6].

To increase the chance of success and to acknowledge the limitations of the numerical model, the main focus is on short fetch lengths, defined here as the first 5000 m after the roughness change. Furthermore It is not expected that the immediate disturbance of the flow, seen as a peak of the IBL height near the roughness change, can be included in the expression to be found. For this reason the first 160 m after the change is disregarded.

Two different approaches are considered. The first is to find an expression on the same form as e.g. the Elliot formula (equation (18)). In general such an expression can be written as:

$$\frac{\delta}{z_1} = f_1\left(\frac{x}{z_2}\right)^{\alpha} \qquad (25)$$

z_1 and z_2 are length scales, for instance upstream and/or downstream roughness lengths.

α is normally assumed to be a constant around 0.8.

f_1 is a function of $\frac{z_{02}}{z_{01}}$.

The challenge of this first approach is to determine appropriate values for these parameters as well as the form of the function f_1. In the following this is done by fitting equation (25) to the simulations of Table 2.

The second approach is to use equation (24) suggested by Savelyev and Taylor and fit the constants A_1 and A_2 to the simulations.

[6]Note that the two most extreme cases of $\frac{z_{02}}{z_{01}} = 5000$ and $\frac{z_{02}}{z_{01}} = 0.0002$ appearing in the table are not included in any of the following derivations.

In each approach TKE and velocity based IBL definitions are considered in both smooth-to-rough and rough-to-smooth simulations.

4.3.2.1 The "Elliot approach"

Below follows a description of how equation (25) is fitted to the simulations of Table 2. The velocity based IBL height in the smooth-to-rough cases is used as an example to demonstrate the procedure.

To simplify the task a bit, only the four different combinations of $z_1 = [z_{01}, z_{02}]$ and $z_2 = [z_{01}, z_{02}]$ are considered.

Plotting $f_1 = \frac{\delta}{z_1}\left(\frac{x}{z_2}\right)^{-\alpha}$ against $\mathrm{M} = \ln\frac{z_{02}}{z_{01}}$ gives four different shapes of the function depending on the combination of z_1 and z_2. In this case a choice is made to use $z_1 = z_2 = z_{01}$. This gives the simplest functional form of the four combinations – an approximately straight line as shown in Figure 22 (made with $\alpha = 0.8$). Note that hereby it is not assumed that the growth of the IBL is controlled by the upstream roughness length alone. The downstream roughness length is still included in $\mathrm{M} = \ln\frac{z_{02}}{z_{01}}$.

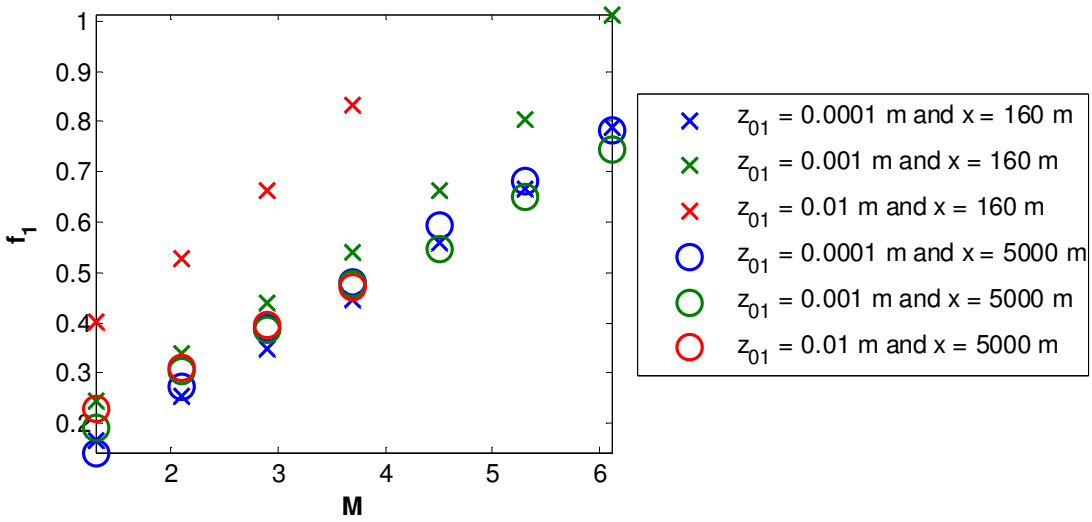

Figure 22: Simulated values of f_1 with $z_1 = z_2 = z_{01}$ are plotted against M. A linear dependency is observed. α is set to 0.8.

As seen in Figure 22 the value of f_1 depends not only on *M* but also on the value of the upstream roughness length and the distance from the roughness change.

An attempt to minimize the dependency on the upstream roughness length is made by adjusting the value of α. At each value of *x,* the value of α giving the smallest mean difference between $f_{1,z_{01}=0.0001}$ and $f_{1,z_{01}=0.01}$ is found. These values are plotted in Figure 23 along with a fitted function given by:

$$\alpha_{fit} = 0.58(x - 136.9)^{0.034} \qquad (26)$$

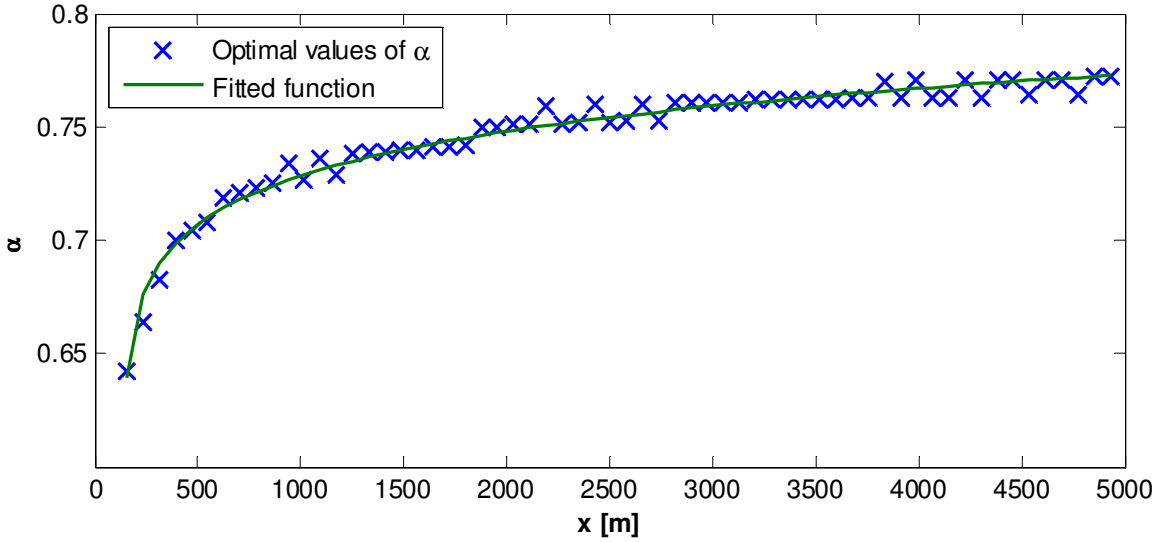

Figure 23: A function is fitted to the values of α making f_1 depend as little as possible on the upstream roughness length.

Using the fitted function for α, equation (25) can now be rewritten into:

$$\frac{\delta}{z_{01}} = (aM + b)\left(\frac{x}{z_{01}}\right)^{0.58(x-136.9)^{0.034}} \qquad (27)$$

All that remains now is to find *a* and *b*. That is, to find the slope of lines corresponding to those shown in Figure 22 and their intersection with the vertical axis. At each value of *x,* the single best fitting straight line through the points of $\left(M, f_{1,z_{01}=0.0001}\right)$, $\left(M, f_{1,z_{01}=0.001}\right)$ and $\left(M, f_{1,z_{01}=0.01}\right)$ is determined through linear regression. Both *a* and *b* is found to vary with *x* as shown in Figure 24 and Figure 25.

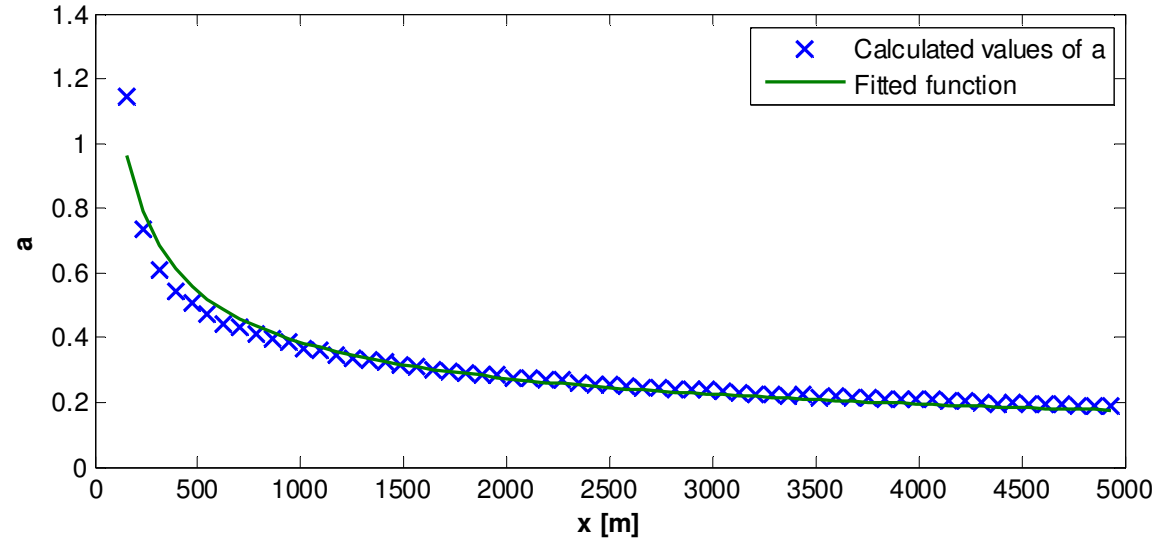

Figure 24: Plotting f_1 versus M at a given position gives more or less a straight line when $z_1 = z_2 = z_{01}$. The slope of this line varies with x as shown here.

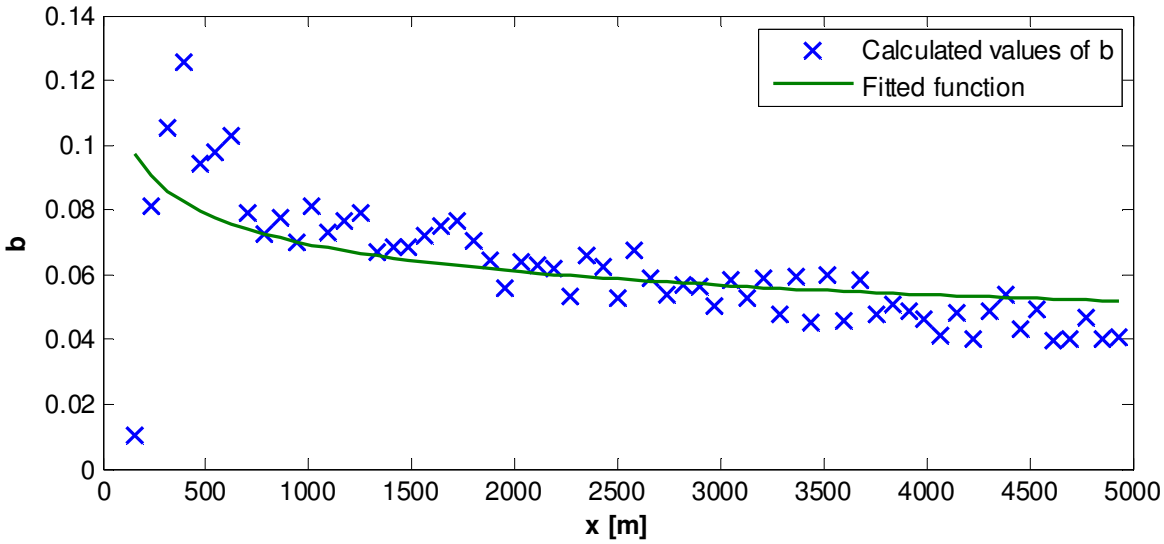

Figure 25: Plotting f_1 versus M at a given position gives more or less a straight line when $z_1 = z_2 = z_{01}$. The intersection of this line with the vertical axis varies with x as shown here.

The fitted functions for *a* and *b* are given by:

$$a_{fit} = 11.62x^{-0.49} \tag{28}$$

$$b_{fit} = 0.25x^{-0.18} \tag{29}$$

Using equations (27), (28) and (29) it is now possible to predict the velocity based IBL height in the case of smooth-to-rough changes in the roughness length. As examples, the predicted and simulated IBL heights are compared in Figure 26 in the cases with $z_{01} = 0.0001$ m. Full lines represent simulated heights and dashed lines predicted heights.

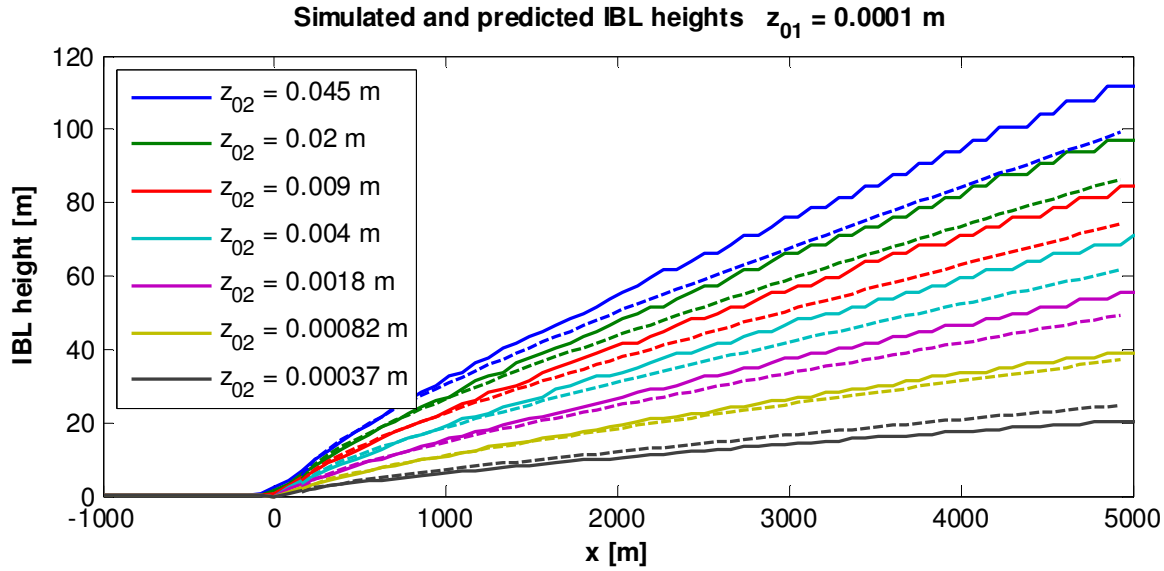

Figure 26: Full lines represent simulated IBL heights and dashed lines represent IBL heights predicted with equations (27), (28) and (29) combined.

The relative differences between predicted and simulated IBL heights in all the smooth-to-rough cases are shown in Figure 27 to Figure 29:

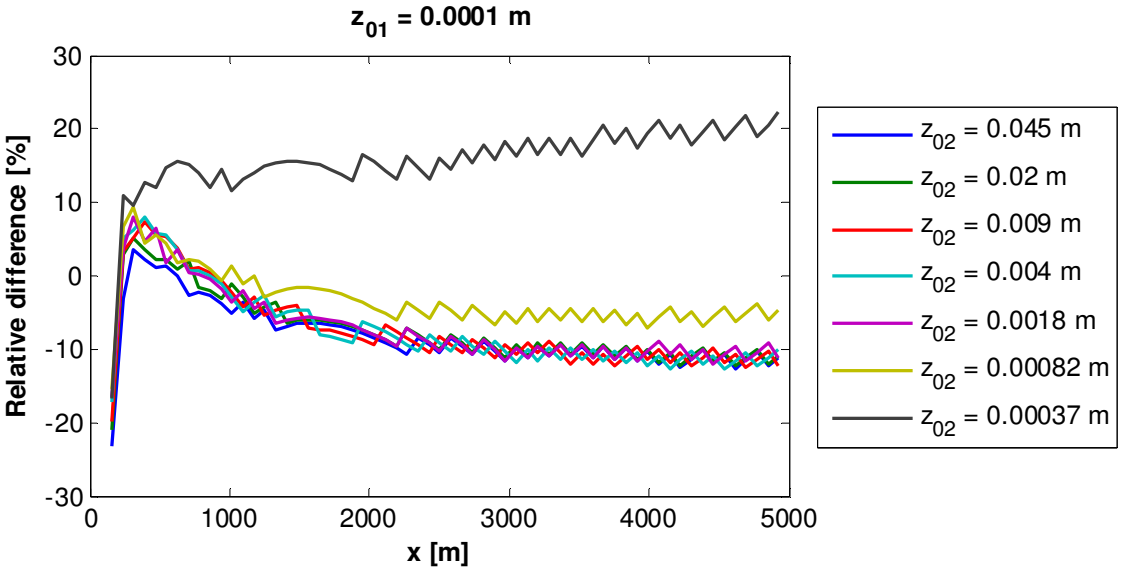

Figure 27: Relative differences between simulated and predicted IBL heights found with the "Elliot approach".

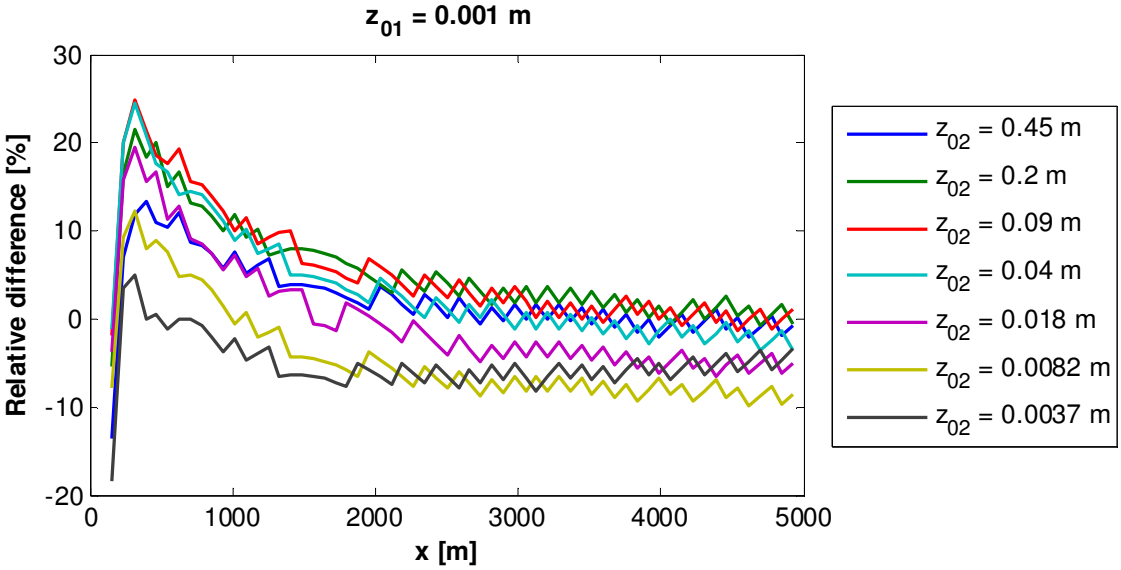

Figure 28: Relative differences between simulated and predicted IBL heights found with the "Elliot approach".

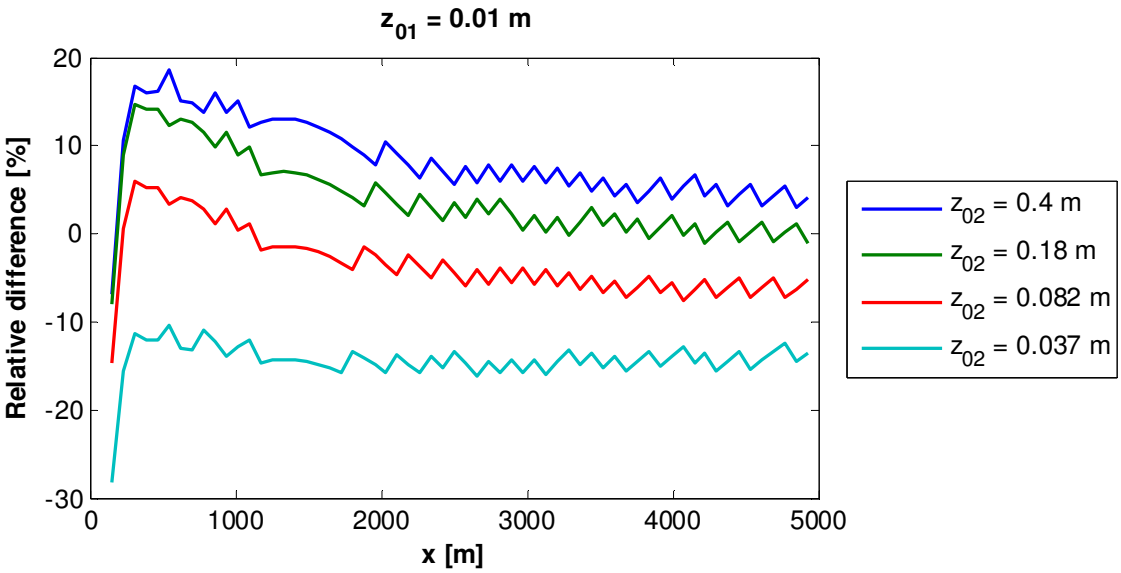

Figure 29: Relative differences between simulated and predicted IBL heights found with the "Elliot approach".

The general tendency of the relative differences is to vary quite a lot with *x* up to fetch lengths of about 1000 or 2000 m. At longer fetch lengths they seem to stabilize at certain levels. In most cases around 10 % or less.

The procedure described above is repeated to find expressions for the TKE based IBL height in the smooth-to-rough cases as well as the TKE and velocity based IBL heights in the rough-to-smooth cases.

The limit defining the TKE based IBL heights is increased to 4%. Lower values are in some cases seen to result in a substantial growth of the IBL immediately after the inlet. This is assumed to be a non-realistic behavior caused by numerical inaccuracies.

The upstream roughness length is in all cases used for both z_1 and z_2, although the linear relationship between f_1 and M shown in Figure 22 is not as pronounced in the rough-to-smooth cases as in the smooth-to-rough cases.

The resulting IBL height expressions are summarized in Table 3.

Smooth-to-rough	Velocity based IBL height (2%)	$\frac{\delta}{z_{01}} = (aM + b)\left(\frac{x}{z_{01}}\right)^{0.58(x-136.9)^{0.034}}$	$a = 11.62x^{-0.49}$	$b = 0.25x^{-0.18}$
	TKE based IBL height (4%)	$\frac{\delta}{z_{01}} = (aM + b)\left(\frac{x}{z_{01}}\right)^{0.61(x-71.9)^{0.039}}$	$a = 5.21x^{-0.51}$	$b = 3.53x^{-0.36}$
Rough-to-smooth	Velocity based IBL height (2%)	$\frac{\delta}{z_{01}} = (aM + b)\left(\frac{x}{z_{01}}\right)^{0.49(x-117.58)^{0.052}}$	$a = -0.91x^{-0.41}$	$b = 6.52x^{-0.39}$
	TKE based IBL height (4%)	$\frac{\delta}{z_{01}} = (aM + b)\left(\frac{x}{z_{01}}\right)^{0.61(x+39.13)^{0.036}}$	$a = -0.051x^{-0.11}$	$b = 1.27x^{-0.21}$

Table 3: IBL height expressions found with the "Elliot approach".

All four expressions are compared to the corresponding simulations. The observed deviations are in general on the same level as those shown in Figure 27 to Figure 29 or smaller.

To sum up, it should in most cases be possible with the found expressions to determine the IBL height with an accuracy of about 10 % at fetch lengths between 2000 and 5000 m. Considering the amount of curve fitting gone into the derivations, this is seen as reasonable good accuracy. The expressions should however also be validated against measured IBL heights. Unfortunately, it has not been possible to find such data with a fetch length in the desired range.
Note also that the expressions must be assumed to underestimate the actual IBL heights a little due to the fact that simulated IBL heights is defined by limits of either 2% or 4% and not 0%.

4.3.2.2 The "Savelyev/Taylor approach"

The "Elliot approach" described above for finding expressions for the IBL height gave quite good results, but the derivation proved to be quite cumbersome and involved a lot of curve fitting.
The more simple "Savelyev/taylor" approach is outlined below.

The idea is to use equation (24) proposed in (Savelyev & Taylor, 2005) and determine the values of A_1 and A_2 from the range of simulations given in Table 2. Equation (24) is repeated here for convenience:

$$\frac{d\delta}{dx} = \left(C\kappa A_1 + A_2\frac{\delta}{x}M\right)\left(\ln\frac{\delta}{z_{01}}\right)^{-1} \qquad (30)$$

The value of C is kept at 1.25, and again the velocity based IBL height in the smooth-to-rough cases is used as an example to demonstrate the procedure.

For each combination of z_{01} and z_{02}, equation (30) is solved in Matlab using the ODE-solver `ODE45`. Best fitting values of A_1 and A_2 are found using the Matlab curve fitting tool `lsqcurvefit`. To get useful results it is found necessary to narrow the range of studied fetch lengths to $500 \leq x \leq 5000$.

In Figure 30 the value of $A = A_1 + \frac{A_2}{C\kappa}\left(\frac{\delta}{x}\right)M$ is plotted against $\left(\frac{\delta}{x}\right)M$. The ratio between IBL height and fetch length is taken as the mean value over $500 \leq x \leq 5000$. As in (Savelyev & Taylor, ., 2005) a linear function is fitted through the points.

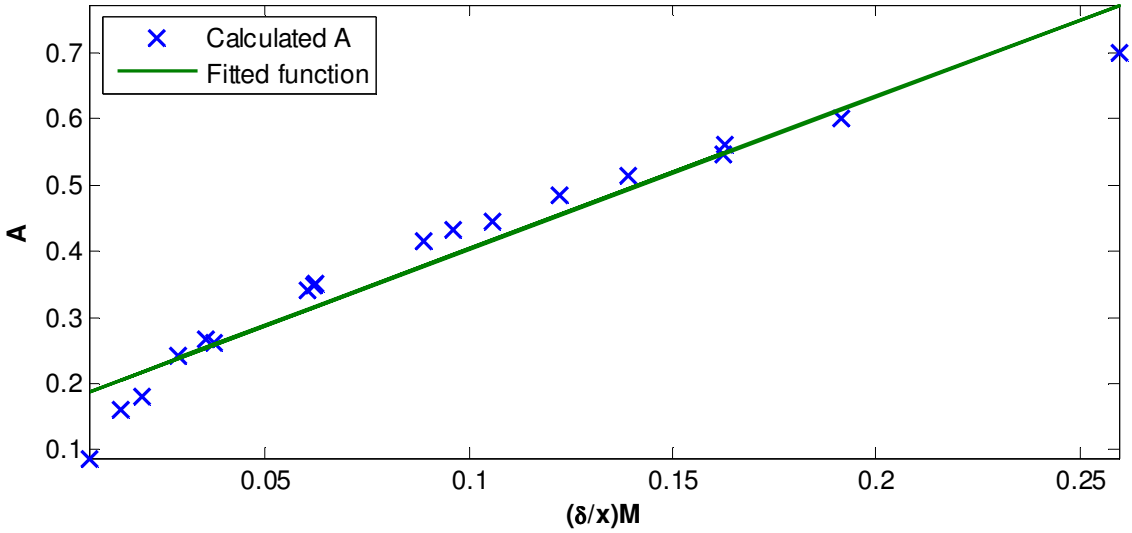

Figure 30: A function is fitted to values of A found through simulations.

A_1 is now approximated as the value of the fitted function where it intersects the vertical axis $\left(\left(\frac{\delta}{x}\right)M = 0\right)$ and $\frac{A_2}{C\kappa}$ as the slope of the fitted function. It is found that:

$$A_1 = 0.17$$

$$A_2 = 1.16$$

With these values equation (30) can be solved to get a prediction of the IBL height.

Figure 31 shows predicted and simulated IBL heights of the cases with $z_{01} = 0.0001$ m. Full lines represent simulated heights and dashed lines predicted heights.

To solve equation (30) it is necessary to specify an initial height of the IBL. The results presented below are found using an initial height equal to the simulated IBL height at $x = 500$ m. In general this value is unknown and one has to come up with a guess. This is obviously a major drawback of this approach. Specifying a height close to zero at a low value of *x* does unfortunately not give very good results. It seems that the IBL growth in the area of $0 \leq x \leq 500$ is poorly described by the suggested expression.

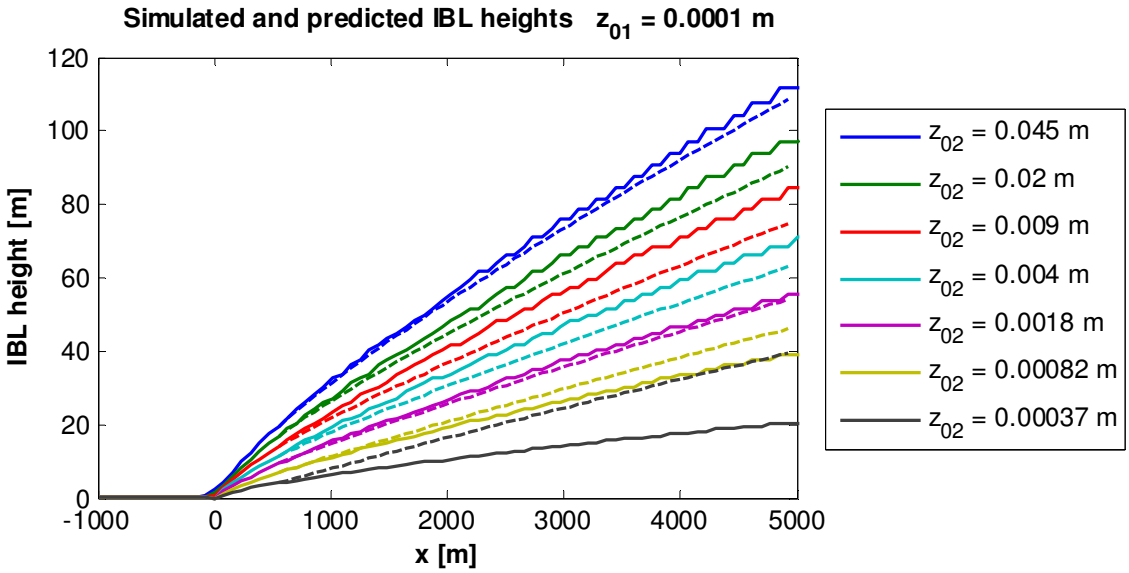

Figure 31: Full lines represent simulated IBL heights and dashed lines represent IBL heights predicted with equation (30).

The relative differences between the simulated and the predicted IBL heights are shown in Figure 32 to Figure 34 for the three different values of z_{01}.

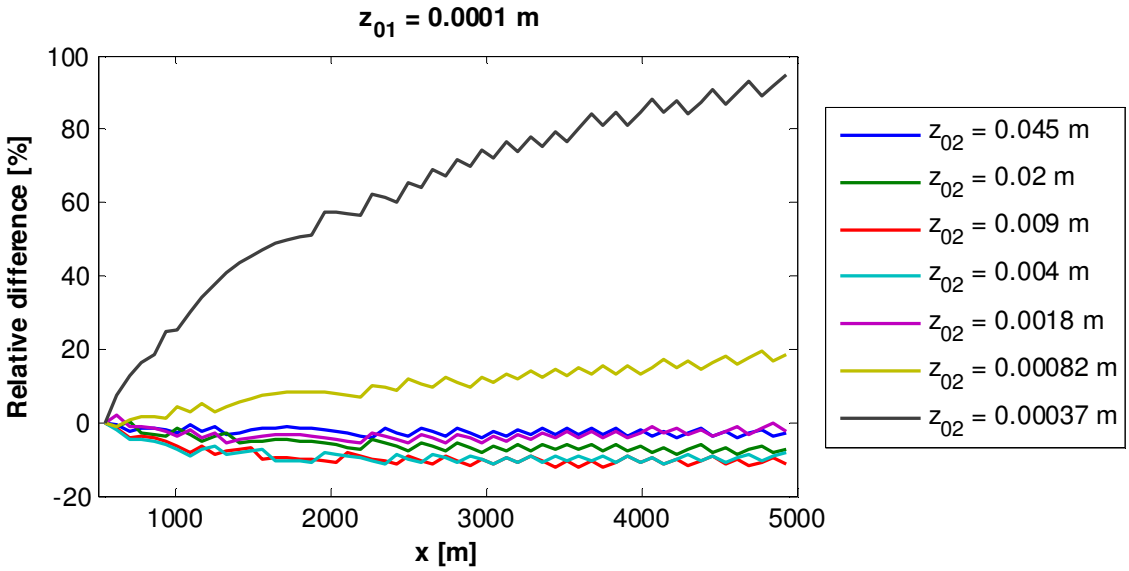

Figure 32: Relative differences between simulated and predicted IBL heights found with the "Savelyev/Taylor approach".

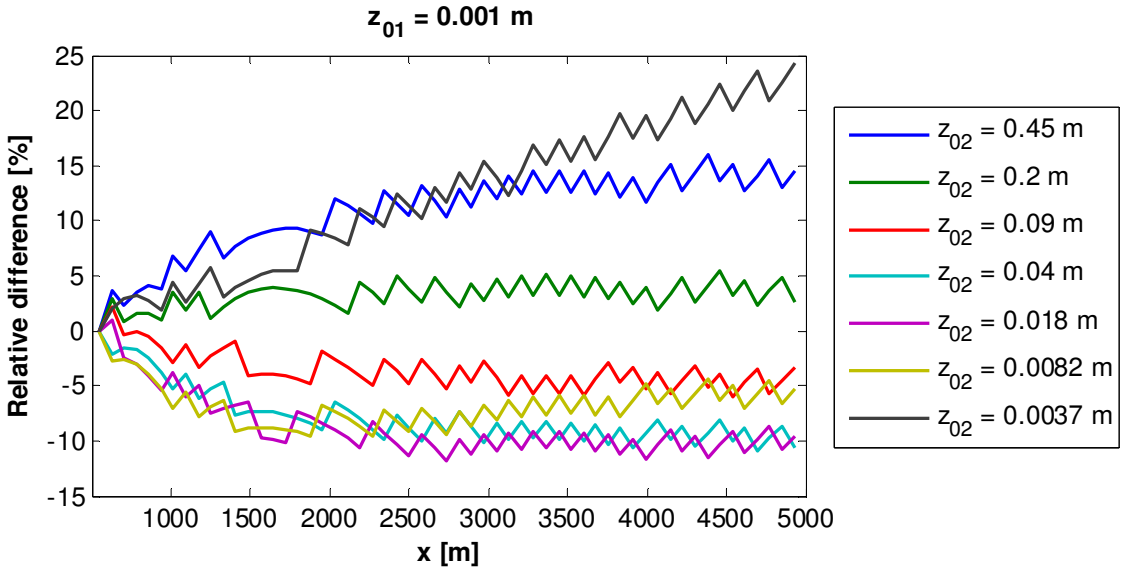

Figure 33: Relative differences between simulated and predicted IBL heights found with the "Savelyev/Taylor approach".

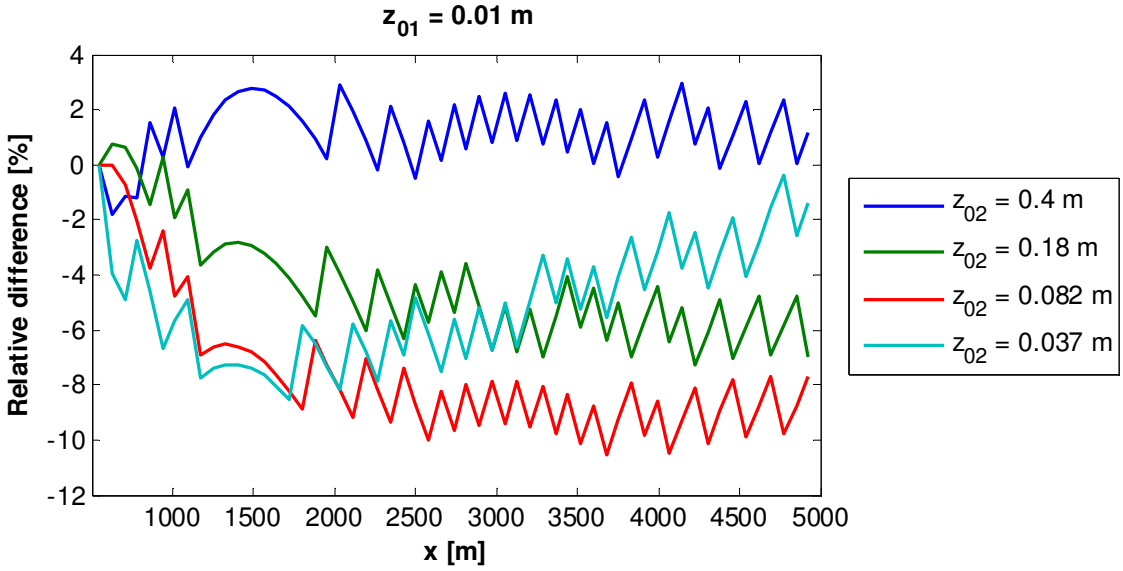

Figure 34: Relative differences between simulated and predicted IBL heights found with the "Savelyev/Taylor approach".

The largest relative difference by far is seen in the case of $z_{01} = 0.0001$ m and $z_{02} = 0.00037$ m where it goes up to almost 100 %. Disregarding this case the differences generally stay within 25 % and in most cases below 10 %. Note however, that these results are obtained using simulated values as initial conditions in the expression for the predicted values.

The derivation described above is repeated for the TKE based IBL height in the smooth-to-rough cases as well as the TKE and velocity based IBL heights in the rough-to-smooth cases.
In all cases, the relative differences between simulated and predicted IBL heights are of the same magnitude as in the cases shown in Figure 32 to Figure 34.
The set of expressions found with "Savelyev/Taylor approach" are given in Table 4.

Smooth-to-rough	Velocity based	$\frac{d\delta}{dx} = \left(0.17C\kappa + 1.16\frac{\delta}{x}M\right)\left(\ln\frac{\delta}{z_{01}}\right)^{-1}$
	TKE based	$\frac{d\delta}{dx} = \left(0.45C\kappa + 1.09\frac{\delta}{x}M\right)\left(\ln\frac{\delta}{z_{01}}\right)^{-1}$
Rough-to-smooth	Velocity based	$\frac{d\delta}{dx} = \left(0.19C\kappa - 0.37\frac{\delta}{x}M\right)\left(\ln\frac{\delta}{z_{01}}\right)^{-1}$
	TKE based	$\frac{d\delta}{dx} = \left(0.4C\kappa - 0.39\frac{\delta}{x}M\right)\left(\ln\frac{\delta}{z_{01}}\right)^{-1}$

Table 4: IBL height expressions found with the "Savelyev/Taylor approach".

Comparing the two approaches described above, the expressions found with the "Elliot approach" seem to be the most useful and the most reliable. They can be used in a wider range of fetch lengths, they agree better with the simulations and does not require an initial guess for the IBL height.

With this said none of the expressions are completely satisfying. To get better agreement with the simulations and thereby supposedly also with atmospheric measurements one could narrow down the range of roughness lengths included in the study or perhaps the range of fetch lengths. This would most likely make the expressions more accurate but of course also less versatile.

Furthermore, the suggested expressions are quite complicated. One simple "rule-of-thumb" expression dependent on fetch length only for rough estimates would be very convenient to have. However, due to the high degree of dependency on both upstream and downstream roughness length, it does not really seem possible to find a such.

4.4 Downstream profiles

So far, the vertical profiles of velocity and TKE downstream of a roughness change have been compared to the corresponding inlet profiles to find the height of the developing IBL. Below follows a more detailed look at the downstream profiles themselves.

The goal is to find expressions for velocity, TKE and dissipation after a roughness change, which can be used to define inlet conditions for other terrain simulations.

Going back to Figure 13, Figure 14, Figure 15 and Figure 16 downstream profiles are compared to inlet profiles. As seen in the previous section regarding the IBL height, the downstream profiles of velocity and TKE follow the inlet profile from the top of the domain down to some height above the ground. Below this height the flow either slows down and becomes more turbulent or speeds up and becomes less turbulent.

At some point after the roughness change, the flow is assumed to become in equilibrium with the new roughness length. That is, a new layer in which the velocity and TKE profiles again become logarithmic and constant is assumed to grow within the IBL. This behavior is, however, not very clearly seen in any of the performed roughness change simulations – at least not with respect to TKE. The general tendency of the simulations is an increase or decrease of TKE from δ_{TKE} and all the way to the wall as seen in Figure 13 and Figure 15.

4.4.1 Velocity profiles

Regarding the velocity on the other hand, adjustment to the new surface is quite clearly seen from logarithmic scaled plots of the downstream velocity. Figure 35 and Figure 36 show logarithmic plots of the

same velocities as in Figure 14 and Figure 16. That is, the velocities after changes in roughness lengths from 0.0001 m to 0.5 m and from 0.5 to 0.0001 m.

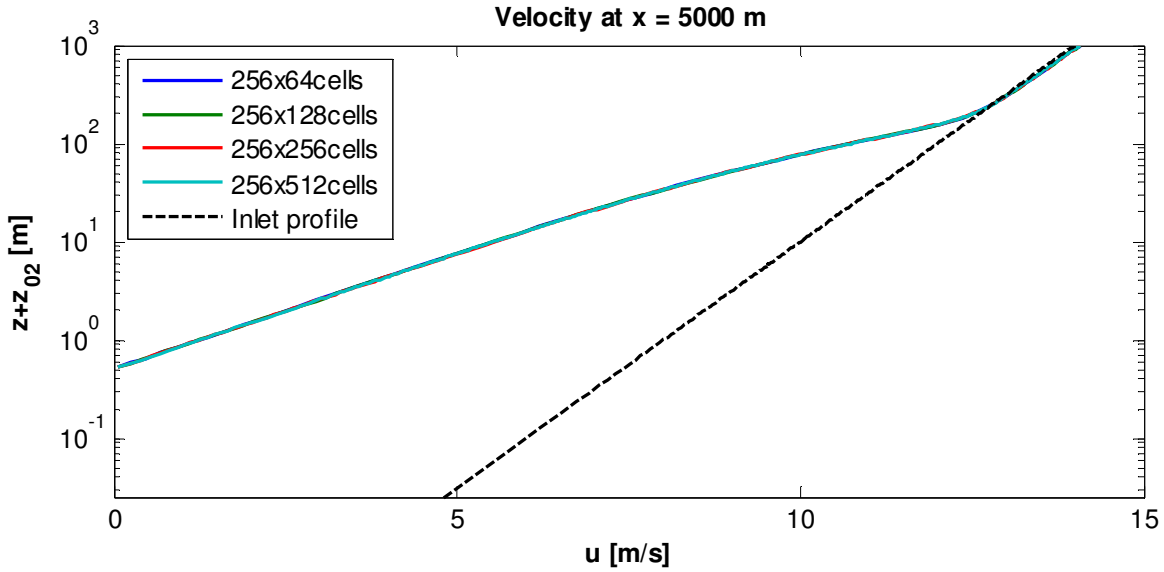

Figure 35: Velocity profiles at x = 5000 m after a change in roughness length from 0.0001 m to 0.5 m at x =0.

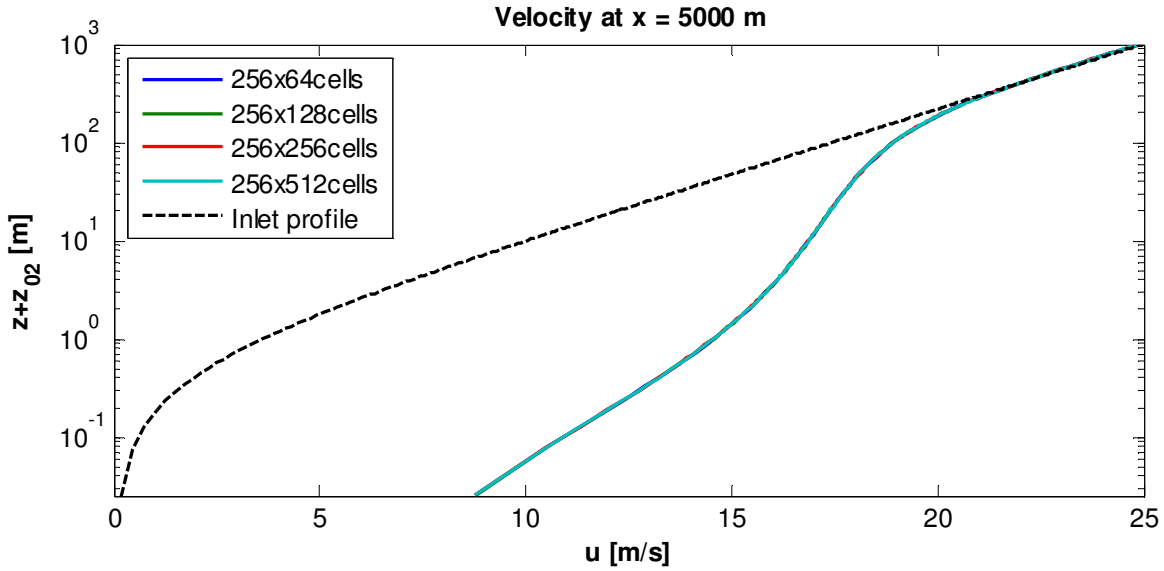

Figure 36: Velocity profiles at x = 5000 m after a change in roughness length from 0.5 m to 0.0001 m at x =0.

In both cases the lowest part of the velocity profile seems very close to being a straight line, meaning the velocity depends more or less logarithmically on the height close to the ground. In the smooth-to-rough case this continues up to around 30 m while in the rough-to-smooth case only up to around 1 m. Above these heights there is a curved non-logarithmic transition zone until the profiles again become logarithmic above the IBL. Note that the inlet velocity profile shown in Figure 36 is in fact logarithmic although it does not resemble a straight line. The curved shape of the profile close to the ground is caused by the definition of the vertical axis of the plot. Had $z + z_{01}$ been used instead of $z + z_{02}$, the inlet profile would have been a straight line.

One classical way to describe the velocity profile downstream of a roughness change is to divide it into three logarithmic sections as shown in Figure 37. The first covering the range of $0 \leq z \leq c_1 \cdot \delta$, the second covering $c_1 \cdot \delta \leq z \leq c_2 \cdot \delta$ and the third $z \geq c_2 \cdot \delta$.
The lower section is defined by z_{02} and a friction velocity found as described previously in equation (22):

$$\begin{gathered} u_1(\delta) = u_2(\delta) \quad => \\ \frac{u_{*1}}{\kappa} \ln \frac{\delta}{z_{01}} = \frac{u_{*2}}{\kappa} \ln \frac{\delta}{z_{02}} \quad => \\ u_{*2} = u_{*1} \frac{\ln \frac{\delta}{z_{01}}}{\ln \frac{\delta}{z_{02}}} \end{gathered} \tag{31}$$

The upper section is defined by z_{01} and u_{*1} as the upstream profile, while the middle section is defined to match the lower and upper sections at $z = c_1 \cdot \delta$ and at $z = c_2 \cdot \delta$ respectively. The values of c_1 and c_2 lie somewhere between 0 and 1 and $c_2 > c_1$.

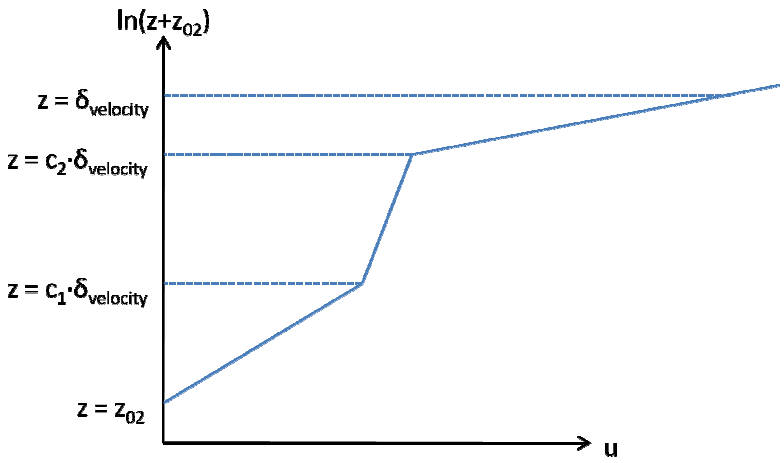

Figure 37: Schematic drawing of a velocity profile downstream of a roughness change divided in three logarithmic sections.

Examples of profiles defined this way with $c_1 = 0$ and $c_2 = 1$ are shown in Figure 39 and Figure 40. They are denoted by 'method 1'. In the same figures are also downstream profiles found by a 'method 2' described below.

The basic idea of 'method 2' is the same as in 'method 1'. Only the slope of the of the lowest section is defined differently and a value of $c_1 = 0.1$ is used for smooth-to-rough cases and a value of $c_1 = 0.01$ for rough-to-smooth cases. The value of c_2 is kept at 1.
In each of the simulations shown in Table 2, a function with the form of equation (32) is fitted to the lowest section of the velocity profile at each value of x between 500 m and 5000 m.

$$u_2(z) = C_1 \ln(z + z_{02}) + C_2 \tag{32}$$

It turns out that C_1 depends more or less linearly on $\mathrm{M} = \ln \frac{z_{02}}{z_{01}}$ as shown in Figure 38 for the rough-to-smooth cases. That is,

$$C_1 = C_3 M + C_4 \tag{33}$$

For each value of z_{01} C_3 and C_4 are determined through linear regression. C_1 is taken as the average value over $500 \leq x \leq 5000$.
In the smooth-to-rough cases C_3 and C_4 are found to depend linearly on $\ln z_{01}$ and in the rough-to-smooth cases exponentially. Note however that these relations are based only on the three values of z_{01} in each category.

In the smooth-to-rough cases it is found that:

$$C_{1,fit} = (0.02 \ln z_{01} + 0.3) \ln \frac{z_{02}}{z_{01}} + (0.1 \ln z_{01} + 1.9) \tag{34}$$

And in the rough-to-smooth cases it is found that:

$$C_{1,fit} = (0.2 \exp(0.5 \ln z_{01}) + 0.1) \ln \frac{z_{02}}{z_{01}} + (2.7 \exp(0.4 \ln z_{01}) + 0.9) \tag{35}$$

Equation (35) is the fitted function shown in Figure 38.

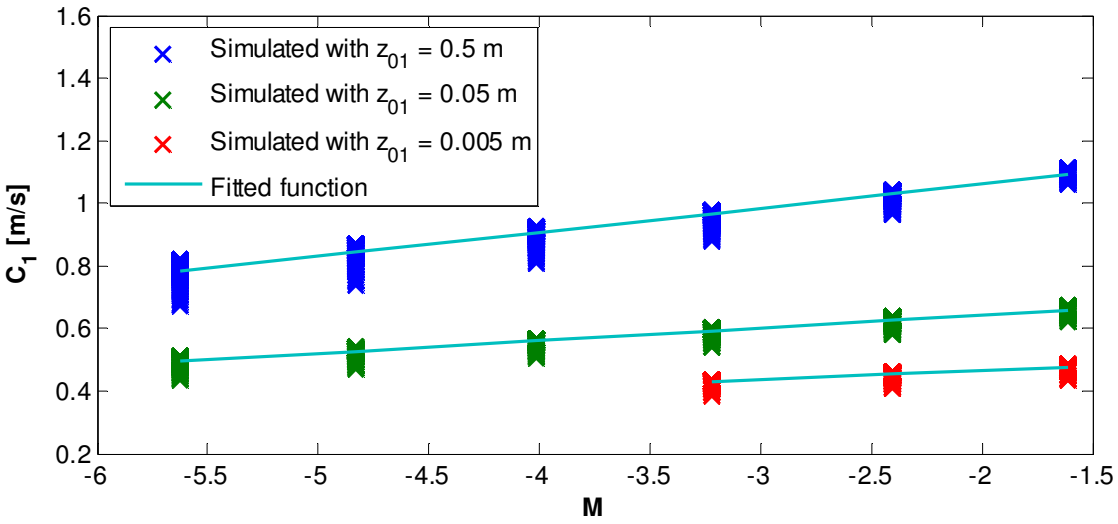

Figure 38: C_1 is plotted against M = $\ln(z_{02}/z_{01})$ for each value of x and a function is fitted through the points

By substituting the fitted functions of C_1 into equation (32) and assuming $C_2 = -C_1 \ln z_{02}$ an expression for the velocity profile up to $z = c_1 \cdot \delta$ is found (equation (36)). Above this height the velocity is determined in the same way as in 'method 1'.

$$u_2(z) = C_{1,fit} \ln\left(\frac{z + z_{02}}{z_{02}}\right) \tag{36}$$

The two methods of approximating the velocity profiles are compared to the simulated profiles at 500 m and 5000 m after a given roughness change. In each case the relative difference between the approximated and the simulated velocity is found at heights of 1, 25, 50 and 100% of the velocity based IBL height, and the average values of these differences are given in Table 5.

		Smooth-to-rough			
		x = 500 m		x = 5000 m	
z_{01} [m]	z_{02} [m]	Error [%] Method 1	Error [%] Method 2	Error [%] Method 1	Error [%] Method 2
0.0001	0.045	-8.5	0.3	-6.3	-1.9
	0.02	-7.9	-1.0	-5.8	-2.6
	0.009	-6.9	-1.7	-5.0	-2.8
	0.004	-6.2	-2.1	-4.3	-2.7
	0.002	-5.1	-1.9	-3.6	-2.3
	0.001	-4.1	-1.4	-3.1	-1.7
	0.0004	-3.3	-0.7	-2.8	-0.8
0.001	0.45	-9.5	0.4	-7.4	-3.1
	0.2	-8.8	-1.4	-6.4	-4.1
	0.09	-7.4	-2.5	-5.7	-5.0
	0.04	-6.9	-4.0	-5.2	-5.7
	0.02	-6.7	-5.1	-4.6	-5.7
	0.01	-5.5	-4.9	-4.1	-5.3
	0.004	-4.6	-4.4	-3.3	-4.2
0.01	0.4	-6.5	1.3	-5.9	-1.6
	0.2	-5.9	-0.1	-5.0	-2.0
	0.08	-5.5	-1.2	-4.4	-2.1
	0.04	-5.0	-1.7	-4.0	-1.9

		Rough-to-smooth			
		x = 500 m		x = 5000 m	
z_{01} [m]	z_{02} [m]	Error [%] Method 1	Error [%] Method 2	Error [%] Method 1	Error [%] Method 2
0.5	0.002	1.6	-6.6	3.7	-0.1
	0.004	2.0	-5.8	3.8	-0.2
	0.009	2.2	-5.1	3.6	-0.2
	0.02	2.3	-4.0	3.4	0.1
	0.045	2.5	-2.4	3.3	0.7
	0.1	3.0	-0.7	3.0	1.4
0.05	0.0002	3.4	-3.3	3.7	0.4
	0.0004	3.5	-3.0	3.7	0.3
	0.0009	3.4	-2.7	3.7	0.3
	0.002	3.3	-2.1	3.3	0.3
	0.0045	2.8	-1.5	3.0	0.5
	0.01	2.0	-1.2	2.4	0.7
0.005	0.0002	3.2	-0.9	3.2	0.8
	0.00045	2.9	-0.6	2.9	0.8
	0.001	2.4	-0.4	2.5	0.8

Table 5: Mean errors between approximated and simulated velocity profiles within the IBL.

In general 'method' 2 gives smaller errors than 'method 1' in both the smooth-to-rough cases and rough-to-smooth cases. There is however a few exceptions. For instance at x = 500 m after the change from 0.5 m to 0.002 m. In this case 'method 2' results in a mean error of -6.6% which is the worst of the 'method 2' errors. In Figure 39 this case is given as an example of how the approximated velocity profiles look like compared to the simulated.

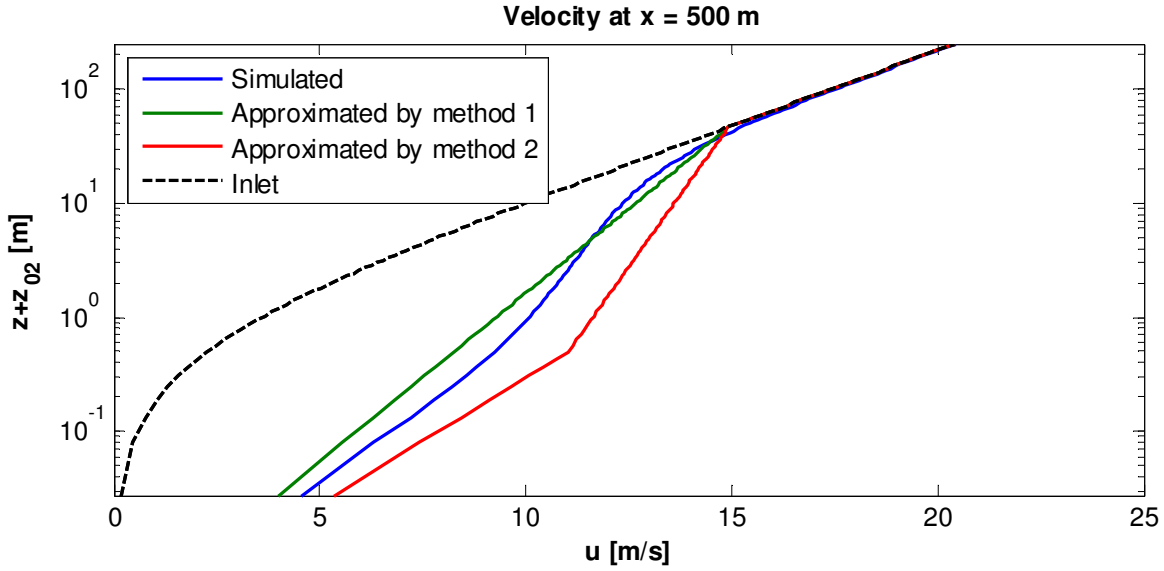

Figure 39: Simulated and approximated velocity profiles 500 m downstream of a change in roughness length from 0.5 m to 0.002 m. The black line represents the upstream velocity profile.

'Method 1' is seen to be much better than 'method 2' in this case. Moving downstream to x = 5000 m however 'method 2' gives the best approximation as shown in Figure 40.

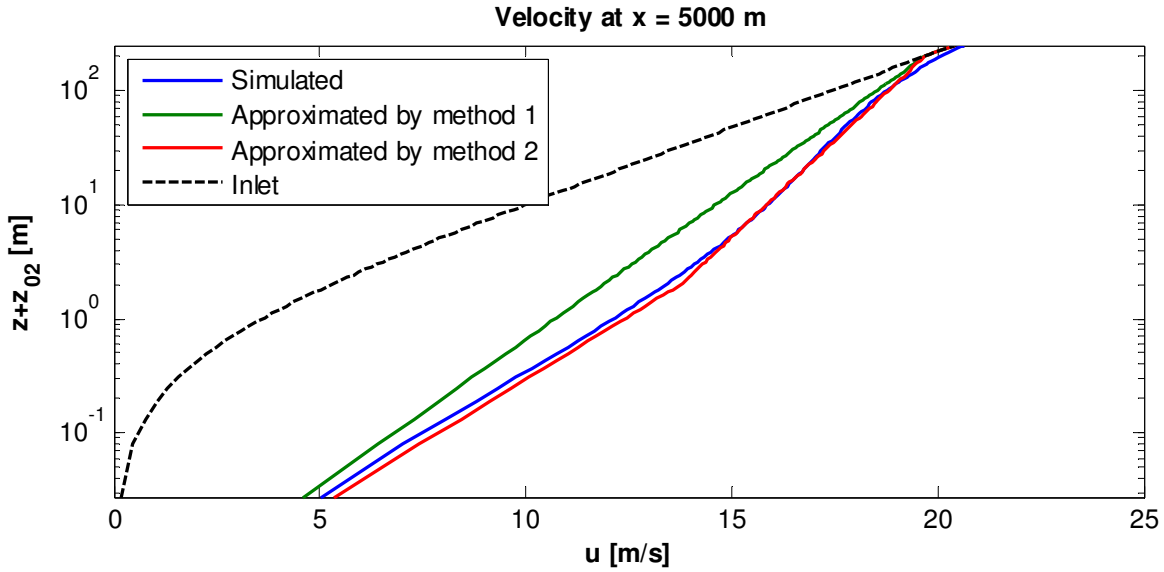

Figure 40: Simulated and approximated velocity profiles 5000 m downstream of a change in roughness length from 0.5 m to 0.002 m. The black line represents the upstream velocity profile.

It seems the only situation where 'method 1' performs significantly better then 'method 2' is at a short distance after a change from a very high roughness length to a very low roughness length.
Both methods, but in particular 'method 1', could most likely be improved by choosing other values of c_1 and c_2.

4.4.2 TKE profiles

Regarding the downstream profiles of TKE, one could simply let them follow the logarithmic velocity profiles found by either 'method 1' or 'method 2'. That is, to assume $k_2 = \frac{u_{*2}^2}{\sqrt{c_\mu}}$ and determine u_{*2} from the slope of the logarithmic velocity profiles through the standard logarithmic description:

$$u_2 = \frac{u_{*2}}{\kappa} \ln \frac{z + z_{02}}{z_{02}} \tag{37}$$

This would, however, result in constant or piecewise constant TKE profiles which fit poorly with the profiles seen for instance in Figure 13 and Figure 15. Instead a second order polynomial is assumed to fit the TKE profiles from the ground and up to δ_{TKE}.

$$k_2(z) = az^2 + bz + c \tag{38}$$

Above the IBL it is assumed that $k_2 = k_1$.
The constants of the polynomial are determined by:

$$k_2(\delta_{TKE}) = k_1(\delta_{TKE}) \tag{39}$$

$$k_2(0) = \frac{u_{*2}^2}{\sqrt{c_\mu}} \tag{40}$$

u_{*2} in equation (40) is found either through equation (31) or by multiplying the values of C_1 from equation (34) and (35) with the von Karman constant. The two methods are referred to as 'method 1' and 'method 2' respectively.

Finally to make k_2 blend smoothly with k_1 the following must be satisfied:

$$\left.\frac{dk_2}{dz}\right|_{z=\delta_{TKE}} = 0 \qquad (41)$$

The errors between the approximated TKE profiles and the simulated profiles at x = 500 and x = 5000 are given in Table 6. The shown errors are average values of the errors found at heights of 1, 25, 50, 75 and 100% of the TKE based IBL height.

		Smooth-to-rough			
		x = 500 m		x = 5000 m	
z_{01} [m]	z_{02} [m]	Error [%] Method 1	Error [%] Method 2	Error [%] Method 1	Error [%] Method 2
0.0001	0.045	-10.4	13.3	-6.5	4.9
	0.02	-7.1	10.2	-5.1	2.7
	0.009	-4.9	7.7	-3.1	2.0
	0.004	-3.4	5.8	-2.6	0.9
	0.002	-2.4	4.7	-1.4	1.5
	0.001	-1.2	4.6	-0.8	2.3
	0.0004	0.2	5.4	-0.2	3.6
0.001	0.45	-22.5	10.9	-12.6	0.5
	0.2	-17.2	5.6	-9.1	-2.7
	0.09	-11.2	2.7	-6.2	-4.3
	0.04	-7.5	0.3	-3.7	-4.7
	0.02	-4.5	-0.7	-1.8	-4.3
	0.01	-2.2	-0.9	-0.7	-3.4
	0.004	-0.2	0.2	0.4	-1.4
0.01	0.4	-21.9	3.2	-8.5	2.9
	0.2	-14.7	1.7	-5.5	1.9
	0.08	-9.0	1.8	-2.4	2.7
	0.04	-4.1	3.1	-0.3	4.0

		Rough-to-smooth			
		x = 500 m		x = 5000 m	
z_{01} [m]	z_{02} [m]	Error [%] Method 1	Error [%] Method 2	Error [%] Method 1	Error [%] Method 2
0.5	0.002	14.2	5.6	11.3	8.1
	0.004	13.2	3.0	10.4	5.8
	0.009	11.8	0.6	9.1	3.6
	0.02	10.1	-1.1	7.6	1.8
	0.045	8.3	-2.0	6.0	0.6
	0.1	6.0	-2.2	3.7	-0.1
0.05	0.0002	9.7	0.8	8.0	4.7
	0.0004	8.9	-1.2	6.9	2.3
	0.0009	7.7	-3.1	5.9	0.4
	0.002	6.8	-4.1	4.9	-0.8
	0.0045	5.5	-4.4	3.9	-1.5
	0.01	4.1	-3.8	2.8	-1.7
0.005	0.0002	4.4	-4.4	3.2	-1.8
	0.00045	3.2	-5.3	2.2	-3.0
	0.001	2.1	-5.3	1.2	-3.5

Table 6: Mean errors between approximated and simulated TKE profiles within the IBL.

As for the velocity profiles 'method 2' gives in most cases better estimates of TKE than 'method 1'.
Overall the TKE errors are somewhat higher than the corresponding velocity errors. Two examples of approximated profiles are shown in Figure 41 and Figure 42. The first one shows the profile 5000 m after the change from 0.5 m to 0.002 m, and the second one shows the profile 5000 m after the change from 0.0001 m to 0.004 m

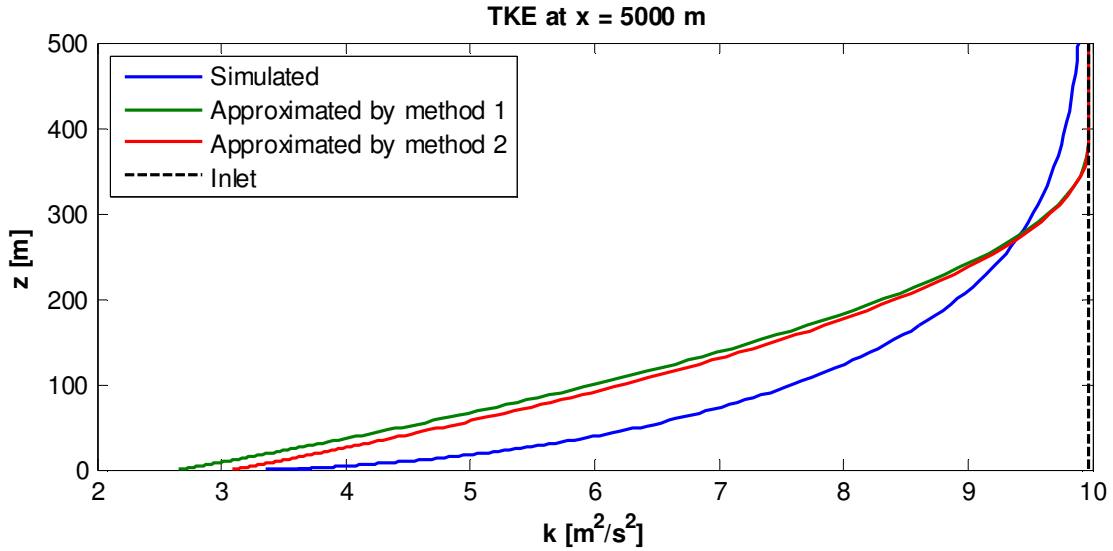

Figure 41: Simulated and approximated TKE profiles 5000 m downstream of a change in roughness length from 0.5 m to 0.002 m. The black line represents the upstream TKE profile.

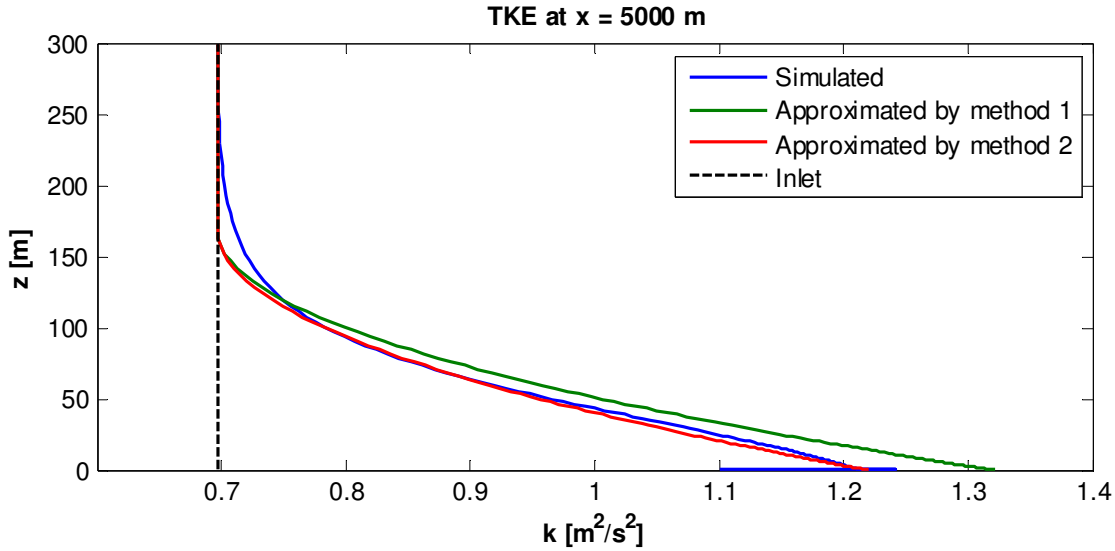

Figure 42: Simulated and approximated TKE profiles 5000 m downstream of a change in roughness length from 0.0001 m to 0.004 m. The black line represents the upstream TKE profile.

Results as shown in Figure 41 are not satisfying. The main problem seems to be the shape of the approximated curves. The second order polynomial looks like a bad choice in this case. The approximations shown in Figure 41 are better. There is still some deviation near the top of the IBL. This might be related to the way the IBL height is defined (equation (16) with $\mathrm{IBL}_{\mathrm{limit}} = 0.04$).

Near the wall the 'method 2' approximation is seen to be quite good in both cases, but at the short fetch length (x = 500 m) some deviations are also seen in this area. This was however to be expected. A potential developing equilibrium layer must be assumed to be very shallow here - especially after a rough-to-smooth change as seen Figure 36 for instance. Even very close to the wall, some fetch length is required for the flow to adapt to the new surface.

4.4.3 Dissipation profiles

Finally the downstream dissipation is approximated by equation (42):

$$\epsilon = \frac{c_\mu^{\frac{3}{4}} \cdot k^{\frac{3}{2}}}{\kappa z} \tag{42}$$

It is the same relation used to describe logarithmic conditions, only now the TKE is not constant. Using the approximated values of the TKE found above with method 1 and 2 gives the errors shown in Table 7 between simulated and approximated dissipation – averaged at heights of 1, 25, 50, 75 and 100% of the TKE based IBL height.

		Smooth-to-rough			
		x = 500 m		x = 5000 m	
z_{01} [m]	z_{02} [m]	Error [%] Method 1	Error [%] Method 2	Error [%] Method 1	Error [%] Method 2
0.0001	0.045	5.8	36.5	11.3	25.5
	0.02	10.7	32.4	11.0	20.9
	0.009	12.2	28.0	11.4	18.1
	0.004	11.7	23.5	9.5	14.2
	0.002	10.4	19.5	8.7	12.7
	0.001	9.4	17.0	7.2	11.4
	0.0004	8.5	15.5	5.3	10.8
0.001	0.45	-39.3	23.1	2.3	20.0
	0.2	-16.2	20.4	5.9	14.5
	0.09	-1.3	18.9	8.1	10.6
	0.04	3.9	14.8	9.3	7.9
	0.02	6.5	11.8	9.5	6.0
	0.01	7.4	9.3	8.3	4.5
	0.004	7.4	8.0	7.1	4.5
0.01	0.4	-31.2	11.6	1.8	17.9
	0.2	-15.7	10.1	4.2	14.6
	0.08	-6.7	9.3	6.2	13.3
	0.04	-1.6	9.0	6.4	12.5

		Rough-to-smooth			
		x = 500 m		x = 5000 m	
z_{01} [m]	z_{02} [m]	Error [%] Method 1	Error [%] Method 2	Error [%] Method 1	Error [%] Method 2
0.5	0.002	-1.6	-17.0	-4.2	-9.5
	0.004	-1.2	-18.9	-3.3	-11.0
	0.009	-2.1	-21.2	-3.7	-12.8
	0.02	-3.2	-22.3	-4.0	-13.4
	0.045	-4.4	-22.2	-4.0	-12.6
	0.1	-6.8	-21.4	-5.1	-11.2
0.05	0.0002	-8.4	-23.7	-6.5	-12.1
	0.0004	-7.5	-24.6	-6.9	-14.5
	0.0009	-7.8	-25.7	-6.8	-15.8
	0.002	-6.8	-24.4	-6.1	-15.4
	0.0045	-6.2	-22.3	-5.1	-13.9
	0.01	-5.2	-17.8	-4.0	-11.0
0.005	0.0002	-7.8	-21.8	-7.3	-15.3
	0.00045	-7.2	-20.5	-6.6	-14.8
	0.001	-5.6	-16.9	-5.4	-12.8

Table 7: Mean errors between approximated and simulated dissipation profiles within the IBL.

The errors vary a lot from case to case and from method to method. In most cases however 'method 1' seems to be better than 'method 2'.

The very high mean errors seen in some cases are suspected to be caused mainly by high errors close to the wall. This is for instance the case in the example shown in Figure 43. It is the case of a roughness change between 0.0001 m to 0.045 m. The mean error of the 'method 2' approximation is found to be 36.5%, but looking at the plot the approximation does not seem to be that bad after all.

Due to these difficulties of estimating the accuracy of the approximations , it is hard to say anything general about which method is the best, or how well they can be trusted.

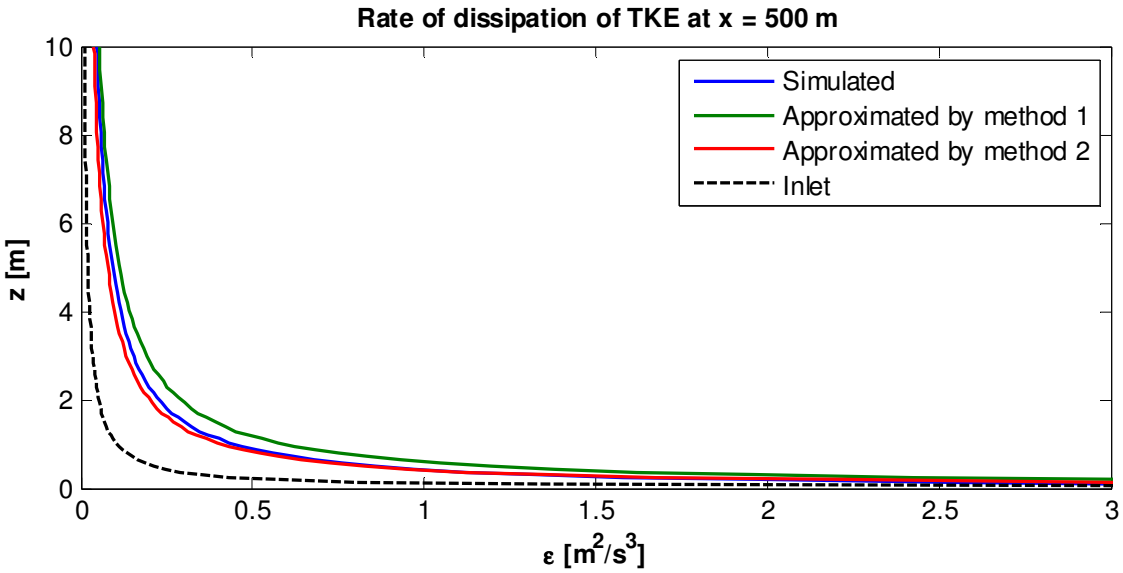

Figure 43: Simulated and approximated dissipation profiles 500 m downstream of a change in roughness length from 0.0001 m to 0.045 m. The black line represents the upstream dissipation profile.

4.5 Closure

In this chapter simulations of the flow over flat terrain with a change in roughness length have been studied.

Based on a range of simulations divided into rough-to-smooth cases and smooth-to-rough cases, empirical expressions for the velocity and TKE based IBL heights as functions of the fetch length and the roughness lengths have been found.

Two different approaches have been considered leading to the expressions of Table 3 and Table 4 respectively. The rather complicated but explicit expressions found by the "Elliot approach" (Table 3) were found to give the best results. They were derived for fetch lengths between 160 and 5000 m and for upstream roughness lengths between 0.0001 and 0.01 m in smooth-to-rough cases and between 0.005 and 0.5 m in rough-to-smooth cases.

At fetch lengths between approximately 2000 and 5000 m IBL heights within 10 % of the simulated heights were found in most cases.

The expressions have unfortunately not been compared to experiments. It seems like most existing experimental results regarding the development of the IBL, is for fetch lengths up to around 100 m. It would be very interesting to have more far-reaching measurements. This would, however, ideally require a number of high meteorological masts - with instrumentation at many different heights - spread out over a large flat area with a uniform surface roughness. Furthermore the incoming flow should be undisturbed and the atmospheric stratification preferably neutral.

In the following chapter simulations are compared to measurements made at the Høvsøre test site, which in fact is a flat area with a uniform surface roughness. Different wind directions are studied giving fetch lengths between 1800 and 3240 m from the coast to the meteorological mast. Unfortunately the mast is not quite high enough to clearly reveal the IBL heights, and the observed fetch dependency of the measured parameters is furthermore found to be inconsistent with what is expected.

In the last part of the present chapter, expressions for approximating the velocity, the TKE and the dissipation downstream of a roughness change have been studied.

Two methods of estimating the near wall friction velocity were considered. ‘Method 1’ was the classical approach of assuming a logarithmic velocity profile within the IBL and setting this equal to the undisturbed velocity profile at the top of the IBL. ‘Method 2’ was to determine an empirical expression from a range of simulated values.
Regarding the velocity, approximations based on ‘method 2’ was in general seen to give the smallest errors when compared to simulated values. The same goes for the TKE, which was approximated by a second order polynomial within the IBL.
The accuracy of the approximated dissipation profiles are more difficult to evaluate because of the very high gradient near the wall. But since they are based on the TKE approximations it seems natural to assume, that ‘method 2’ is also the most accurate here – although the errors shown in Table 7 seem to say the opposite.
Examples of velocity, TKE and dissipation profiles have been shown in Figure 39 to Figure 43 to give a general idea of the quality of the approximations.

To sum up, based on a range of roughness change simulations, empirical expressions for describing the flow after a change in the roughness length have been suggested. They are thought to offer a reasonable alternative to the standard logarithmic inlet conditions, when doing simulations over terrain where an upstream roughness change is suspected to have some influence on the flow.
The expressions have only been compared to simulations included in the derivations of the expressions. It is however assumed they will work equally well for other simulations, as long as fetch lengths and roughness lengths are kept within the range of values used for the derivations.
A more accurate approach, however, would still be to include the roughness change in the computational domain or do a precursor simulation.

5. Høvsøre measurements

5.1 Introduction

In this chapter measurements made at the Høvsøre test site (near the west coast of Jutland, Denmark) are studied and compared to simulated wind profiles downstream of a roughness change.

The roughness change in this case is due to the transition from sea to farmland. Measurements with wind directions in the range of 270° to 330° are studied. This corresponds to distances between 1800 m and 3240 m from the roughness change to the position of the Høvsøre mast.
The measurements are furthermore sorted to get near neutral conditions only. To do this, only entries with wind speeds above 6 m/s and absolute values of the Obukhov length[7] above 1000 m are used.

The test site of Høvsøre is chosen because the fields around the mast are relatively flat as seen in the map of Figure 44, and have a more or less uniform roughness. Thus the effects of a single roughness change can be studied without the influence of hills and so on. Each contour on the map represents a difference in height of 1.8 m.

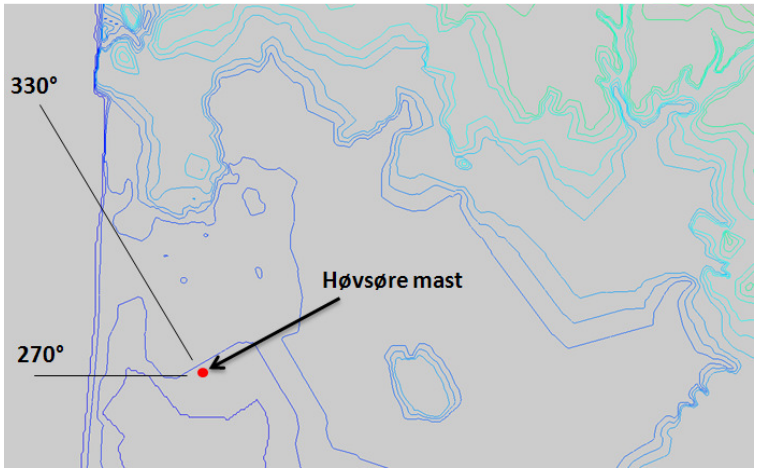

Figure 44: Map of height contours around the Høvsøre test site. Each contour on the map represents a difference in height of 1.8 m.

5.2 Measurements

The measurements at Høvsøre are made with cup anemometers at heights of 2, 10, 40, 60, 80, 100 and 116.5 m, with sonic anemometers at heights of 10, 20, 40, 60, 80, 100 m and with a wind vane at 10 m. Figure 45 and Figure 46 show the measured wind speed and turbulent kinetic energy normalized with the mean of the measured friction velocities at 10 and 20 m height.

The TKE is found through the mean-square values of the velocity fluctuations:

$$k = \frac{1}{2}(\overline{u'u'} + \overline{v'v'} + \overline{w'w'}) \qquad (43)$$

[7] Measured at a height of z = 10 m

The friction velocity is found as:

$$u_* = \sqrt{\frac{\tau_0}{\rho}} \tag{44}$$

τ_0 is the wind shear at ground level or in this case the mean value between 10 and 20 m height. It is calculated as:

$$\tau_0 = \sqrt{\left(-\rho\overline{u'w'}\right)^2 + \left(-\rho\overline{v'w'}\right)^2} \tag{45}$$

For simplicity only measurements from the sonic anemometers are shown here. The velocities are mean values over 30 minute periods. For each wind direction a number of data sets are obtained through the sorting explained above and it is the mean values of these that are shown below.

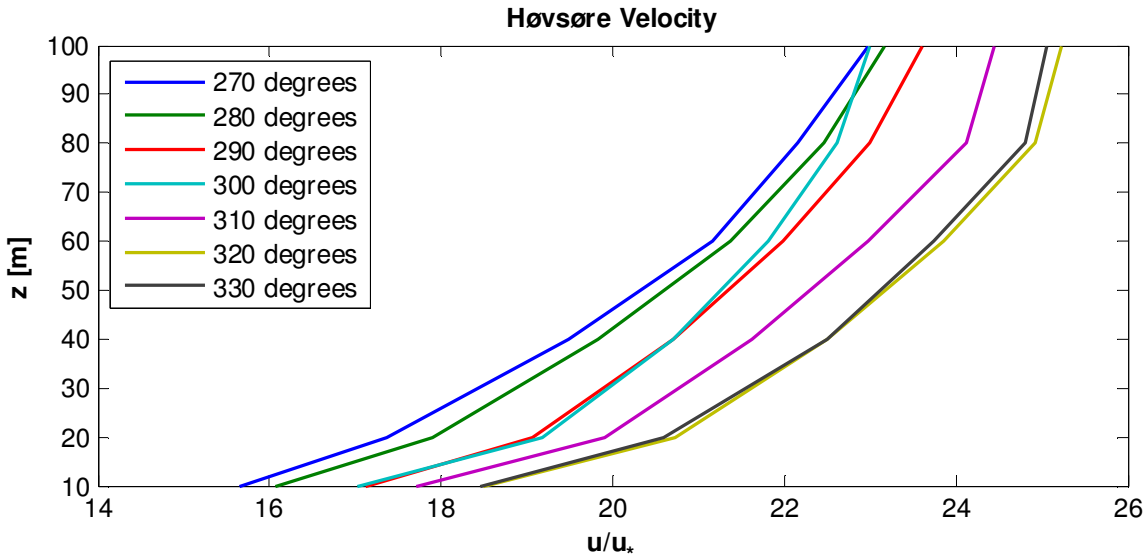

Figure 45: Measured velocities at Høvsøre – normalized with the mean of the measured friction velocities at z = 10 m and z = 20 m.

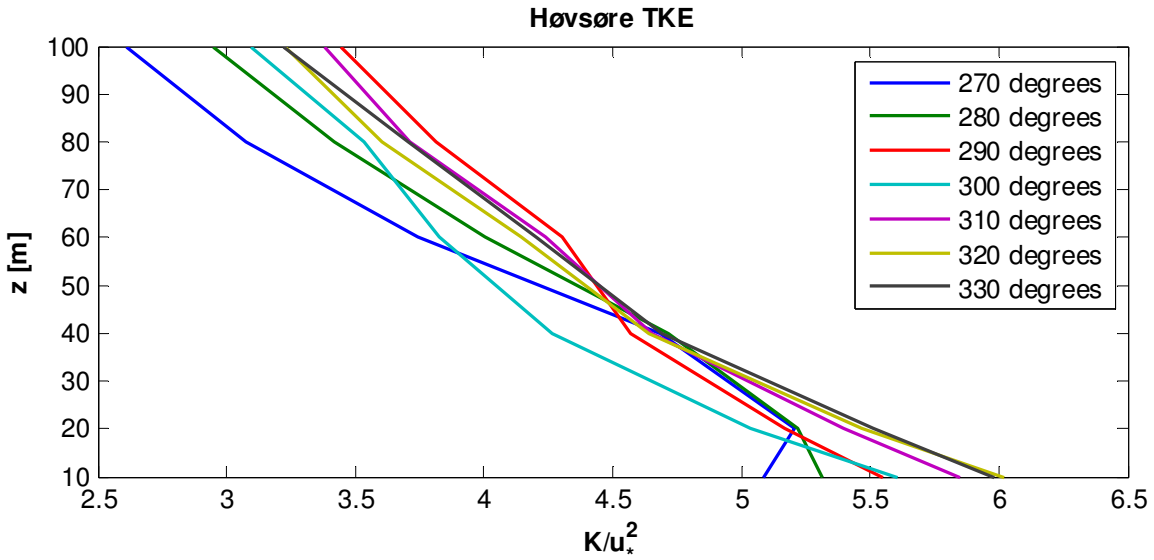

Figure 46: Measured values of TKE at Høvsøre – normalized with the mean of the measured friction velocities at z = 10 m and z = 20 m.

First of all it is noticed that the velocity in general seems to increase with the fetch length, which is opposite to what was expected. One would naturally assume the wind to continuously slow down when moving inland from the sea, and at the same time that the wind shear and thereby the friction velocity would increase.

The observed behavior cannot really be explained except from the way the data is obtained and from measuring inaccuracy.

Though the data is sorted to get neutral conditions only, other factors such as the temperature difference between water and land might play a role. One could for instance imagine, that the long fetch measurements were obtained during periods, where the land surface was significantly warmer than the sea, whereby the air was accelerated in the coastal region, and that the short fetch measurements were obtained under opposite conditions. Unfortunately no temperature measurements from Høvsøre are available for further analysis in this direction[8].

One could also imagine that changes in the surface roughness related to the time of year could have influenced the measured velocities.

The meteorological mast itself, should not have any influence on the measurements. The studied wind directions are primarily westerly and the anemometers are placed on booms pointing north and south of the mast.

The standard deviations of the averaged normalized velocities in Figure 45 lie between 0.5 and 2.5 depending on height and wind direction.

The TKE measurements show no clear dependency on the wind direction. This could be taken as a confirmation that measuring inaccuracy actually dominates over the fetch dependency in this case. The standard deviations of the averaged TKE values lie between 0.6 and 1.2.

[8] Temperature and stability measurements from the offshore wind farm of Horns Rev about 150 km south of Høvsøre could perhaps be used to understand the results seen in Figure 45. This is however outside the scope of this project.

Focusing on measurements with a specific velocity such as 12 m/s at a height of 10 m for all the directions, gives more or less the same results as shown above.

5.3 Simulations

To simulate the wind at the Høvsøre site, the roughness lengths of sea and land is needed. At sea the relationship proposed by Charnock is used to get the roughness length[9]:

$$z_0 = a_{charnock}\left(\frac{u_*^2}{g}\right) \tag{46}$$

The friction velocity is defined by assuming a logarithmic velocity profile with 10 m/s at a height of 10 m.

$$u_* = \frac{u\kappa}{\ln\left(\frac{z+z_0}{z_0}\right)} \tag{47}$$

Combining equations (46) and (47) leads to a roughness length of 0.00026 m. The empirical constant $a_{charnock}$ is set to 0.018 and the gravitational acceleration to 9.81 m/s^2.
Over land a roughness length of 0.02 m is used – corresponding to farmland with uncut grass[10].

Figure 47 shows the simulated velocity profiles at fetch lengths corresponding to wind directions of 270° and 330° at Høvsøre, normalized with the simulated friction velocity at z = 15 m. The terrain is assumed to be completely flat. In the plot is also the mean of the measured velocities at all the considered wind directions, normalized with the measured near wall friction velocity, along with the theoretical logarithmic profiles based on the water- and land-roughness.

The simulated friction velocity is estimated by:

$$u_* = k^{\frac{1}{2}} \cdot c_\mu^{\frac{1}{4}} \tag{48}$$

The computational domain is similar to the one used for the simulations in the previous chapter; 20x5 km with 256x512 cells stretched in the vertical direction. The near wall cells have a height of 0.052 m.

[9] (Arya, 2001) page 198
[10] (Arya, 2001) page 199

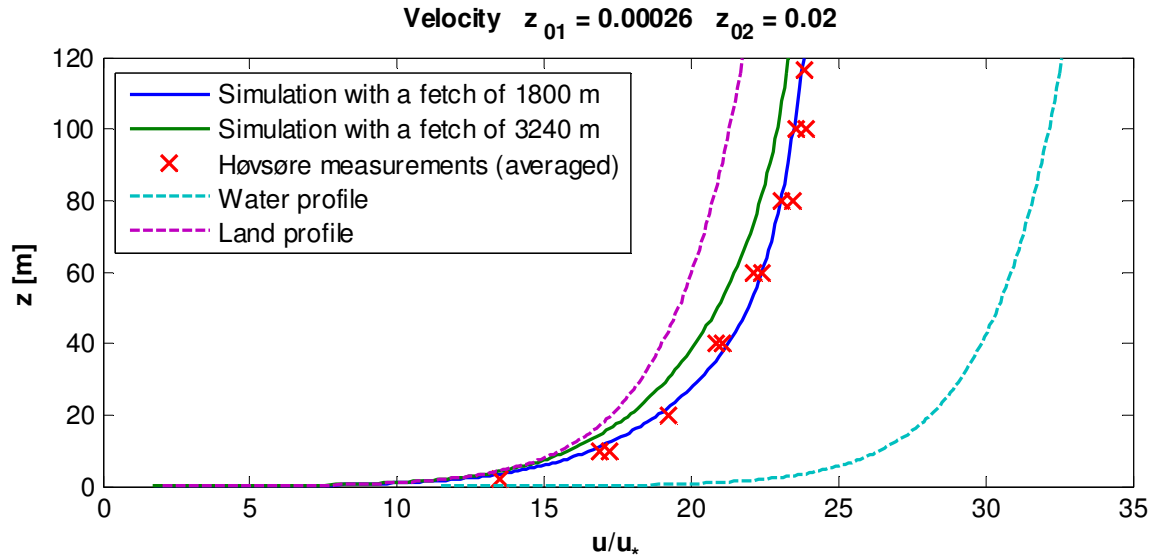

Figure 47: Simulated, measured and logarithmic velocities – normalized with the corresponding near wall friction velocities

As opposed to the measurements the simulated velocities actually decrease with the fetch length as expected; moving from the water profile towards the land profile. The averaged measurements (from both sonic and cup anemometers) seem to fit quite well with the short fetch simulation. However, with the small difference between the fetch lengths it seems unrealistic in this case to find measurements with good enough accuracy to relate them to one or the other fetch length. The exact choice of roughness lengths for the simulations is also a significant factor in this respect.

Figure 48 shows the development of the simulated friction velocity used for normalizing the simulated velocities in Figure 47. As expected, it increases with fetch length – an observation which does not help to explain the unexpected fetch dependency of the measured velocity shown in Figure 45.

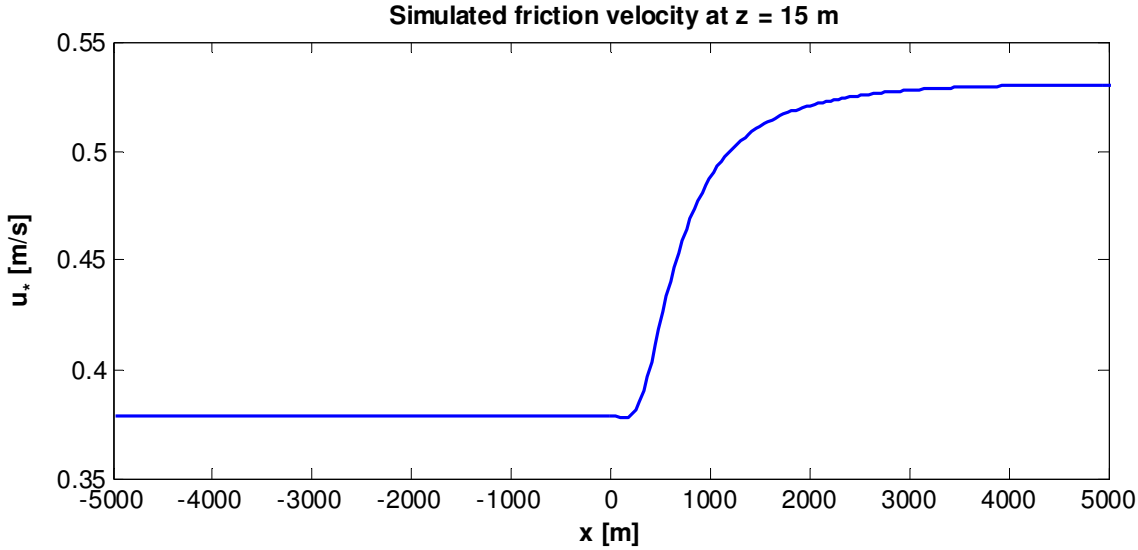

Figure 48: Development of the simulated friction velocity at z = 15 m. The change in roughness length from 0.00026 m to 0.02 m takes place at x = 0.

Figure 49 shows the velocities on a logarithmic scale from 1 to 500 m above ground level. The simulated profiles exhibit a clear change from a logarithmic profile (a straight line) in the top of the domain to

something else from around 100 m and down. A similar but not as pronounced tendency could be transferred to the measurements. A straight line through for instance the three highest measurement points will deviate somewhat from the lower points. Measurements from higher altitudes would might have made the tendency clearer.

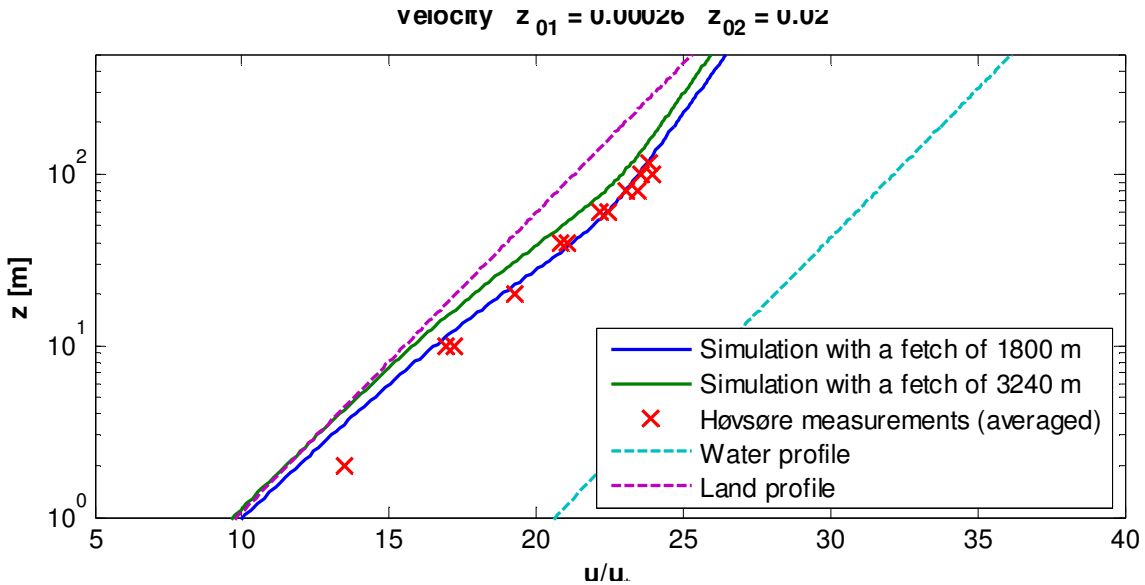

Figure 49: Simulated, measured and logarithmic velocities – normalized with the corresponding near wall friction velocities – on a logarithmic scale.

Figure 50 shows the development of the IBL heights based on the simulated TKE and velocity. As it was also seen in Figure 49, the velocity based IBL height at the studied fetch lengths is just within the height of the Høvsøre mast. The TKE based IBL height is on the other hand predicted to be above the height of the mast.

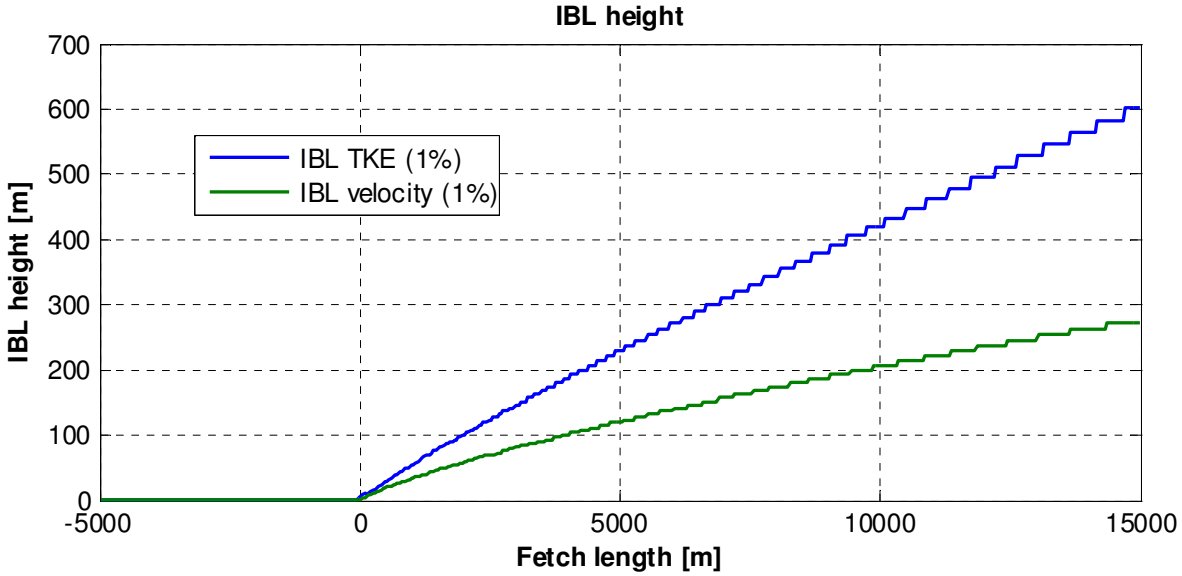

Figure 50: IBL heights defined as the heights at which the simulated TKE or velocity starts to differ more than 1% from the inlet values. The change in roughness length from 0.00026 m to 0.02 m takes place at x = 0.

Measured and simulated TKE profiles are plotted in Figure 51, and as for the velocity quite good agreement is observed. The measured profile lies somewhere in between the two simulated profiles.

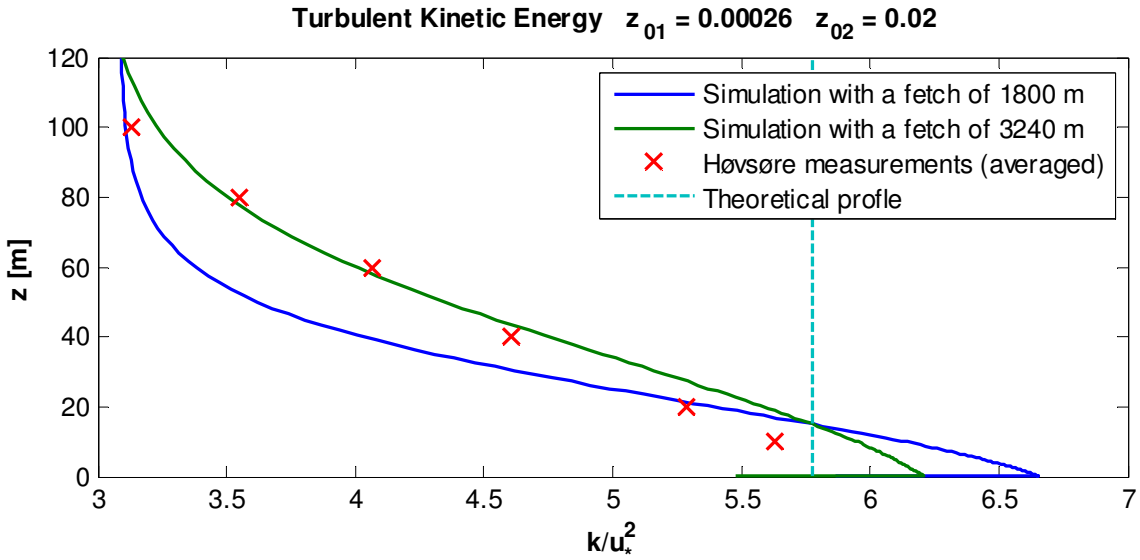

Figure 51: Simulated, measured and equilibrium TKE – normalized with the corresponding near wall friction velocities.

The theoretical profile in Figure 51 is defined by equation (49) which comes from the $k-\epsilon$ turbulence model:

$$C_\mu = \left(\frac{u_*^2}{k}\right)^2 \tag{49}$$

5.4 Closure

Regarding the velocity and TKE averaged over the studied range of wind directions, the Høvsøre measurements show good agreement with simulations made with *Ellipsys* under the specified conditions. Unfortunately, no clear conclusion regarding the fetch dependency of velocity and TKE can be made. In particular the measured velocity behaves opposite of what was expected. Factors such as horizontal temperature gradients and offshore atmospheric stratification, which are not included the present analysis, might be the cause of the unexpected behavior.

In the presented simulations, the terrain was assumed to be completely flat. To validate this assumption they are compared to simulations including the actual terrain of the area. The computational domain of these terrain simulations are more or less similar to that of the original simulations – except of course for the variations in the elevation of the wall boundary.

Two terrain simulations are made; one along the 300°-direction and one along the 330°-direction. These directions correspond to fetch lengths of 1875 and 3240 m.

Figure 52 shows the simulated velocities versus the height above ground level at the position of the mast. The velocities are normalized with the simulated friction velocity at 15 m above ground level.

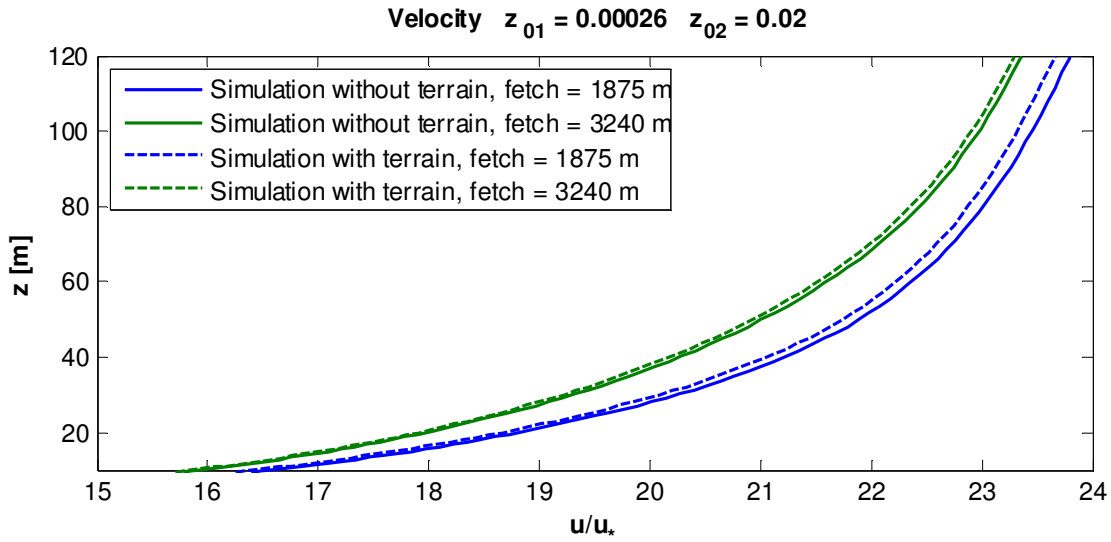

Figure 52: Comparison of velocities from simulations with and without the terrain of the Høvsøre area included. Two different fetch lengths are considered.

As seen in Figure 52, including the terrain in the Høvsøre simulations has very little effect on the velocity. It seems very unlikely that it is terrain effects which causes the measured velocities to increase with the wind direction and thereby with the fetch length.

Regarding the IBL, the simulations predicts heights of around 80-100 m at the studied fetch lengths. A similar IBL height can be deduced from the averaged velocity measurements, but it is not seen very clearly. Velocities measured at higher altitudes, with for instance a LIDAR system, would most likely make the top of the IBL stand out more distinctly.

The measurements presented in this chapter have been provided by the Test and Measurement Programme (TEM) of the wind energy department (VEA) at Risø DTU. An overview of the Høvsøre project can be found at the web site of (VEA online).

6. Askervein – 2D simulation

6.1 Introduction

Askervein is a hill with a height of 116 m located on the west coast of South Uist - an island of the Outer Hebrides, Scotland. In 1982 and 1983 a range of measurements were made at this location to get a better understating of how the wind behaves, when it encounters a low hill. These measurements have become a widely used reference for numerical models dealing with flow over hills. The background of the experiments is given in (Taylor & Teunissen, 1985).

As seen in Figure 53 the shape of the hill is more or less elliptical with line B-B defining the major axis of about 2 km and lines A-A or AA-AA defining the minor axis of about 1 km. The measurements were made along these lines.
Below follows a study of the influence of the surface roughness and of an upstream roughness change on the flow over Askervein.
It has been shown earlier in this report how a roughness change affects the vertical profiles of velocity and TKE. The effect of using such modified profiles as inlet conditions instead of the standard logarithmic equilibrium profiles for a simulation of the flow over Askervein is investigated.

Simulations are compared to the measurements, but the main concern is however to compare simulations of different conditions to each other. Exact agreement with the measurements can after all not be expected due to the approximations of the numerical model.
The most obvious and probably also most arguable approximation of the simulations presented in this chapter, is an assumption of the flow being two dimensional. For this to be valid, the flow can have no lateral velocity components. But since the hill has a limited extent in the lateral direction, some flow around the hill and not only over the hill must be expected. The influence of the 2D approximation is looked upon in the following chapter in which the full three dimensional flow is simulated.

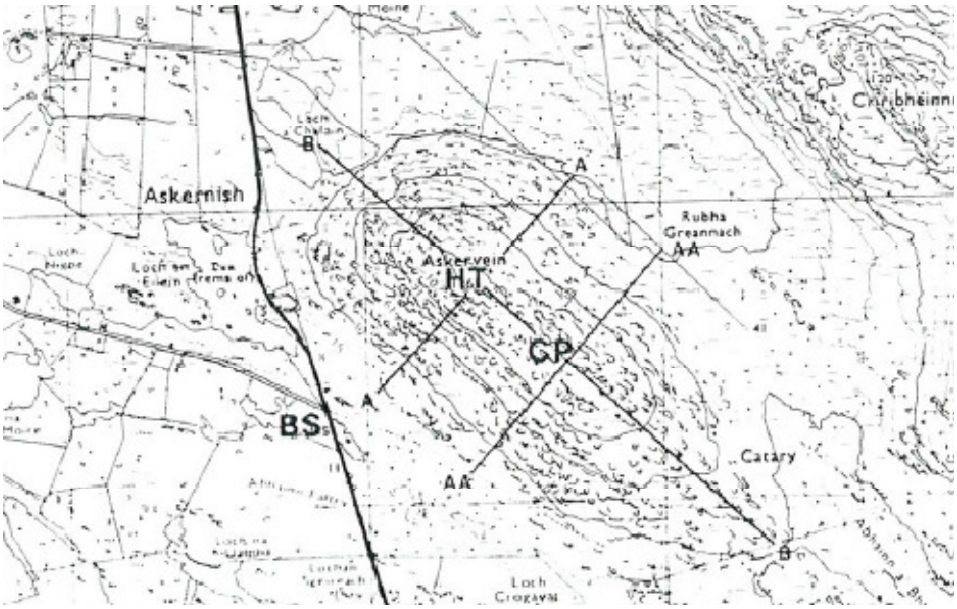

Figure 53: Section of map of Askervein (copied from (Taylor & Teunissen, 1985))

This chapter is divided in four parts. The first part deals with grid dependency, the second with the dependency on the Reynolds number, the third with the influence of the surface roughness and finally the last part deals with the influence of upstream changes of the surface roughness.

The topic of flow over hills is covered in several texts concerning experimental work, numerical models and analytical relations. (Jackson & Hunt, 1975) is often referred to as a key work (e.g. in (Kaimal & Finnigan, 1994) and (Taylor & Teunissen, 1985)) introducing a division of the flow over a low hill into an inner layer where turbulent friction have a large effect on the mean flow, and an outer layer in which the mean flow can be treated as being inviscid. The background of the theory will not be discussed in detail here, but it is merely noted that it appears to have had a substantial influence on later work within the topic.
An important parameter, which also seem to have received a great deal of attention, is the fractional speed-up ratio. It is defined as the relative difference between the undisturbed upstream velocity and the local velocity over the hill:

$$\Delta S = \frac{u(z) - u_{ref}(z)}{u_{ref}(z)} \tag{50}$$

This number is of great interest when choosing sites for wind turbines or when estimating loads on other structures in complex terrain since the available power or the potential loads depend on the velocity cubed or squared respectively. It will be the main parameter looked upon in this chapter along with the variation of TKE over the hill.
Note that *z* refers to the height above ground level.

6.2 The measurements – Inlet conditions

The specific measurements used for comparison, is the data set called TU03-B in (Taylor & Teunissen, 1985) - the same used in (Sørensen, 1995). As described in (Sørensen, 1995), the wind direction in this case is approximately from southwest to northeast along line A-A and the atmosphere nearly neutrally stratified. Line A-A is at 223° and the wind direction is 210°.

Measurements made at the reference site (RS) located approximately 3 km south of the hill top (HT) are used to define the inlet conditions for the following simulations. The inlet velocity is to begin with assumed to be logarithmic with a velocity of 8.9 m/s at a height of 10 m. Using a roughness length of 0.03 m as suggested in (Taylor & Teunissen, 1985) a friction velocity of 0.6125 is obtained. The logarithmic profile with these parameters is shown in Figure 54 along with measurements made at RS.

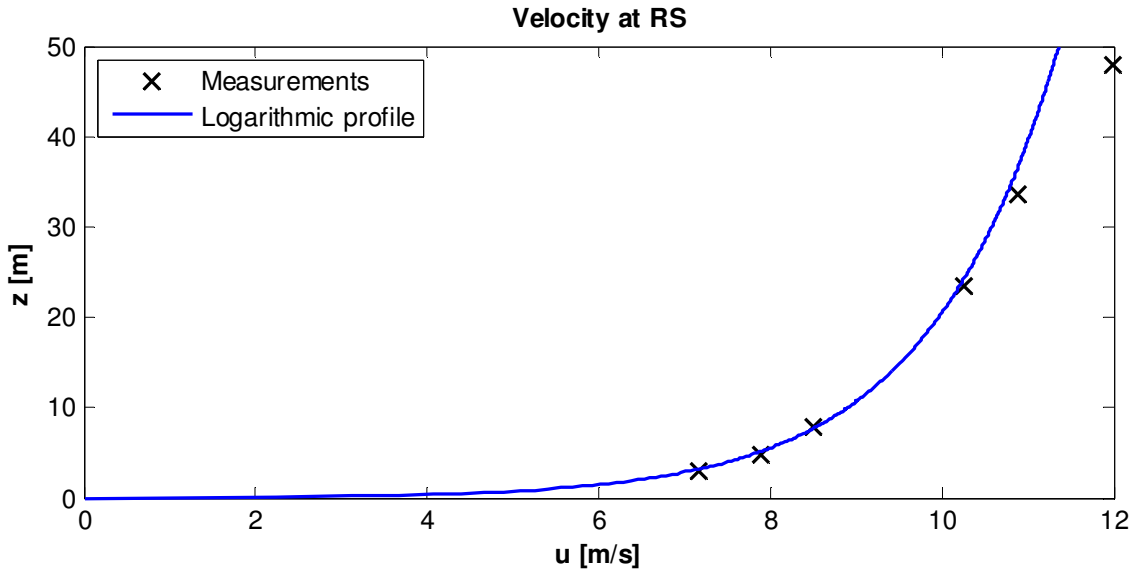

Figure 54: Logarithmic velocity profile fitted to measurements at the Askervein reference site.

The logarithmic velocity profile is seen to fit quite well up to a height of about 25 m. At the two highest measuring points it starts to deviate from the measurements. More on this will follow later. As suggested in (Sørensen, 1995) the constants C_μ and $C_{\epsilon 1}$ of the $k-\epsilon$ turbulence model are adjusted to obtain the turbulence intensity measured at RS. The values shown in Table 8 are used.

κ	C_μ	σ_k	σ_ϵ	$C_{\epsilon 1}$	$C_{\epsilon 2}$
0.4	0.11	1.00	1.30	1.54	1.92

Table 8: Constants of the $k-\epsilon$ turbulence model adjusted to the measured turbulence intensity at the Askervein reference site.

6.3 Computational domain and grid dependency

A rectangular domain with a length of 7.1 km and a height of 2.5 km is used for the simulations. The used boundary conditions are as described Figure 1.

The distance from the coast to the hill top is estimated to 3.3 km (from the map in (Taylor & Teunissen, 1985)) and the distance from the reference site to a line orthogonal to line A-A is estimated to 2.6 km.

The computational domain is designed to have its inlet 2.6 km before HT and its outlet 4.5 km after HT. HT is placed at $x = 0$. The height of the domain goes from ground level at $z = 0$ to $z = 2500$ m.

The grid is generated using *Hypgrid* (see (Sørensen, 1998)). The near-wall cell height is set to approximately 0.05 m and the grid is stretched towards the top of the domain using a sine hyperbolic stretch function. The cell width is set to its minimum of about 10 m in the vicinity of the hill, from where it is stretched toward inlet and outlet. Three different grid resolutions with respectively 64x64, 128x128 and 256x256 cells are examined. As an example the 128x128 grid is shown in Figure 55. In *Hypgrid* a volume blend factor of 0.0005 and dissipation factor of 1 is used.

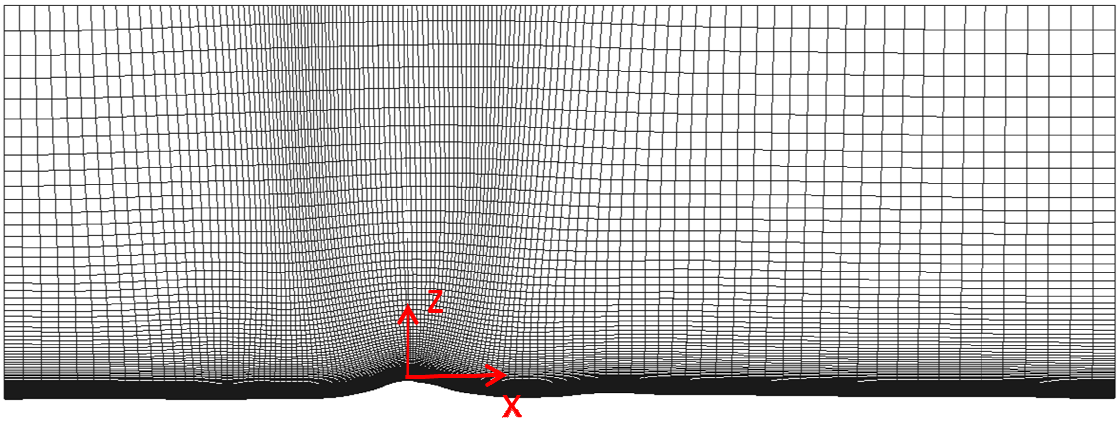

Figure 55: Computational grid with 128x128 cells. HT is placed at x = 0. z is the height above ground level.

With the inlet conditions described above, a study of the grid dependency is made. Three parameters are evaluated; the speed-up along line A-A, the speed-up at HT and the TKE along line A-A.

To determine the speed-up, the velocity in the first cell after the inlet is used as the reference velocity. The TKE is normalized with the reference velocity at a height of 10 m.

Figure 56 to Figure 58 show the simulated speed-up and TKE along with the measured values found in the data set TU03-B.

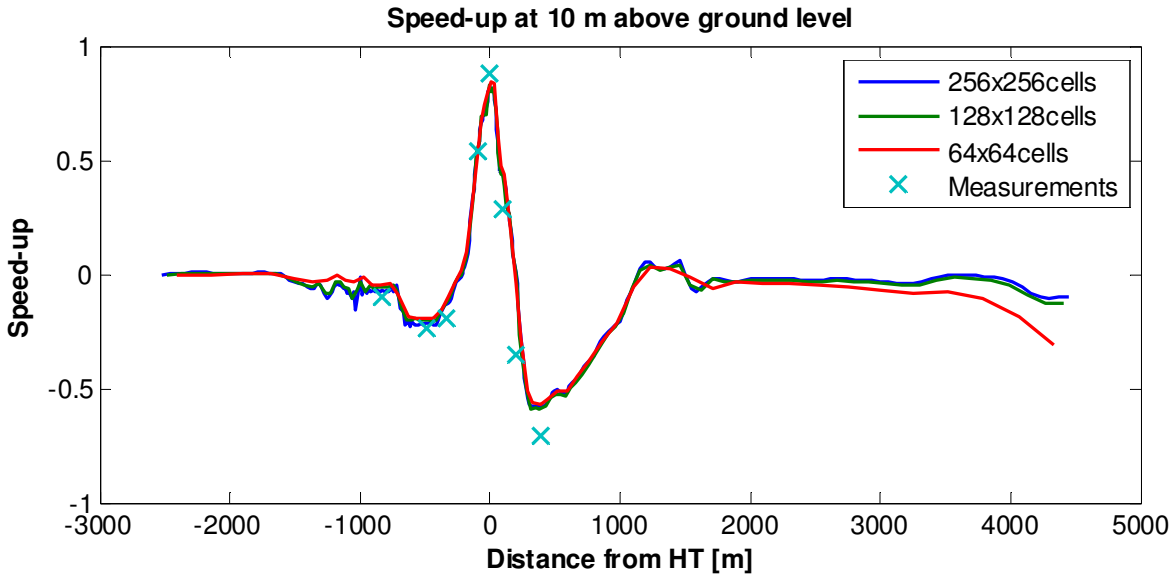

Figure 56: Measured and simulated speed-up along line A-A at a height of 10 m above ground level. Three different grid resolutions are presented.

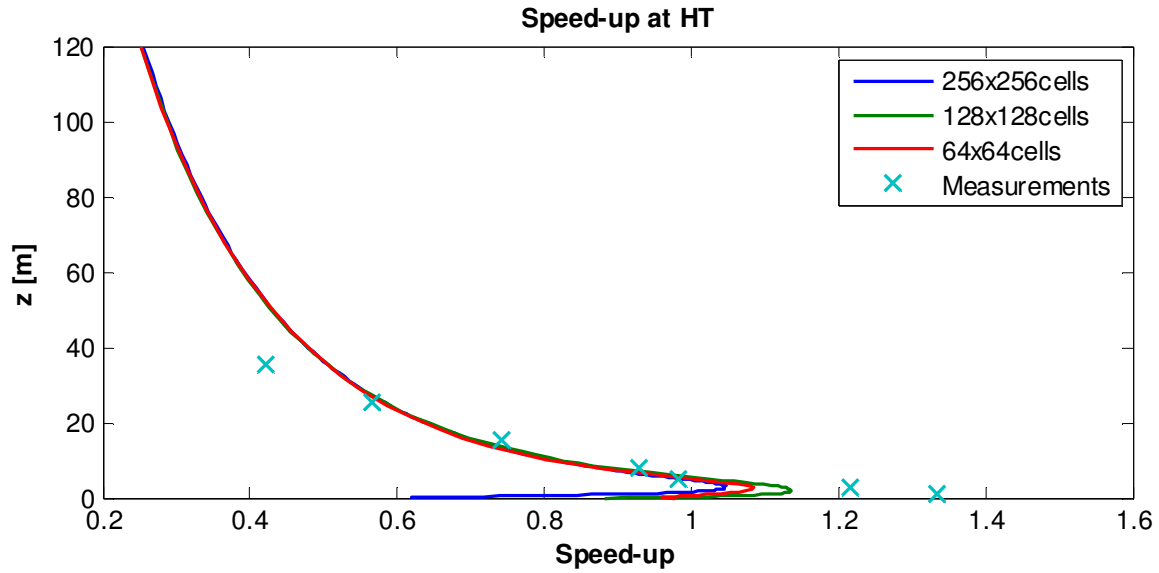

Figure 57 Measured and simulated speed-up at HT as a function of the height above ground level. Three different grid resolutions are presented.

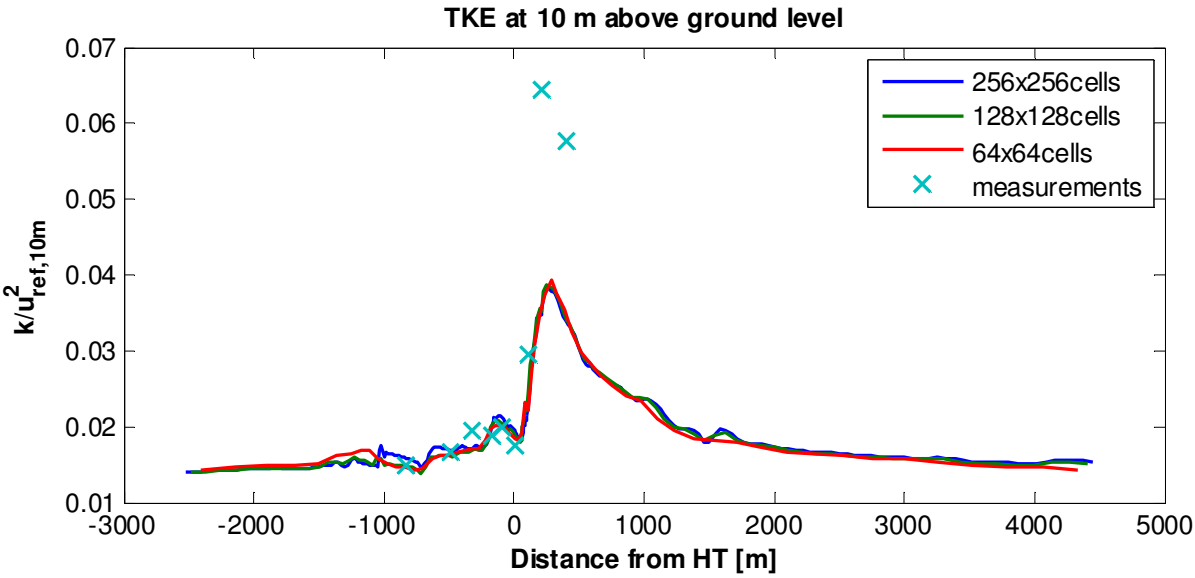

Figure 58: Measured and simulated TKE along line A-A at a height of 10 m above ground level. Three different grid resolutions are presented.

All three grid resolutions give similar results, and they all seem to be equally comparable to the measurements. The speed-up is generally underestimated at HT up to a height of approximately 20 m. Above this height it is overestimated. Also at the point 400 m after HT, almost at the foot of the hill, the simulations clearly overestimate the speed-up.

The TKE show good agreement upstream of and at HT. Further downstream it is underestimated quite substantially.

The differences between the results of the 128x128 cells grid and the 256x256 cells grid are considered to be small enough to assume, that the solution is grid independent at this resolution. The following simulations are made with the 128x128 cells grid.

6.4 Dependency on the Reynolds number

It is assumed that the solution is independent of the Reynolds number of the flow. The Reynolds number is found as $Re = \frac{U_{char} \cdot L}{\nu}$. L and U_{char} are characteristic length and velocity scales.

For all considerable wind speeds the Reynolds number is assumed to be high enough to make inertia forces much more dominant than viscous forces. To test this assumption, a simulation with an inlet velocity of 8.9 m/s is compared to a simulation with an inlet velocity that is ten times lower. Speed-up and TKE is show in Figure 59 to Figure 61.

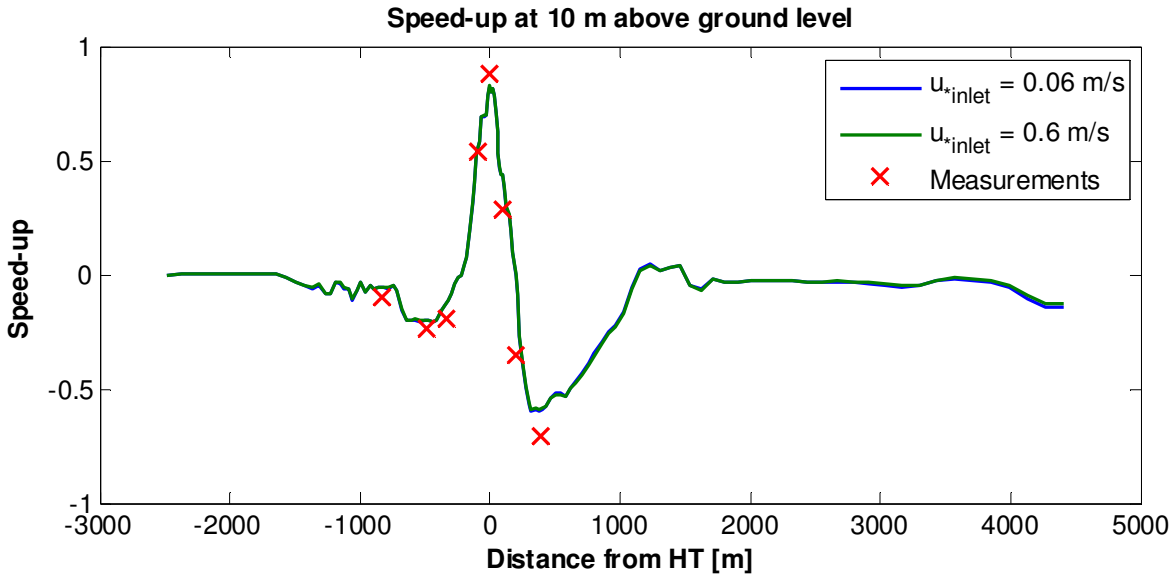

Figure 59 Measured and simulated speed-up along line A-A at a height of 10 m above ground level. Two simulations with different inlet velocities are compared.

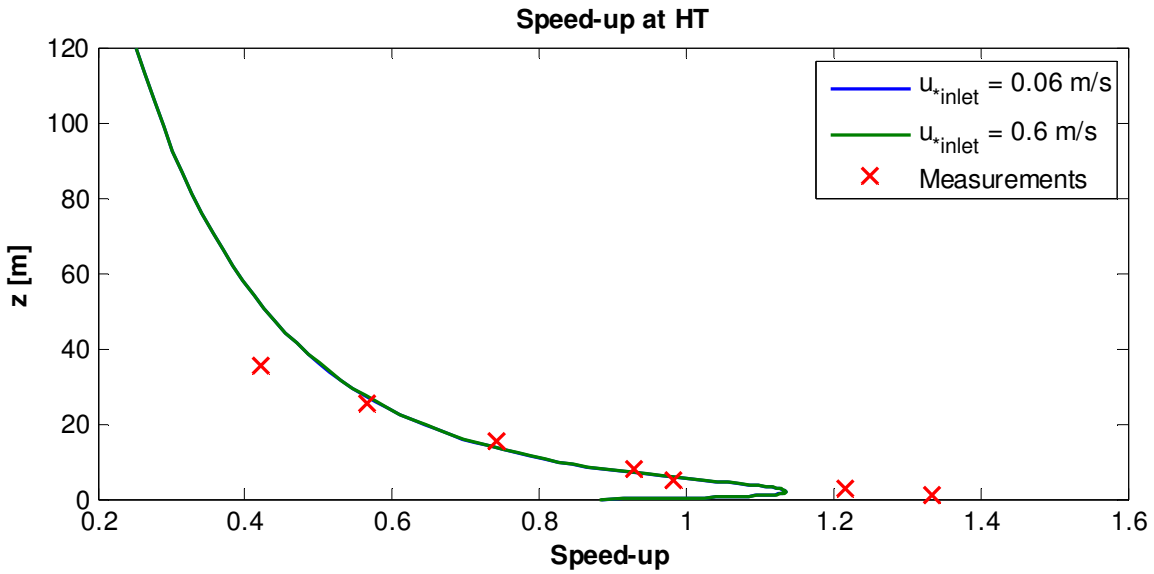

Figure 60: Measured and simulated speed-up at HT as a function of the height above ground level. Two simulations with different inlet velocities are compared.

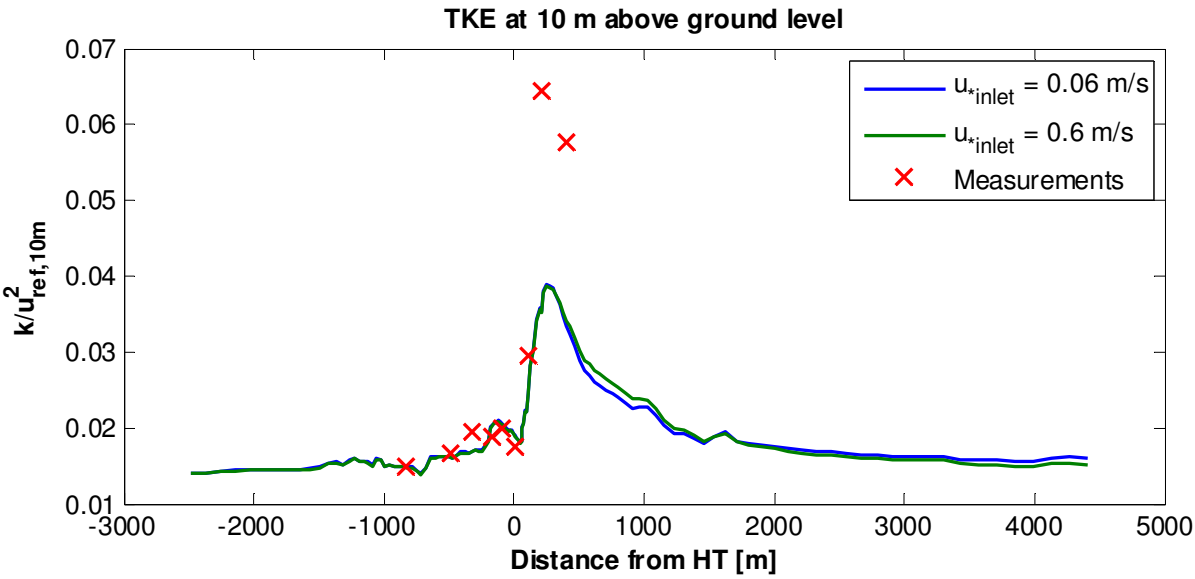

Figure 61 Measured and simulated TKE along line A-A at a height of 10 m above ground level. Two simulations with different inlet velocities are compared.

As expected, the speed-up is not affected by the reduction of the friction velocity. In this sense the flow is independent of the Reynolds number.

Regarding the TKE on the other hand, a small difference between the two simulations is seen on the lee side of the hill and also near the outlet. This could possibly be an effect of the negative speed-up in these areas. The reduction of the initially low velocity, might be enough to make the effect of the viscous forces visible. The conclusion must be that the flow is not fully independent of the Reynolds number, and some care should be taken when choosing inlet velocities.

6.5 Dependency on roughness length

According to (Taylor & Teunissen, 1985) the ground cover of Askervein and its surroundings is primarily heather, grass, low scrub and flat rocks. Based on profiles measured at RS, the authors obtain roughness lengths between 0.01 and 0.03 m. Their subjective estimate is around 0.05 m. In other words there is some uncertainty regarding the exact value of the roughness length. A range of simulations using different roughness lengths is made to study the influence of this parameter on the results.

All simulations are made with logarithmic inlet profiles, specified by a velocity of 8.9 m/s at a height of 10 m. In the two most extreme cases, roughness lengths of 0.0001 and 0.5 m are used. These values give friction velocities of 0.3 and 1.2 m/s respectively. Regarding the Reynolds number dependency, this difference in friction velocities should not significantly influence the results (according to Figure 59, Figure 60 and Figure 61).

The use of these extreme values for the roughness length should not be considered as a realistic attempt to model the flow over Askervein, but just as a method to study the influence of the roughness length.

Figure 62 shows the speed-up found with the different roughness lengths in the interval of $-1000 \leq x \leq 1000$, and Figure 63 shows the speed-up as a function of the height above HT.

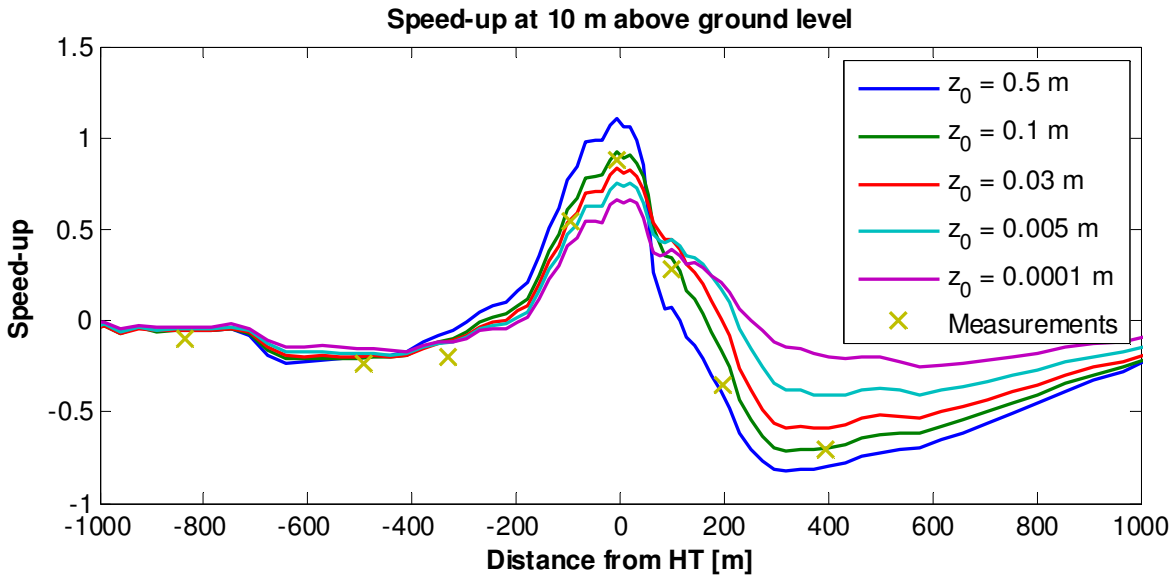

Figure 62: Measured and simulated speed-up along line A-A at a height of 10 m above ground level. Five simulations with different roughness lengths are compared.

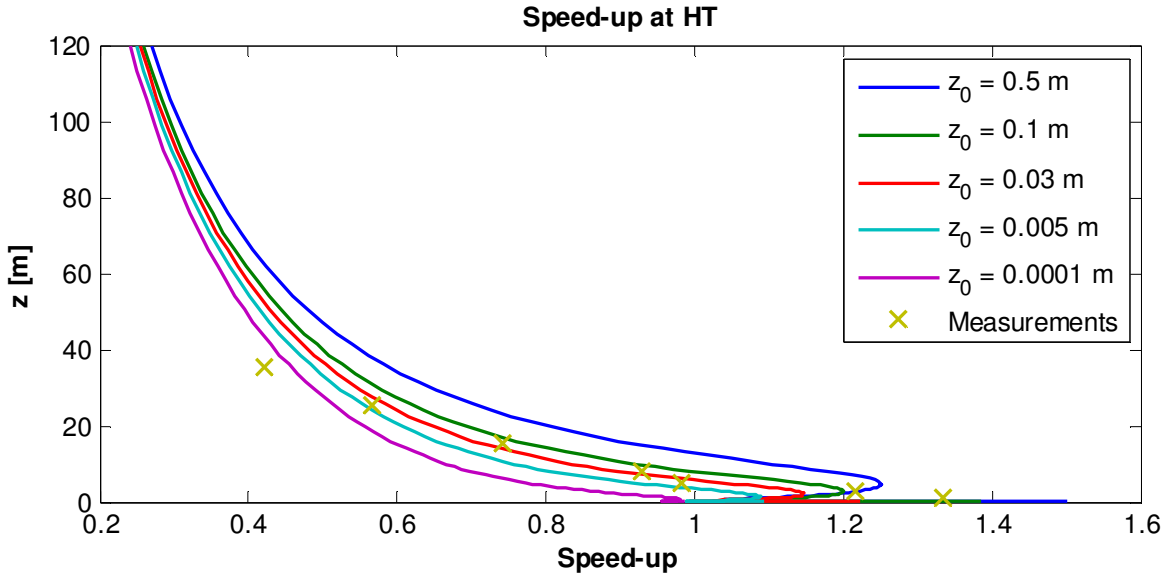

Figure 63: Measured and simulated speed-up at HT as a function of the height above ground level. Five simulations with different roughness lengths are compared.

The general tendency seen in Figure 62 for increasing roughness lengths, is higher speed-up values at HT and more significant velocity reductions behind the hill.

Figure 63 shows that the height at which the maximum speed-up occurs, increases with the roughness length – from around 0.5 m to 4.5 m above ground level. From this height and upwards the speed-up is seen to decrease along with the relative differences between the five curves.

Compared to the measured speed-up at 10 m above ground level, the simulation with $z_0 = 0.1$ m seems to give the best agreement. However, as mentioned in the introduction of this chapter, measured and simulated values cannot really be directly compared. The simulated flow is approximated to be two dimensional and is therefore only allowed to travel over the hill and not around it, as the real flow most likely would do to some extent. Following this thought, one would actually expect the simulation to

overestimate the speed-up at HT. From this point of view a value of $z_0 > 0.1\ \mathrm{m}$ would seem more appropriate. This on the other hand, agrees poorly with the actual surface roughness observed at Askervein.

Figure 64 shows simulated velocity profiles at HT (dashed lines) along with the associated inlet profiles (full lines). A distinct shift of the simulated profiles is observed when going from the low to the high roughness length. The velocity over the smoothest surface is seen to increase with height up to around 1 m above ground level, then to decrease up to 300 m, before it again starts to increase. As the surface gets more rough, the upper limit of the initial velocity increase is moved upwards, and the upper limit of the following decrease downwards. A continuous increase is observed for the highest roughness length.

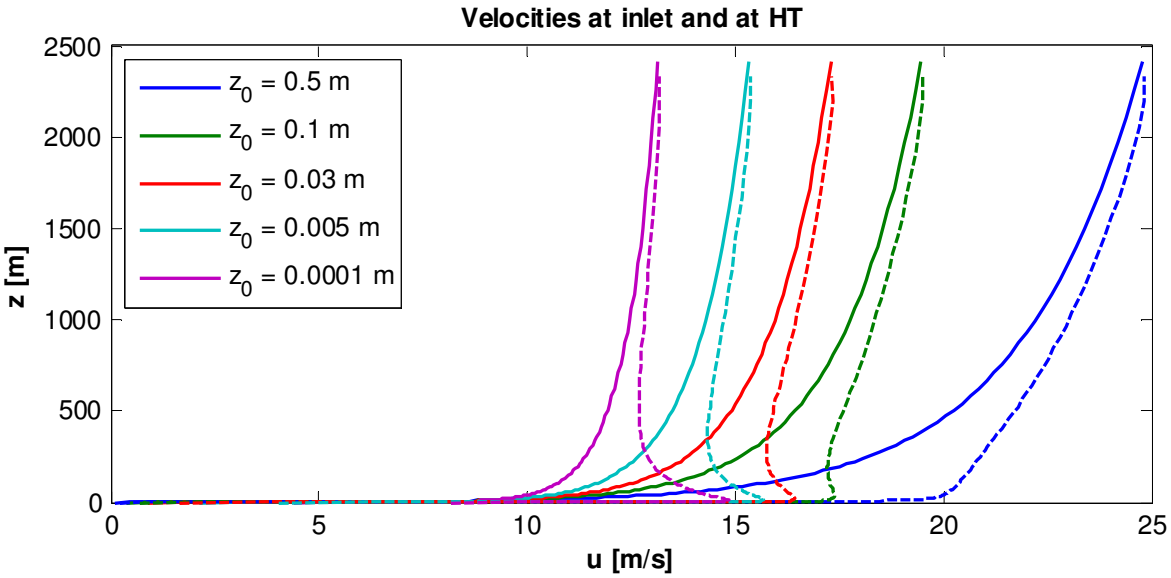

Figure 64: Inlet velocities are compared to velocities at HT taken from simulations with different roughness lengths.

A more detailed look at the development of the velocity over the hill is given in Figure 65 and Figure 66 for $z_0 = 0.0001\ \mathrm{m}$ and $z_0 = 0.5\ \mathrm{m}$ respectively. In each case the velocity has been normalized with the associated inlet velocity.

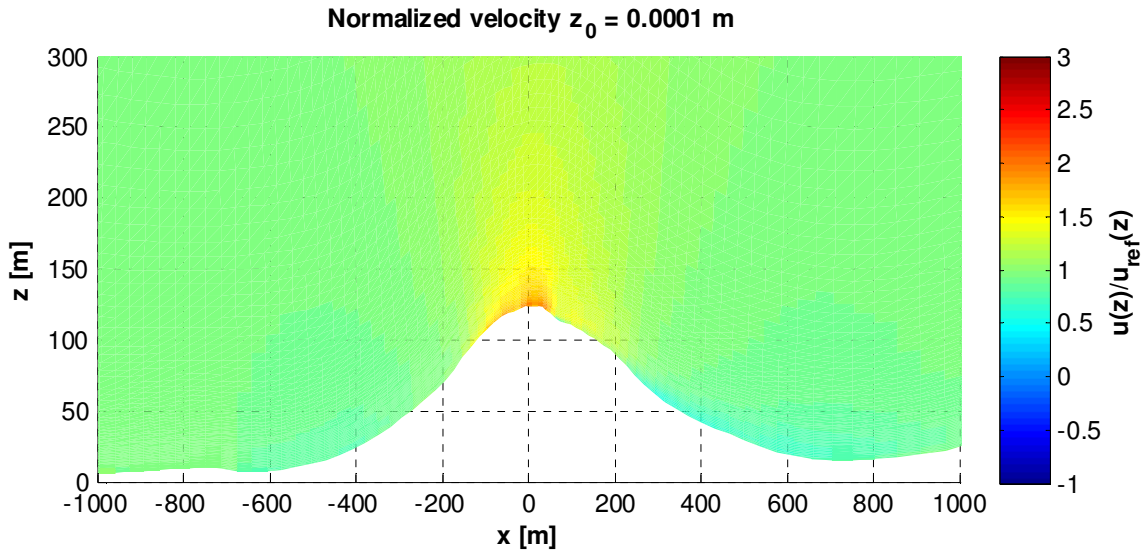

Figure 65: Simulated velocity field over Askervein – normalized with the inlet velocity. The roughness length is set to 0.0001 m.

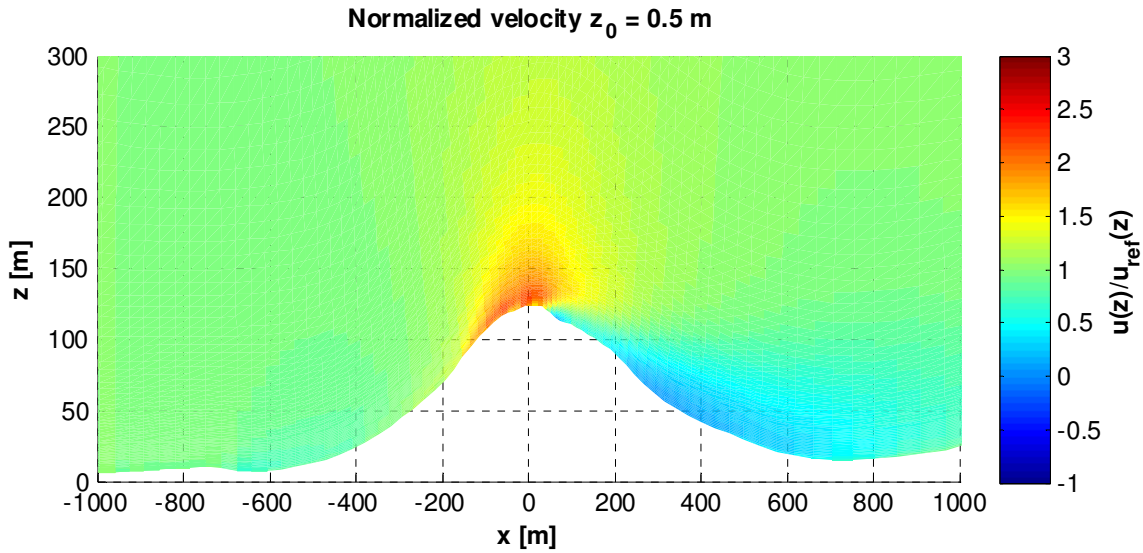

Figure 66: Simulated velocity field over Askervein – normalized with the inlet velocity. The roughness length is set to 0.5 m.

The main thing to observe in these figures is the expansion of the zones of positive and negative speed-up at HT and behind HT, as the roughness length is increased. In the case of $z_0 = 0.5$ m the velocity gets close to zero in an area on the lee side of the hill, but no separation bubble with reversed flow is observed in either case.

Regarding the development of TKE over the hill, a comparison of the different simulations seems inappropriate, since they are all made with the same value of C_μ. One could argue, that this value should be adjusted in each case to fit the inlet TKE to the measured turbulence intensity at RS - in the same way the friction velocity is adjusted to fit the inlet velocity to the measured velocity.
Figure 67 shows the TKE values simulated with a constant value of $C_\mu = 0.11$. Quite large differences are observed.

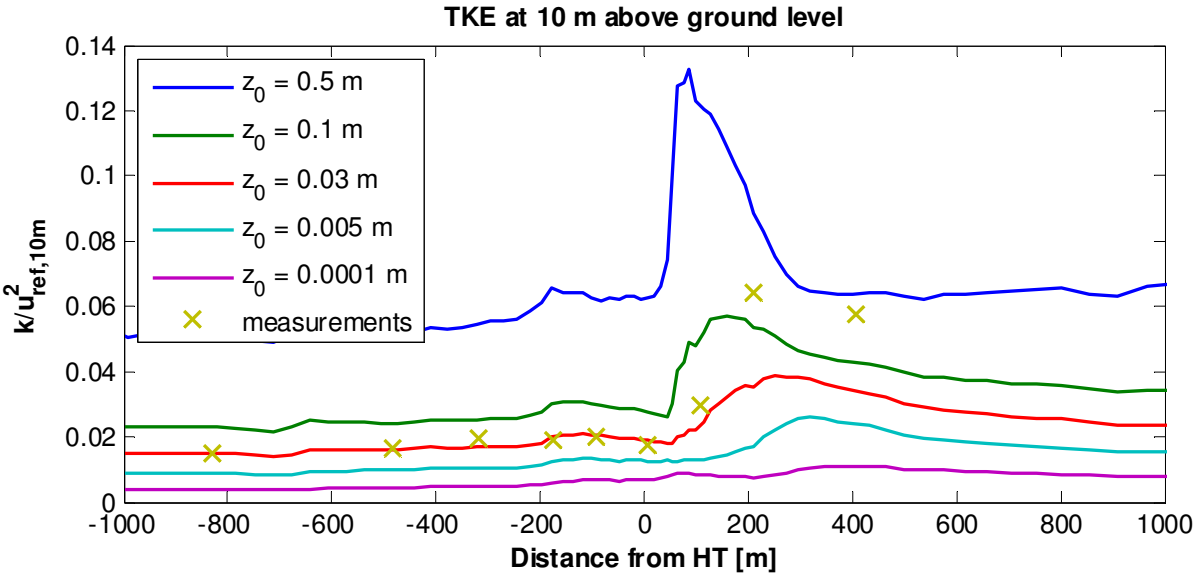

Figure 67: Measured and simulated TKE along line A-A at a height of 10 m above ground level. Five simulations with different roughness lengths are compared. All simulations are made with $C_\mu = 0.11$.

Due to the choice of C_μ, it is only the simulation with $z_0 = 0.03$ that fits the measured values upstream of HT. The other simulations give values on generally too high or too low levels.
At the two last measuring points downstream of HT, it is the simulations with the highest roughness lengths that show the best agreement with the measured values. However for the reason given above no clear conclusions can be drawn from Figure 67. It is primarily shown to give an idea of the influence of C_μ.

Figure 68 shows the TKE values simulated with C_μ adjusted in each case to match the turbulence intensity measured at RS. Its value is determined through:

$$C_\mu = \left(\frac{u_*^2}{k}\right)^2 \tag{51}$$

The measured turbulence intensity is given by:

$$I_{measured} = \frac{k^{\frac{1}{2}}}{u_{ref}} = \frac{k^{\frac{1}{2}}}{8.9\ \mathrm{m/s}} = 0.12 \tag{52}$$

With these relations C_μ is adjusted to the different values of u_* used in each simulation. Note that when changing C_μ one also has to adjust:

$$C_{\epsilon 1} = C_{\epsilon 2} - \frac{\kappa^2}{\sigma_\epsilon \sqrt{C_\mu}} \tag{53}$$

The following values are obtained:

z_0	0.5 m	0.1 m	0.03 m	0.005 m	0.0001 m
u_*	1.17	0.77	0.61	0.47	0.31
C_μ	1.43	0.27	0.11	0.04	0.01
$C_{\epsilon 1}$	1.82	1.68	1.55	1.28	0.45

Table 9: Constants of the $k-\epsilon$ turbulence model adjusted to the measured turbulence intensity at RS and the different roughness lengths.

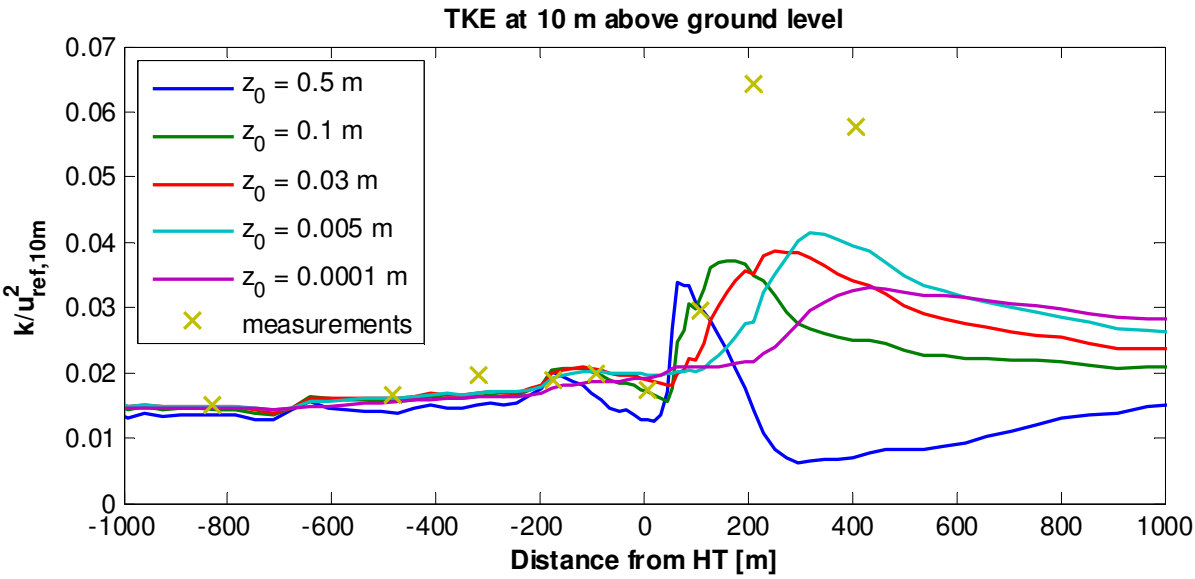

Figure 68: Measured and simulated TKE along line A-A at a height of 10 m above ground level. Five simulations with different roughness lengths are compared. In each simulation the value of C_μ is adjusted to fit the measured turbulence intensity.

The adjustment of C_μ brings the simulated values closer together as expected. Now the maximum value of the TKE is varying very little with the roughness length. The position of this maximum on the other hand, varies quite a lot – moving further downstream of HT – as the roughness length increases.

None of the simulated peak values come close to the measured. Judging from the position of the TKE peaks a roughness length between 0.03 m and 0.1 m would give the best agreement with the measurements. Note that the value of $C_\mu = 0.04$, used in the simulation with $z_0 = 0.005$ m, comes closest to the standard value of $C_\mu = 0.03$ used for atmospheric flows. This simulation does give the highest TKE peak value, but it is still well below the measured values, and the peak is also located further downstream than the measured peak value.

The two most extreme cases behave a bit differently than the trend of the other simulations dictates. In the case of the highest roughness length, a very significant reduction of the TKE is seen downstream of HT, and in the case of the lowest roughness length, the maximum value is somewhat lower than expected from the general trend.

While changing the value of C_μ has a clear effect on the TKE, it is found to have very little influence on the speed-up in the present simulations – except for the one with $z_0 = 0.5$ m. In this case the maximum speed-up at HT is decreased a little, compared to the original simulation with $C_\mu = 0.11$, while the velocity reduction downstream of HT is substantially increased as seen in Figure 69 (comparable to Figure 62).

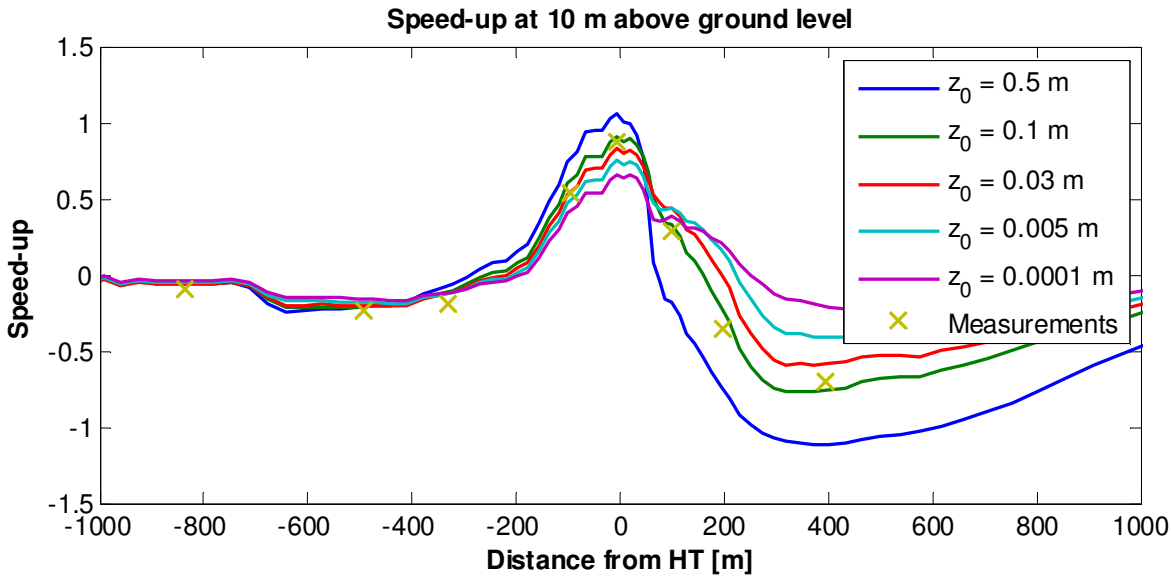

Figure 69: Measured and simulated speed-up along line A-A at a height of 10 m above ground level. Five simulations with different roughness lengths are compared. In each simulation the value of C_μ is adjusted to fit the measured turbulence intensity.

Looking further into this area of very low speed-up and TKE, reveals that the flow is actually reversed here. The normalized velocity field over the hill is shown in Figure 70. The negative speed-up zone after the hill top is much more pronounced than in the corresponding plot of Figure 66.

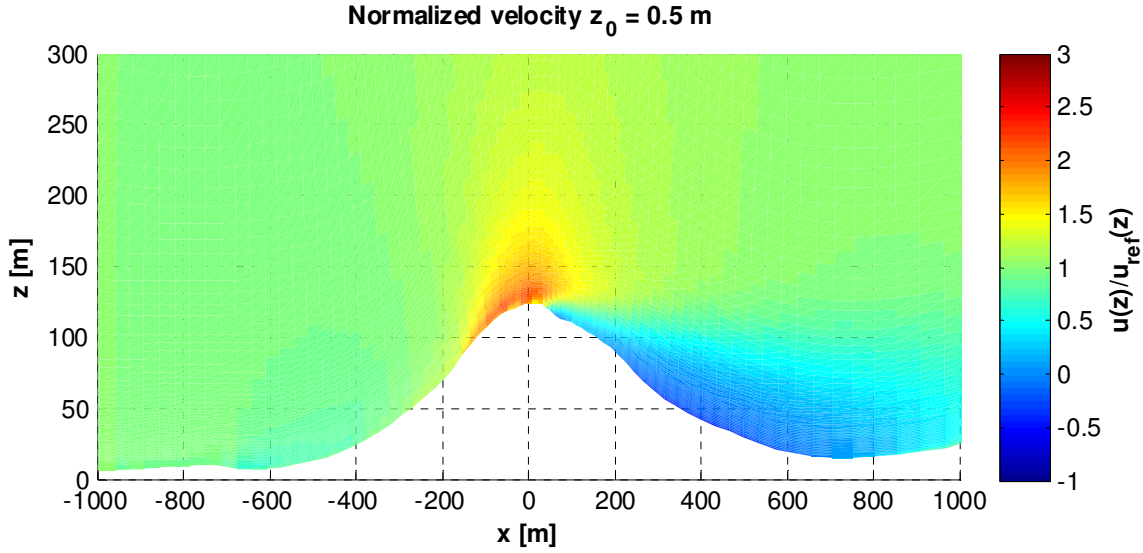

Figure 70: Simulated velocity field over Askervein – normalized with the inlet velocity. The roughness length is set to 0.5 m and C_μ is adjusted to 1.43.

To sum up the effects of changing the roughness length; at the hill top the speed-up increases with the roughness length. For instance when going from 0.03 m to 0.1 m, an increase of about 10 % is observed at z = 10 m. A similar decrease is observed, when going from 0.03 m to 0.005 m. At 80 m above HT, the equivalent changes in speed-up are around 2%.

Behind the hill at z = 10 m a reduction of the velocity is observed. It gets more pronounced as the roughness length is increased. Changes of -20 % and 30 % are found, as the roughness length goes from 0.03 m to 0.1 m and from 0.03 m to 0.005 m respectively.

To get a good overall fit with the measured values, it seems that a roughness length equal to or higher than 0.1 m is needed.

Regarding the normalized TKE, it is found necessary to adjust the value of C_μ to the measured turbulence intensity to get comparable results. By doing this it is found that the maximum value of TKE increases as the roughness length is decreased – at least to a certain extent.
In all cases the maximum value is found downstream of HT as in the measured data, but as the roughness length is decreased, the location moves further downstream. When looking at the maximum value of TKE, the simulation with $z_0 = 0.005$ m comes closest to the measured values, but when looking at the position of the maximum value a roughness length between 0.03 m and 0.1 would give the best fit.

Changing C_μ is found to have little effect on the velocity, except in the case of $z_0 = 0.5$ m where it caused the flow to circulate behind the hill.

6.6 The influence of an upstream roughness change

In this section the influence of an upstream change in roughness length is studied. Following line A-A, the coast is reached at a distance of only 3.3 km southwest of HT. Thus, it seems very likely that flow over Askervein is actually influenced by the change from sea to land. Judging from the simulations presented previously in this report, the flow cannot be expected to be in equilibrium with the land roughness at such a short fetch length.

The simulation of the flow over Askervein is split in two parts. First a precursor simulation over flat terrain with the desired change in roughness is made. Profiles of velocity, TKE and dissipation downstream of the change are stored and used as inlet conditions for the actual terrain simulation of the flow over Askervein. The computational domain, used for the flat terrain simulations, is similar to the one used for the simulations presented in the chapter of "The flow over flat terrain with a single roughness change". A domain as described above in this chapter, is used for the following terrain simulation.

Another method would be to use the empirical expressions found earlier in this report to determine the inlet profiles. But due to the uncertainties of these expressions, the more accurate method of doing a precursor simulation is chosen.

First of all, a test is made of how the numerical model behaves when using inlet profiles taken from a precursor simulation. In this test case the precursor simulation is of the flow over flat terrain with a change in roughness length from 0.0001 m to 0.03 m at $x = 0$. This is referred to as simulation 1. Logarithmic inlet conditions with $u_* = 0.3474$ m/s are specified at $x = -5000$ m and on the top boundary.
The profiles of velocity, TKE and dissipation at $x = 3300$ m are stored and used as inlet conditions for another simulation (referred to as simulation 2) over flat terrain with a uniform roughness length of 0.03 m. Again $u_* = 0.3474$ m/s is specified at the top boundary.
The flow in simulation 2 is expected to develop in the same way as the flow downstream of the roughness change in simulation 1.
Figure 71 and Figure 72 show the profiles of velocity and TKE in the two simulations at positions corresponding to 15000 m after the roughness change. As expected the profiles of simulation 1 and 2 are more or less identical. The numerical model behaves as intended.

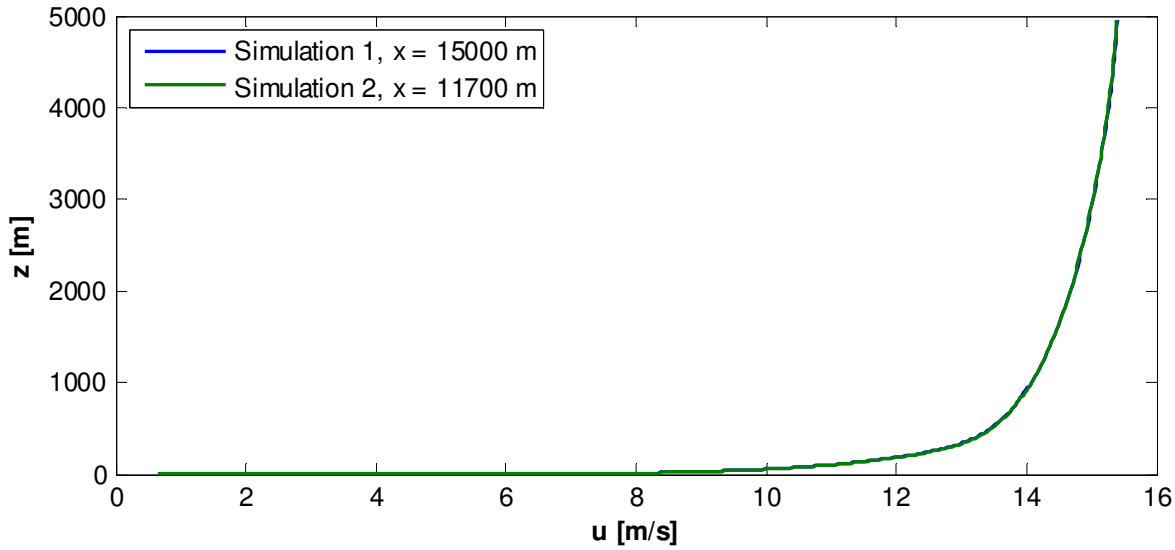

Figure 71: Comparison of velocities from a precursor simulation and from a simulation with inlet conditions taken from the precursor simulation.

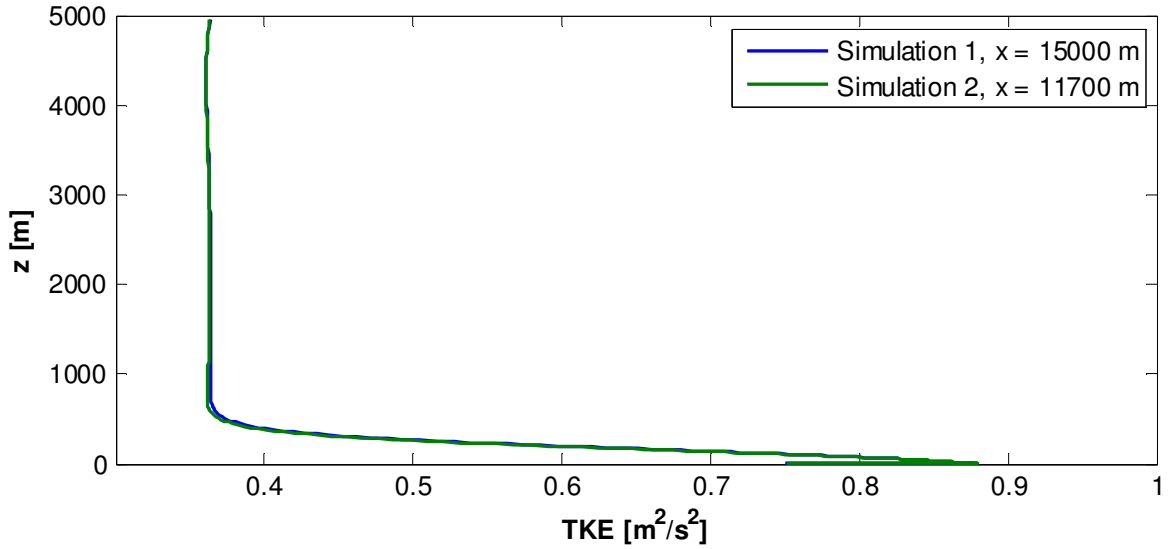

Figure 72: Comparison of TKE from a precursor simulation and from a simulation with inlet conditions taken from the precursor simulation.

Returning now to Askervein, it is assumed that an internal boundary exists as the flow encounters the hill. The influence of this layer is examined in two ways. First the influence of the IBL height alone is studied by comparing simulations made with the same upstream and downstream roughness lengths but with different fetch lengths.
After this follows a study of the effect of changing the upstream roughness length, but keeping the fetch length constant. This will, as shown earlier, also result in different IBL heights.

As shown in Figure 54, the logarithmic velocity profile only follows the measured velocities up to around 30 m above ground level at the reference site. This could indicate the presence of an IBL stretching up to this height. It would however seem more plausible that the velocity profile was logarithmic above 30 m and in

some transitional state below.
Three simulations with $z_{01} = 0.0001$ m and $z_{02} = 0.03$ m are made.
In the first case, the inlet profiles for the actual terrain simulation is taken from the precursor simulation at a position which results in a total fetch length of 3300 m from the roughness change to HT. This length reflects the actual distance from the coast to the HT.
In the second case, a total fetch length of 4100 m is considered. With this fetch length the non-logarithmic velocity profile at x = 0, is found to match the profile measured at RS quite well – as shown in Figure 73. In the same figure is also the standard logarithmic profile.
In the third case a fetch length of 8000 m is used. This is simply to see what happens, when the entire height of the hill is within the IBL.
Looking at simulations over flat terrain with a change in roughness length from 0.0001 m to 0.03 m, the velocity based IBL heights at the three different fetch lengths are respectively 76 m, 90m and 152 m.

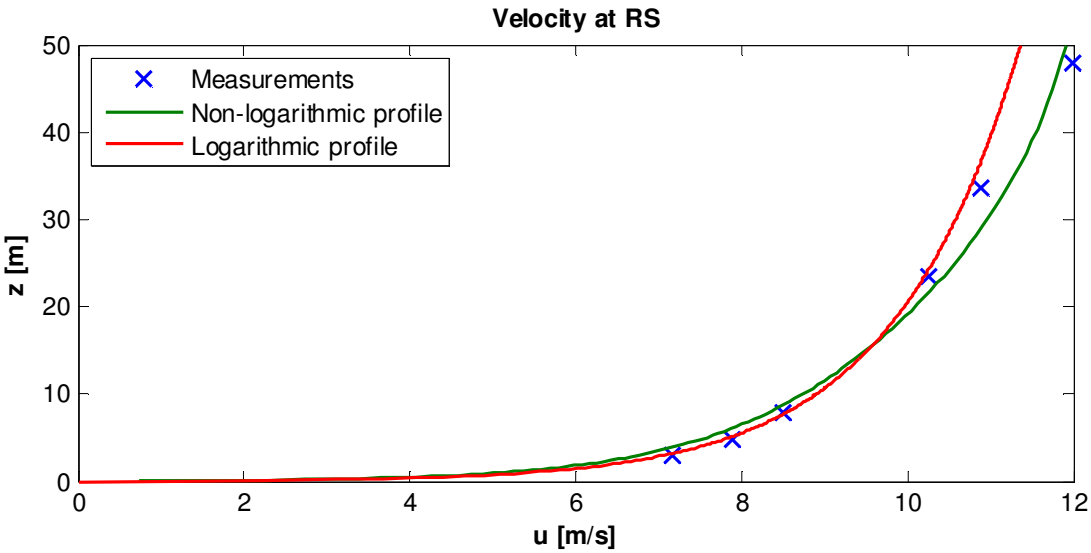

Figure 73: The standard logarithmic velocity profile and a non-logarithmic velocity profile fitted to measurements at the Askervein reference site. The non-logarithmic profile is generated by a change in roughness length from 0.0001 m to 0.03 m 1500 m upstream of RS.

All the precursor simulations are made with logarithmic inlet profiles with a velocity of 12 m/s at a height of 50 m (as measured at RS). For the turbulence model the values in Table 8 are used.

Figure 74 shows the speed-up found with the three roughness change simulations compared to the measured values and to a simulation made with logarithmic inlet conditions (8.9 m/s at a height of 10 m and $z_0 = 0.03$ m). The velocity at 1000 m before HT is used as reference velocity. This is to focus on the speed-up caused by the hill and not by the roughness change.
The effect of the changed inlet conditions is quite small except in the region behind the hill. Here all the roughness change simulations predict a more severe reduction of the velocity than the simulation with no roughness change. At x = 400 m this brings them much closer to the measured value.
The speed-up generally increases with fetch length, and as seen in Figure 75, this tendency becomes more pronounced with the height above ground level – at least at HT up to a certain height.
At a height of 80 m above HT, the speed-up of the long fetch simulation is very close to that of the uniform roughness simulation. The speed-up of the two shorter fetch simulations are approximately 12% below that of the uniform roughness simulation.

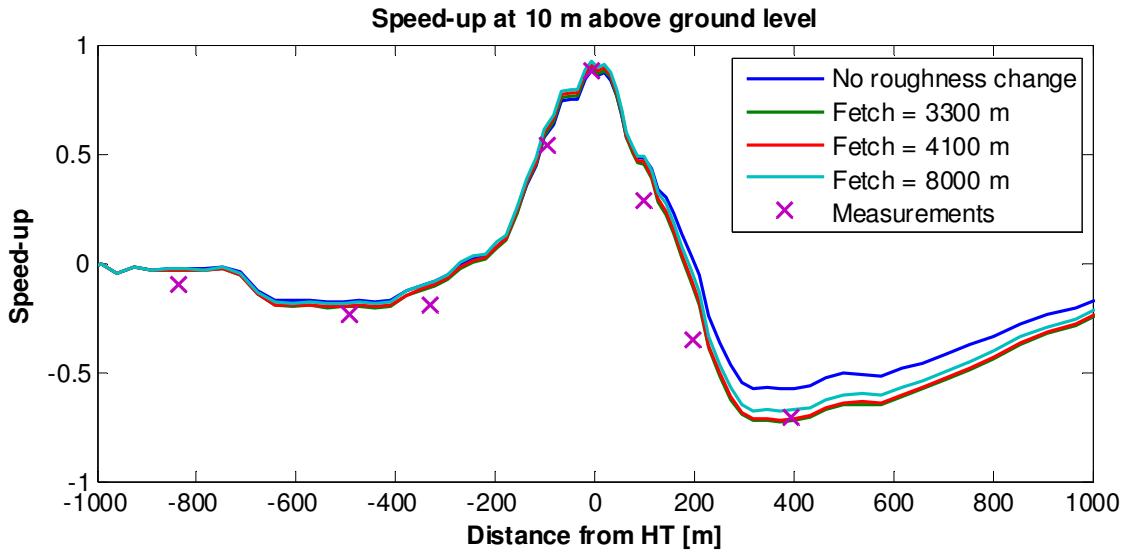

Figure 74: Measured and simulated speed-up along line A-A at a height of 10 m above ground level. Four simulations are presented. One with logarithmic inlet conditions and three with inlet conditions modified by an upstream change in roughness length from 0.0001 m to 0.03 m. The dependency on the fetch length is studied.

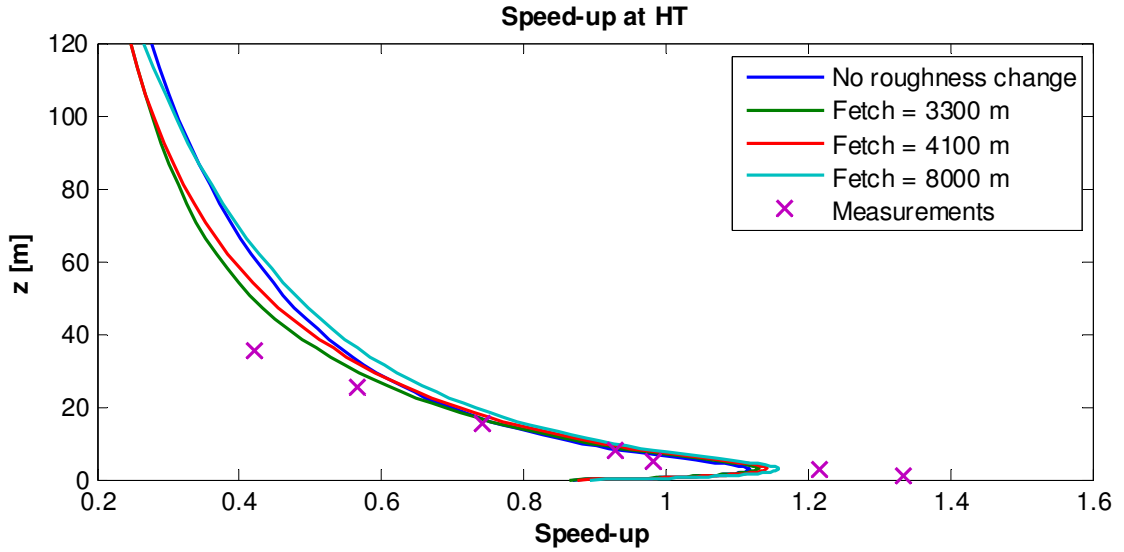

Figure 75: Measured and simulated speed-up at HT as a function of the height above ground level. Four simulations are presented. One with logarithmic inlet conditions and three with inlet conditions modified by an upstream change in roughness length from 0.0001 m to 0.03 m. The dependency on the fetch length is studied.

Figure 76 shows the velocity profiles at HT (dashed lines) and at the reference point of x = -1000 (full lines).

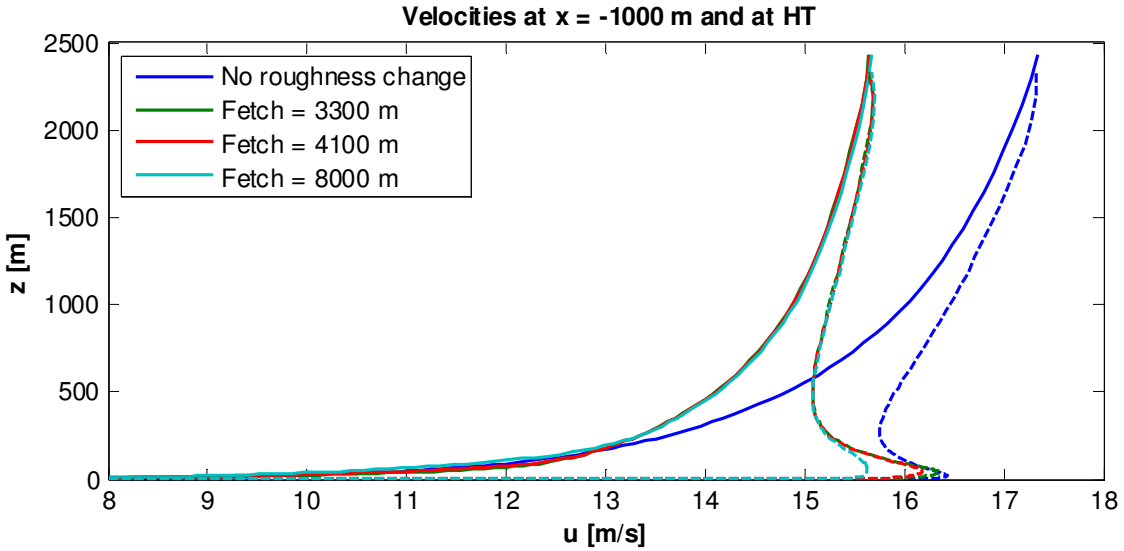

Figure 76: Velocities at x = -1000 m are compared to velocities at HT. Four simulations are presented. One with logarithmic inlet conditions and three with inlet conditions modified by an upstream change in roughness length from 0.0001 m to 0.03 m. The dependency on the fetch length is studied.

Figure 77 shows the TKE along line A-A. It generally increases with the fetch length. The most significant increase is seen at HT, where there is a difference of 26% between the simulation with the shortest fetch length and the simulation with no roughness change. The roughness change simulations generally predicts lower TKE levels than the uniform roughness simulation.

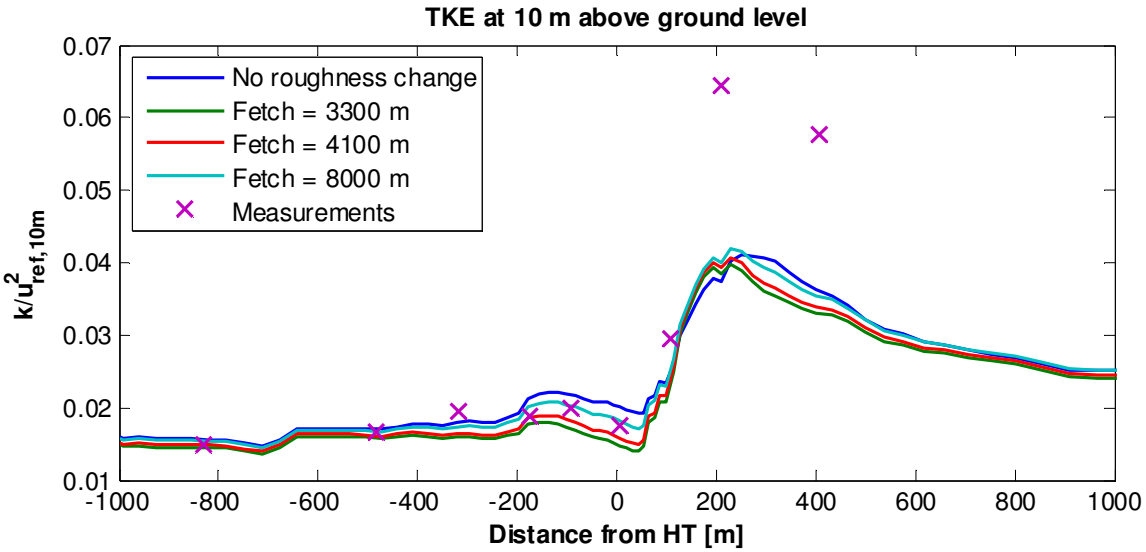

Figure 77: Measured and simulated TKE along line A-A at a height of 10 m above ground level. Four simulations are presented. One with logarithmic inlet conditions and three with inlet conditions modified by an upstream change in roughness length from 0.0001 m to 0.03 m. The dependency on the fetch length is studied.

Finally a test is made of how the ratio between the upstream roughness length z_{01} and the downstream roughness z_{02} influences the flow. Three roughness change simulations with different values for z_{01} is carried out as described above. These values are 0.0001 m, 0.001 m and 0.01 m. z_{02} is kept constant at 0.03 m. In each case a total fetch length of 3300 m is used.

The three different roughness changes would over flat terrain result in velocity based IBL heights of 76 m 74 m and 57 m respectively at the position of HT.

In Figure 78 to Figure 81, the roughness change simulations are compared to measurements and the uniform roughness simulation with logarithmic inlet conditions (8.9 m/s at a height of 10 m and $z_0 = 0.03\ \mathrm{m}$).

The speed-up at 10 m above ground level is only affected by the upstream roughness changes in the region behind the hill. Here it is seen to decrease with z_{01}. At x = 400 there is a difference of about 25% between the simulation with $z_{01} = 0.0001\ \mathrm{m}$ and the simulation with uniform roughness.

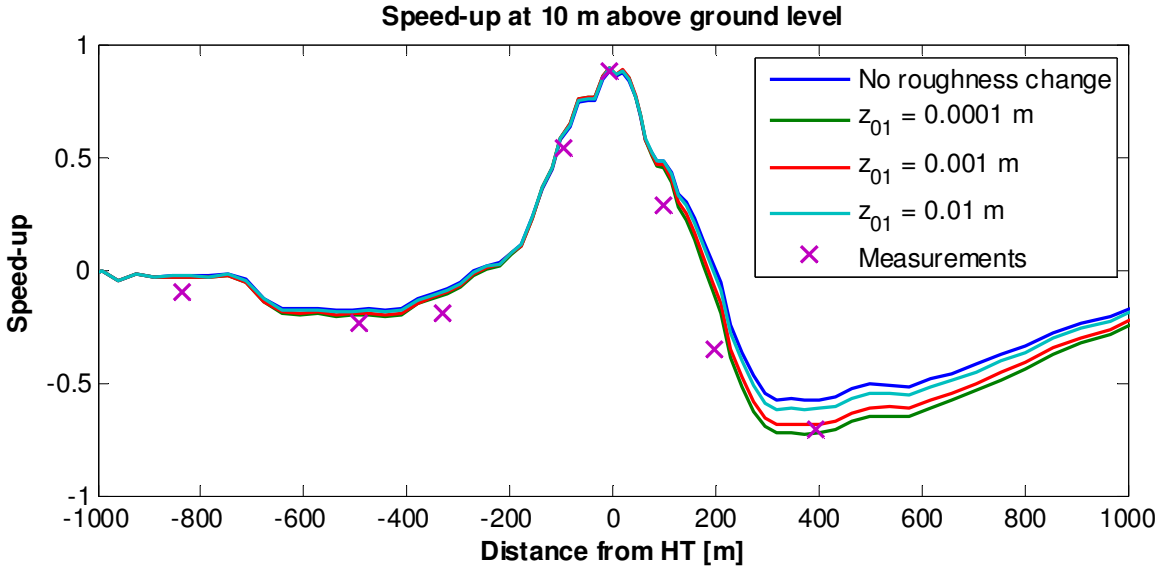

Figure 78: Measured and simulated speed-up along line A-A at a height of 10 m above ground level. Four simulations are presented. One with logarithmic inlet conditions and three with inlet conditions modified by upstream changes in roughness length from 0.0001 m, 0.001 m and 0.01 m respectively to 0.03 m. The roughness change takes place at x = -3300 m.

At HT from around 30 m above ground level and upwards, the speed-up is also seen to decrease with z_{01}. At a height of 80 m there is a difference of 12% between the uniform roughness simulation and the simulation with $z_{01} = 0.0001\ \mathrm{m}$.

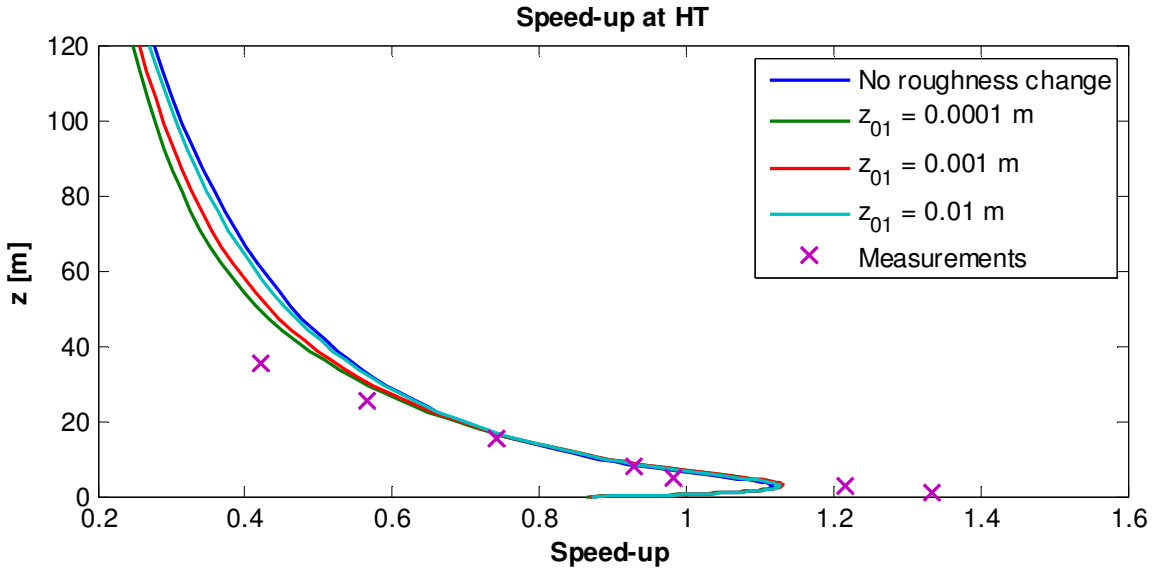

Figure 79: Measured and simulated speed-up at HT as a function of the height above ground level. Four simulations are presented. One with logarithmic inlet conditions and three with inlet conditions modified by upstream changes in roughness length from 0.0001 m, 0.001 m and 0.01 m respectively to 0.03 m. The roughness change takes place at x = -3300 m.

Velocity profiles at HT (dashed lines) and at the reference point of x = -1000 (full lines) are compared:

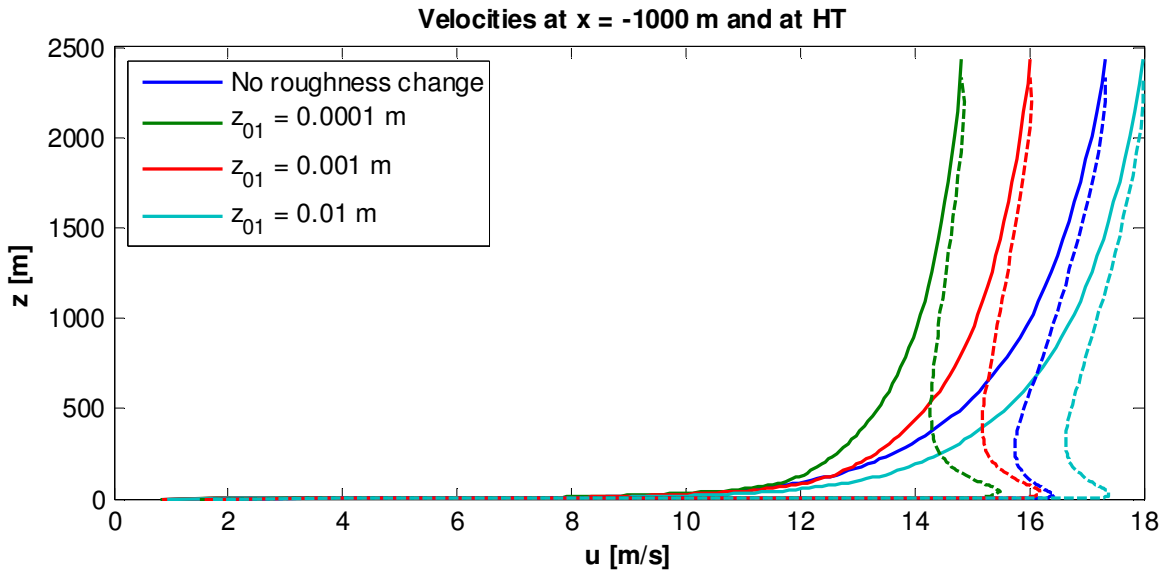

Figure 80: Velocities at x = -1000 m are compared to velocities at HT. Four simulations are presented. One with logarithmic inlet conditions and three with inlet conditions modified by upstream changes in roughness length from 0.0001 m, 0.001 m and 0.01 m respectively to 0.03 m. The roughness change takes place at x = -3300 m.

Regarding the TKE at 10 m above ground level, it is generally seen to decrease with the upstream roughness length. This is most clearly seen at HT and around 300 m downstream of HT.

At HT there is a difference of 25% between the uniform roughness simulation and the simulation with $z_{01} = 0.0001$ m.

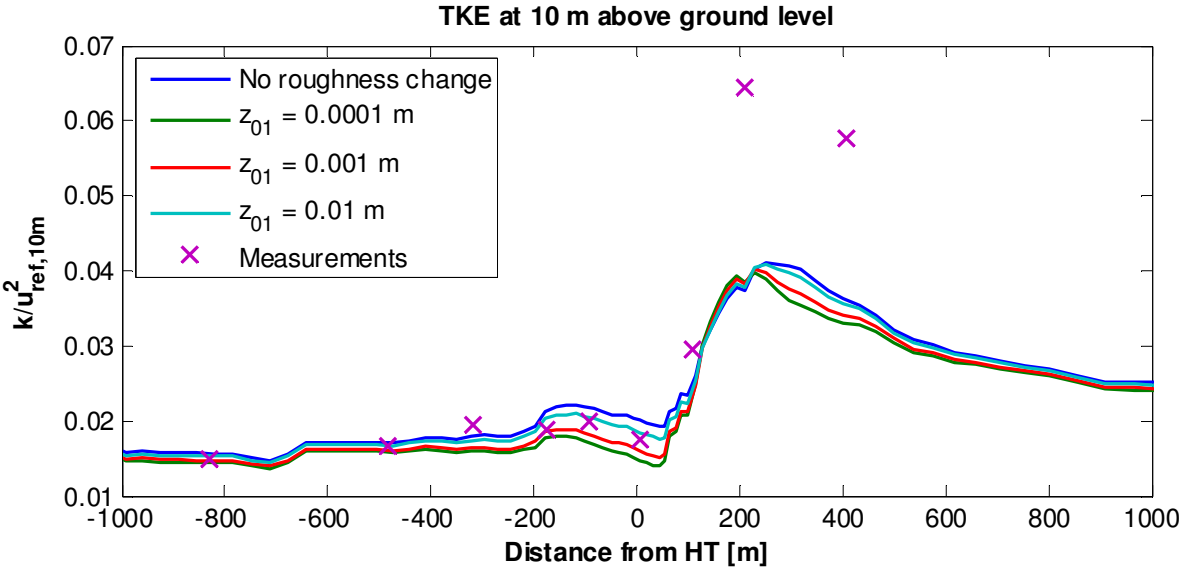

Figure 81: Measured and simulated TKE along line A-A at a height of 10 m above ground level. Four simulations are presented. One with logarithmic inlet conditions and three with inlet conditions modified by upstream changes in roughness length from 0.0001 m, 0.001 m and 0.01 m respectively to 0.03 m. The roughness change takes place at x = -3300 m.

6.7 Closure

Several interesting things have been found in this chapter regarding the simulated flow over Askervein. Both simulations with logarithmic inlet conditions and inlet conditions disturbed by an upstream change in surface roughness have been studied.

In the case of logarithmic inlet conditions, it was found, that the simulated flow is not completely independent of the Reynolds number. A small decrease of the TKE was observed in a region behind the hill top, when reducing the inlet friction velocity from 0.6 m/s to 0.06 m/s. This was found using a roughness length of 0.03 m.
Increasing the surface roughness was found to increase the speed-up at HT and decrease the speed-up in the region after HT.
To get comparable levels of TKE, it was found necessary to adjust the value of C_μ when changing the roughness length. With this done it was found, that the maximum value of TKE generally increases as the roughness length is decreased, while the position of these maximum values moves downstream.
It generally seems like a roughness length around 0.1 m or higher gives the best agreement between simulation and measurements when using logarithmic inlet conditions. The TKE downstream of the hill is however still substantially underestimated.
Note also that the adjusted values C_μ in the most extreme differs quite a lot from the standard value 0.03, and the results might not be very reliable.

Using inlet conditions disturbed by an upstream roughness change generally gave lower levels of speed-up and TKE than using logarithmic inlet conditions. Both increasing the fetch length and increasing the upstream roughness length was found to increase speed-up and TKE – bringing the results closer to those of the uniform roughness simulation.

When using inlet conditions modified by an upstream roughness change, the combination of the shortest fetch length (3300 m) and the lowest upstream roughness length (0.0001 m) was found to give the best agreement between simulated speed-up and measurements.
Regarding the TKE, the simulations closest to the uniform roughness simulation were seen to give the best agreement with the measurements.

Another approach to make the simulations agree better with the measurements could be to add an extra roughness change somewhere between the inlet and the hill top. This is however not considered here.

7. Askervein – 3D simulation

7.1 Introduction

In the previous chapter, the flow over the low hill of Askervein was studied through 2D simulations. The effects of changing the surface roughness of the hill and the upstream area was examined. But, as it was also mentioned, the assumption of the flow being purely two dimensional is questionable. Some of the incoming air must be assumed to go around the hill and not only across it. This behavior is not recognized by the 2D model, and for a more realistic analysis a 3D model is needed. The advantage of using a 2D model instead of a 3D model is of course the reduced computational time.

The purpose of this chapter is to verify that the conclusions made in the previous chapter regarding the 2D simulations are also applicable for corresponding 3D simulations. Such a verification would make the results more reliable and thereby more useful when for instance choosing a site for a wind farm.

7.2 Results

The 3D simulations are made on a computational grid with 128 cells in the x, y and z directions. The main flow is in the x-direction which is aligned with line A-A shown in Figure 53 . The y-direction is perpendicular to this, and z is the height above ground level.
The extent of the domain is defined by -2600 m <x< 4500 m, -4000 m <y< 2000 m and 0 m <z< 4000 m. Line A-A is at y = 0 and the hill top at x = 0.

The boundary surface at x = -2600 is defined as inlet along with the top boundary, while the surface at x = 4500 is defined as outlet. The bottom boundary is defined as a no-slip wall, and the two remaining boundary surfaces are defined by symmetry conditions.

First of all a simulation with logarithmic inlet conditions and uniform surface roughness is made. As in the corresponding 2D simulation of the previous chapter, the roughness length associated with the wall boundary is set to 0.03 m, and the inlet conditions are specified by a friction velocity of 0.61 m/s.
The speed-up along line A-A of the two simulations (2D and 3D) is shown in Figure 82 below. The inlet velocity is used as reference velocity.

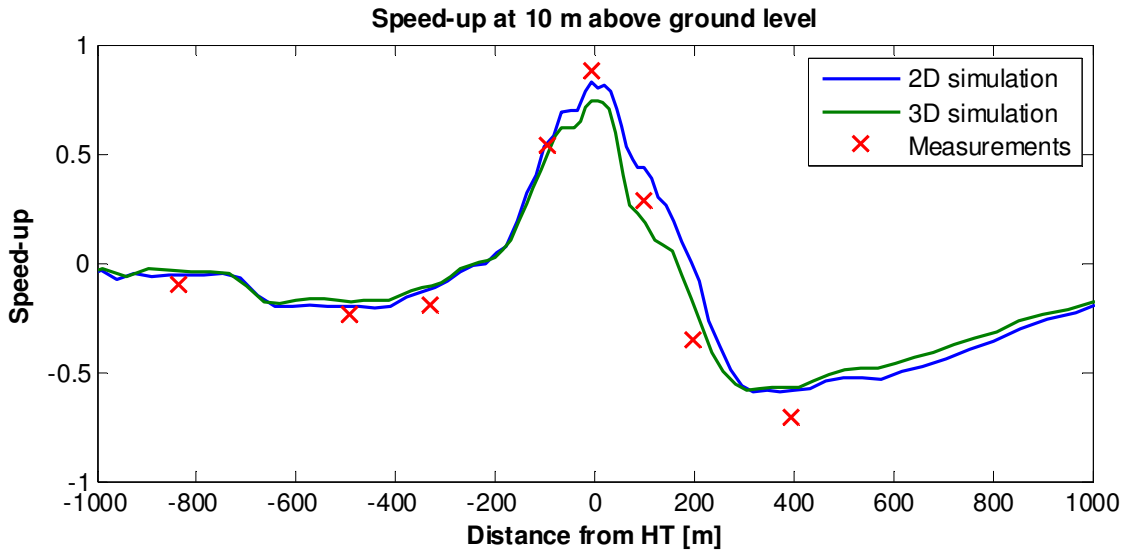

Figure 82: Comparison of 2D and 3D simulations of the flow over Askervein using logarithmic inlet conditions and a uniform roughness length of 0.03 m.

As expected, the speed-up at HT is lower in the 3D simulations – most likely because the air is allowed to flow around the hill. As shown in Figure 83 this is true for all heights up to at least z = 100 m.

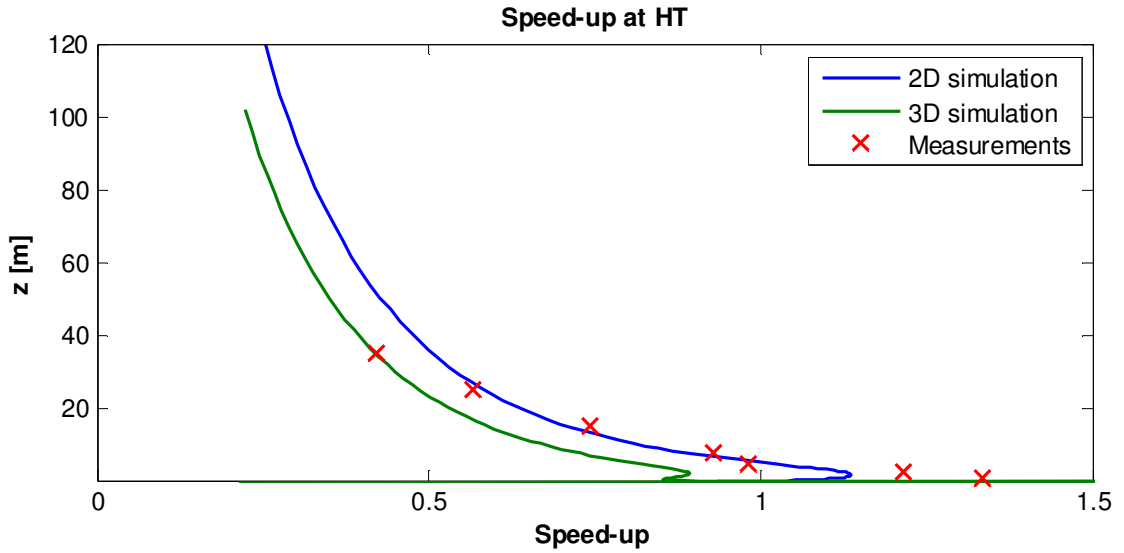

Figure 83: Comparison of 2D and 3D simulations of the flow over Askervein using logarithmic inlet conditions and a uniform roughness length of 0.03 m.

Regarding the TKE along line A-A shown in Figure 84, it is found to be higher in the 3D simulation than in the 2D simulation in the region immediately after HT, but from around x = 200 and downstream it stays lower than in the 2D simulation. Upstream of HT the simulations give similar results.

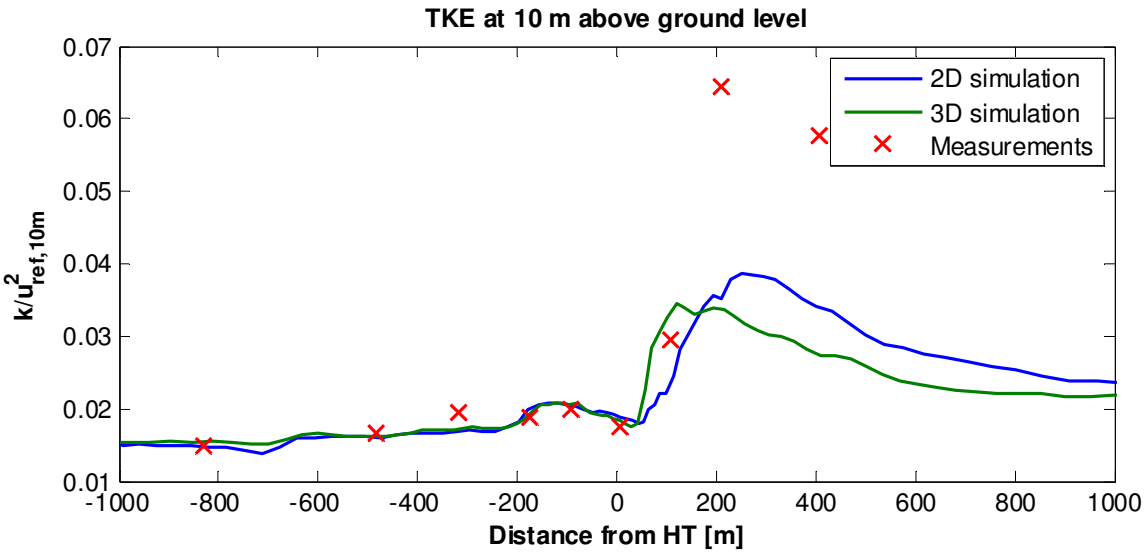

Figure 84: Comparison of 2D and 3D simulations of the flow over Askervein using logarithmic inlet conditions and a uniform roughness length of 0.03 m.

In Figure 85, Figure 86 and Figure 87 the influence of an upstream change in roughness length from 0.0001 m to 0.03 m is studied. Simulations with three different fetch lengths are considered. The inlet conditions used here, are the same as were used in the simulations presented in Figure 74 to Figure 77 of the previous chapter. The velocity at x = -1000 is used as reference velocity.

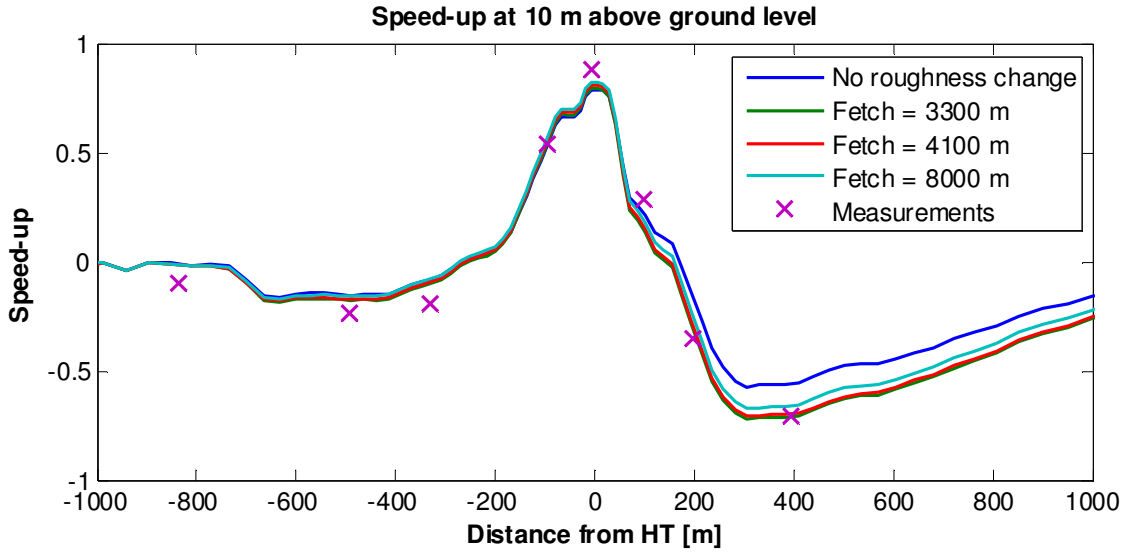

Figure 85: Measured and simulated speed-up along line A-A at a height of 10 m above ground level. Four simulations are presented. One with logarithmic inlet conditions and three with inlet conditions modified by an upstream change in roughness length from 0.0001 m to 0.03 m. The dependency on the fetch length is studied.

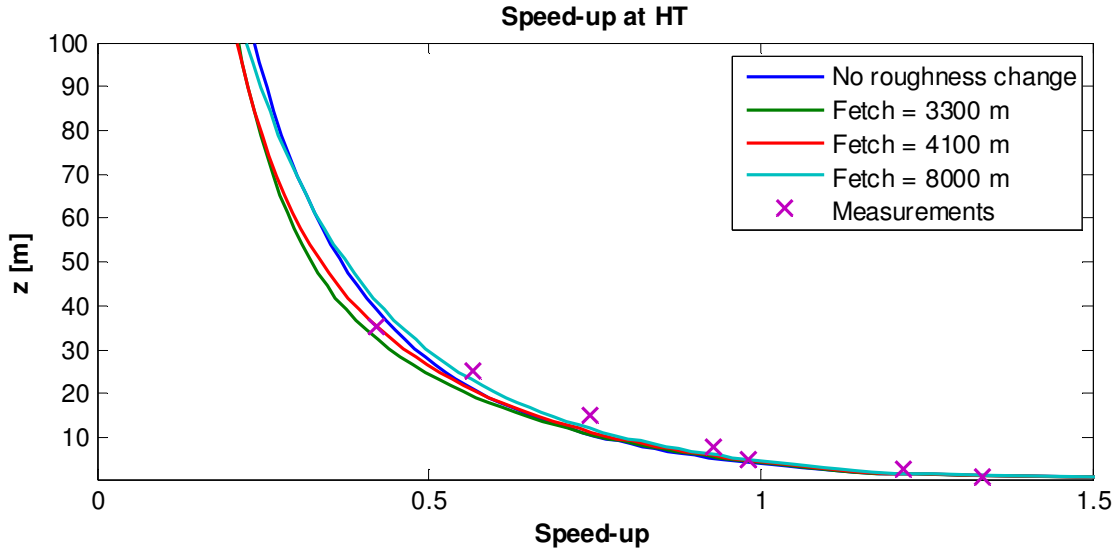

Figure 86: Measured and simulated speed-up at HT as a function of the height above ground level. Four simulations are presented. One with logarithmic inlet conditions and three with inlet conditions modified by an upstream change in roughness length from 0.0001 m to 0.03 m. The dependency on the fetch length is studied.

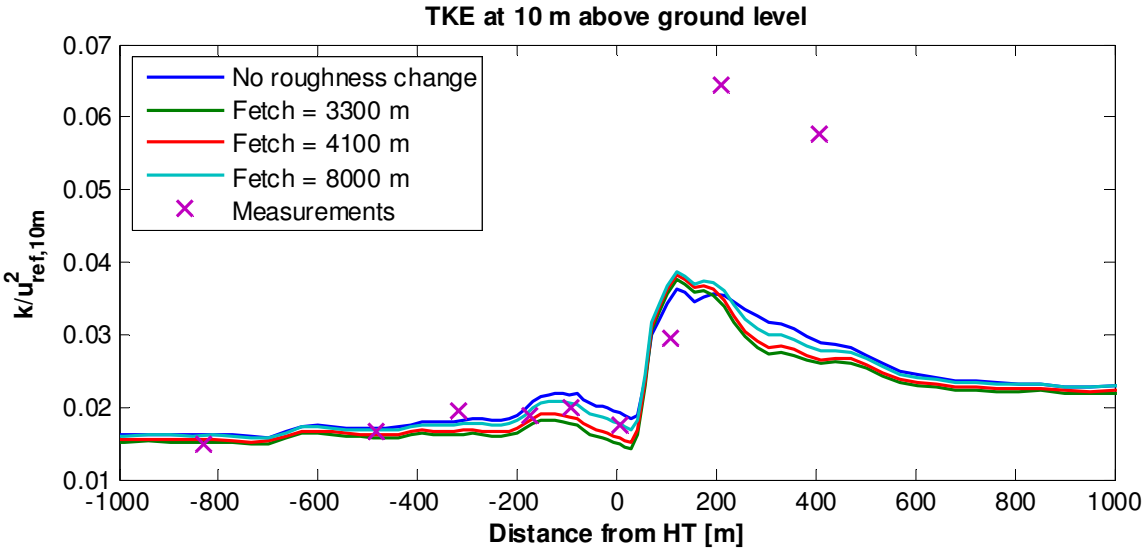

Figure 87: Measured and simulated TKE along line A-A at a height of 10 m above ground level. Four simulations are presented. One with logarithmic inlet conditions and three with inlet conditions modified by an upstream change in roughness length from 0.0001 m to 0.03 m. The dependency on the fetch length is studied.

The tendencies observed in Figure 85, Figure 86 and Figure 87 are very close to those of the corresponding 2D simulations. Speed-up and TKE increases with the fetch, and the results of the roughness change simulations are generally seen to be lower than those of the uniform roughness simulation.
80 m above HT the speed-up of the short fetch simulation is approximately 12 % below that of the uniform roughness simulation. The TKE of the short fetch simulation at 10 m above HT is 23 % lower than the TKE of the uniform roughness simulation.

In Figure 88, Figure 89 and Figure 90 the influence of changing the upstream roughness length is studied. Simulations with upstream roughness lengths of 0.0001 m, 0.001 m and 0.01 m are considered. The downstream roughness length is kept at 0.03 m and the fetch at 3300 m.

The inlet conditions used here are the same as were used in the simulations presented in Figure 78 to Figure 81 of the previous chapter. The velocity at x = -1000 is used as reference velocity.

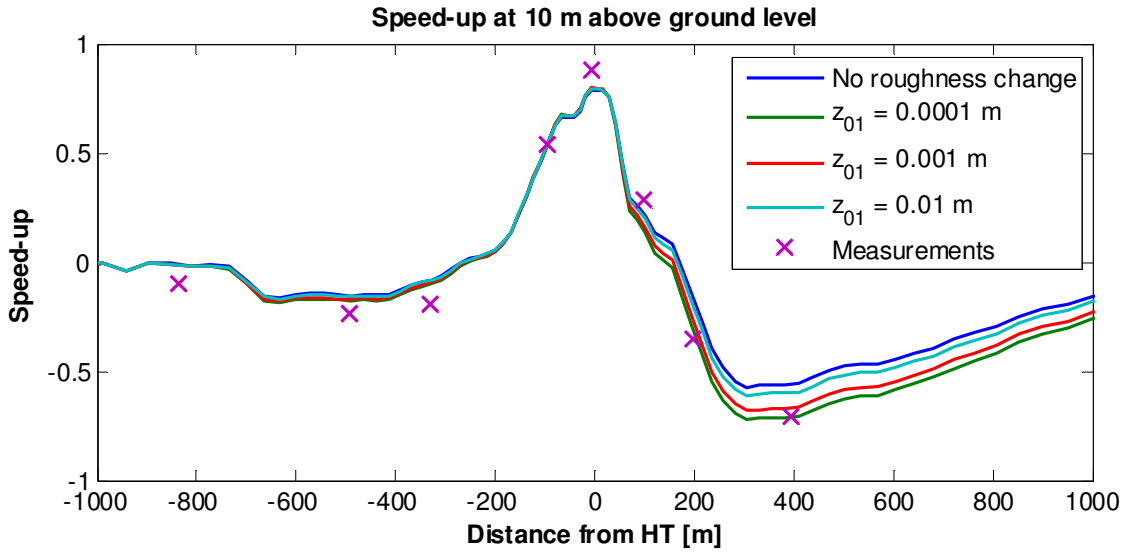

Figure 88: Measured and simulated speed-up along line A-A at a height of 10 m above ground level. Four simulations are presented. One with logarithmic inlet conditions and three with inlet conditions modified by upstream changes in roughness length from 0.0001 m, 0.001 m and 0.01 m respectively to 0.03 m. The roughness change takes place at x = -3300 m.

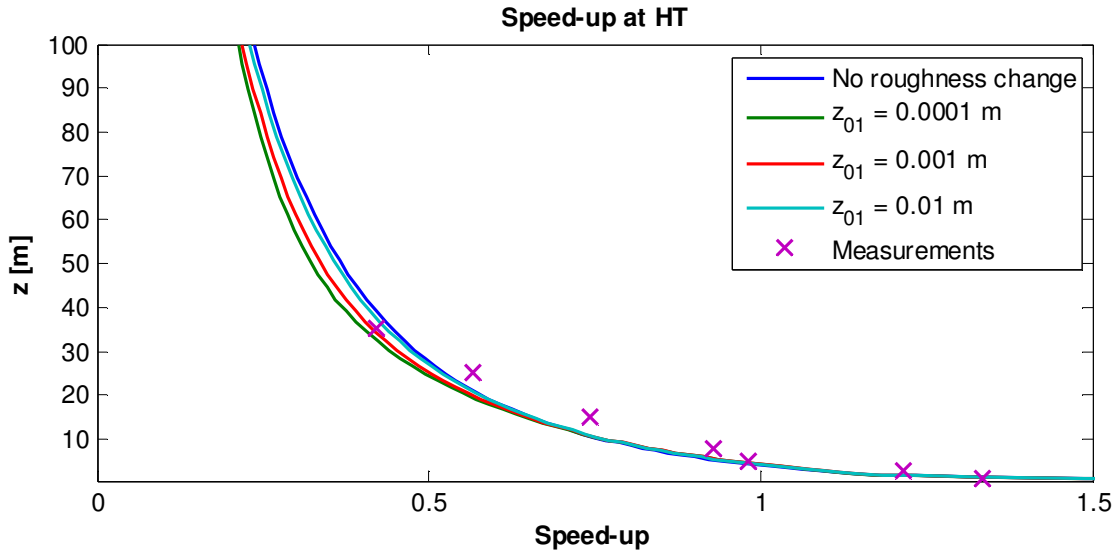

Figure 89: Measured and simulated speed-up at HT as a function of the height above ground level. Four simulations are presented. One with logarithmic inlet conditions and three with inlet conditions modified by upstream changes in roughness length from 0.0001 m, 0.001 m and 0.01 m respectively to 0.03 m. The roughness change takes place at x = -3300 m.

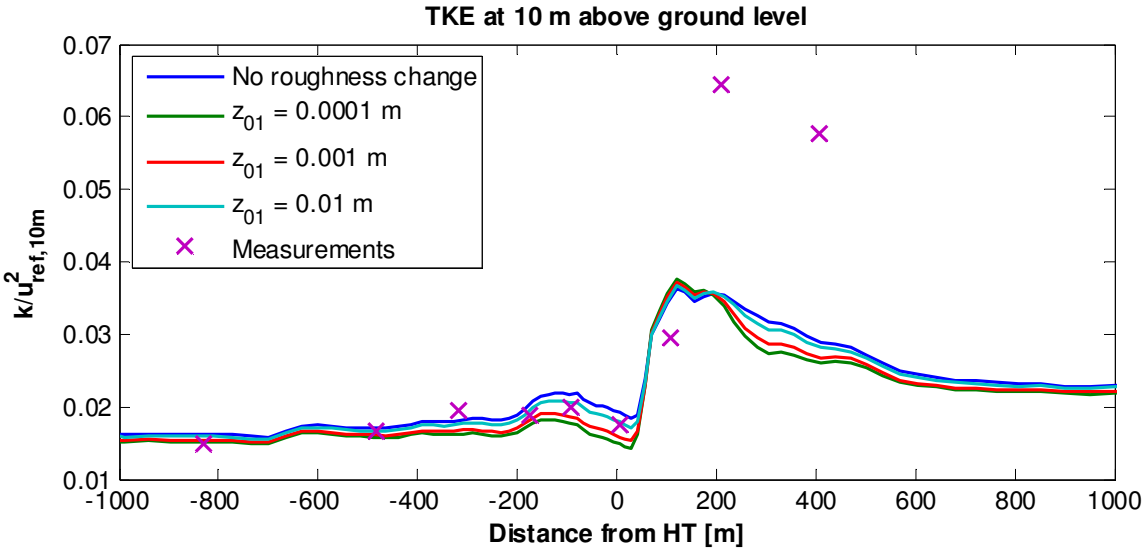

Figure 90: Measured and simulated TKE along line A-A at a height of 10 m above ground level. Four simulations are presented. One with logarithmic inlet conditions and three with inlet conditions modified by upstream changes in roughness length from 0.0001 m, 0.001 m and 0.01 m respectively to 0.03 m. The roughness change takes place at x = -3300 m.

The observed tendencies of the 3D simulations are again very close to those of the corresponding 2D simulations.

At the position 400 m downstream of HT, the speed-up at 10 m above ground level of the simulation with $z_{01} = 0.0001$ m is approximately 27% below that of the uniform roughness simulation. At 80 m above HT the difference in speed-up is 12%. Regarding the TKE there is a difference of 23% between the two simulations at 10 m above HT.

The investigation made in the previous chapter regarding the influence of changing the surface roughness of the hill itself and using logarithmic inlet conditions, is not repeated here due to the uncertainties associated with the adjustment of the turbulence model constants.

The presented simulations of this chapter are all made with $C_\mu = 0.11$ and the corresponding values given in Table 8.

7.3 Closure

The presented 3D simulations of the flow over Askervein give results quite similar to those of the corresponding 2D simulations. The speed-up at HT and in a region behind the hill was as expected found to be a bit lower in the 3D simulations. In the standard case of logarithmic inlet conditions and a uniform roughness length of 0.03 m this brings the simulated results away from the measurements at HT but closer to the measurements downstream of HT.

The effect of using inlet conditions modified by an upstream change in roughness length instead of logarithmic inlet conditions was found to be more or less the same in the 3D simulations as in the corresponding 2D simulations. Thus the conclusions of the previous chapter regarding the 2D simulations are confirmed by the supposedly more realistic 3D simulations.

Judging from the simulations, it seems very plausible that the transition from sea to land upstream of Askervein has a significant influence on the flow over the hill.

Below follows a general discussion of the results presented throughout this report.

8. Closure

The atmospheric boundary layer flow over different types of terrain has been studied through simulations made with the finite volume CFD code of *Ellipsys 2D* and *3D,* and through measurements made at the Høvsøre test site and over the low hill of Askervein.
The primary objective of these investigations has been to find out, how the wind is affected by changes in the surface roughness. Neutral atmospheric stratification has been assumed throughout.

The flow over flat terrain with uniform surface roughness was studied to get an idea of the accuracy of the numerical model.
Simulated flows defined by logarithmic inlet conditions, was found to remain more or less undisturbed throughout the computational domain as expected. The largest deviations between inlet profiles of velocity and TKE and the corresponding downstream profiles was seen in the case of the highest roughness length (0.5 m). With a proper computational mesh these deviations was found to be below 1%.

Regarding the mesh, a resolution of 256x256 cells was found to be adequate for a domain of 20x5 km.
It was also shown, that the height of the near wall cells can have a significant influence on the solution. The accuracy was generally seen to increase, as the cell height was decreased, but only to a certain level. Making the cells too low, was seen to decrease the accuracy. A cell aspect ratio of 1500 was recommended as an upper limit, when simulating flows over flat terrain. For flow simulations over more complex terrain, an aspect ratio of 1500 might be too high.

The flow over flat terrain with a change in surface roughness was simulated to study the development of the IBL and the vertical profiles of velocity, TKE and dissipation downstream of such a roughness change. Four existing formulae for predicting the IBL height was compared to simulations. Poor agreement was observed.
Two different approaches for finding new empirical expressions for the IBL height has been described. The basic idea in both of them, was to fit parameters of existing formulae to the results of a range of roughness change simulations.
The so called “Elliot approach” turned out to give the most reliable and useful set of expressions. Four different expressions was required to describe both TKE and velocity based IBL heights after both smooth-to-rough and rough-to-smooth changes.
The expressions were derived for fetch lengths between 160 and 5000 m, for upstream roughness lengths between 0.0001 and 0.01 m in smooth-to-rough cases and between 0.005 and 0.5 m in rough-to-smooth cases and for roughness length ratios between 4 and 450 in smooth-to-rough cases and between 0.2 and 0.004 in rough-to-smooth cases.
Staying within these limits, the expressions should be capable of predicting an IBL height within 25 % of the simulated height. At fetches between approximately 2000 and 5000 m errors below 10% can be expected. Assuming that the simulated flows are representative of real world atmospheric boundary layer flows, this accuracy is thought to be quite good.
To verify this assumption, the simulated flow was compared to measurements made at the Høvsøre test site.
Regarding the vertical profiles of velocity and TKE, good agreement was observed at all heights between 10 and 116.5 m. The IBL height at Høvsøre could unfortunately not be very accurately deduced from the measurements. It does, however, seem to be quite close to the height predicted by the simulation and

thereby also by the suggested empirical expression. More experiments – preferably with measurements at higher altitudes – are however required to fully validate the suggested expressions.

The fetch dependency of the velocity and TKE profiles at Høvsøre was also studied, but poor agreement between simulations and measurements was observed. The disagreement is thought to be related to factors such as horizontal temperature gradients and the atmospheric stratification upstream of the roughness change, which were not included the present analysis. Experiments including temperature measurements both upstream and downstream of the roughness change would most likely help to understand the observed behavior.

The simulations of the flow over flat terrain has also been used to suggest expressions for the vertical profiles of velocity, TKE and dissipation downstream of a roughness change. Profiles at fetch lengths between 500 and 5000 m were considered.
A main hurdle in this direction was to estimate the near wall friction velocity. Two different methods were considered for this purpose. One was a classical method based on theoretical considerations, and the other was to find an empirical expression based on the range of simulations also used to derive the IBL height expressions.
The velocity was approximated by a profile divided in three logarithmic sections, and the TKE by a second order polynomial within the IBL. The dissipation was approximated by the expression also used for describing standard logarithmic conditions.
The approximated profiles based on the empirical expression for the near wall friction velocity, was seen to give the best agreement with the simulated profiles. This was perhaps to be expected, since the simulated profiles was also used to derive the expression. However, the high number of simulations included in the derivation, is thought to make the approximated profiles quite trustworthy.
The accuracy of these profiles was estimated by looking at the differences between simulation and approximation averaged at heights corresponding to 1, 25, 50, 75 and 100 % of the IBL height. The approximated velocities were found to be within 6.6% of the simulated and the TKE within 13.3%. Regarding the dissipation, differences of up to 36.5% was observed. This is thought be an effect of the very high gradient of the near wall dissipation.
Note that the approximated profiles depend on the IBL height. The presented results were found with use of the simulated IBL heights. Without these, one would have to rely on estimated values.
And, as in the case of prediction of the IBL height, more experiments are needed to verify both the simulated and the approximated profiles.

All said, the derived expressions for describing the flow downstream of a roughness change, are thought to offer a reasonable alternative to the standard logarithmic conditions, when these are not applicable. They are, however, probably not reliable enough to be used in cases where a high accuracy is needed. A cure for this, could be to narrow down the range of fetch and roughness lengths, for which the expressions should apply, i.e. making them a little less general.
There is obviously also a need to develop similar expressions for non-neutral conditions.

Finally, the flow over the low hill of Askervein was simulated to study the effect of an upstream roughness change on the flow over a non-flat terrain. Both 2D and 3D simulations were performed. The results were found to be quite similar.
The effect of introducing an upstream roughness change was generally lower levels of speed-up and

normalized TKE across the hill. Both increasing the fetch length and increasing the upstream roughness length was found to increase speed-up and TKE – bringing the roughness change simulations closer to the uniform roughness simulation. Whether these tendencies also apply for real atmospheric flows remains to be validated.
Of the studied simulations, the quite realistic one with a change in roughness length from 0.0001 m to 0.03 m at a position 3300 m upstream of the hill top, was found to give the best agreement with the measured speed-up. It is still slightly underestimated at the hill top but very well estimated behind the hill.
Regarding the TKE, a longer fetch or a higher upstream roughness length seems to be required, to get good agreement with the measurements. In general, the simulated TKE shows good agreement up to the hill top, but behind the hill it is clearly underestimated.

The effect of changing the roughness length of the hill itself and the surroundings was studied through the 2D simulations. When using logarithmic inlet conditions, it was seen that a roughness length higher than the normally used value of 0.03 m would give better agreement with the measurements. Changing the roughness length, however, brought up a need to adjust the constants of the turbulence model, which in turn added some uncertainty to the results.

The main conclusion, to be drawn from the Askervein simulations, is that the upstream roughness change appears to have a quite significant influence on the flow over the hill.
As an example, the speed-up at 80 m above the hill top was found to be around 0.3 in the case of uniform roughness, and about 12% lower when including the roughness change from 0.0001 m to 0.03 m 3300 m upstream of the hill top. As shown in equation (54) below, this means a reduction of 8% of the potential wind power available at this position.

$$\Delta P_{\text{available}} = \frac{(0.3 \cdot u_{\text{ref}} + u_{\text{ref}})^3 - (0.88 \cdot 0.3 \cdot u_{\text{ref}} + u_{\text{ref}})^3}{(0.3 \cdot u_{\text{ref}} + u_{\text{ref}})^3} = 0.08 \qquad (54)$$

Such a reduction would definitely be worth taking into account, if one was planning to put up a wind turbine on the top of Askervein.
It is also worth noticing that, if the fetch length is increased to 8000 m, the influence of the roughness change on the hill top speed-up becomes very small. Behind the hill however, a significant influence is still observed.

9. References

Arya, S. P. (2001). *Introduction to Micrometeorology.* Academic Press, International Geophysics Series.

Elliot, W. P. (1958). The Growth of the Atmospheric Internal Boundary Layer. *Trans. Amer. Geophys. Un.* (39), pp. 1048-1054.

Garratt, J. R. (1990). The Internal Boundary Layer - A Review. *Boundary-Layer Meteorology* (50), pp. 171-203.

Hansen, M. O. (2008). *Aerodynamics of Wind Turbines.* Earthscan.

Jackson, P. S., & Hunt, J. C. (1975). Turbulent Wind Flow over a Low Hill. *Quart. J. R. Meteorol. soc.* (101), pp. 929-955.

Kaimal, J. C., & Finnigan, J. J. (1994). *Atmospheric Boundary layer flows.* Oxford University Press.

Michelsen, J. A. (1992). *Basis3d - a platform for development of multiblock PDE solvers.* Technical University of Denmark.

Michelsen, J. A. (1994). *Block structured multigrid solution of 2D and 3D elliptical PDE solvers.* Technical University of Denmark.

Savelyev, S. A., & Taylor, P. A. (2005). Internal Boundary Layers: I Height Formulae for neutral and diabatic flows. *Boundary-Layer Meteorology* (115), pp. 1-25.

Savelyev, S. A., & Taylor, P. A. (2001). Notes on an internal boundary-layer height formula. *Boundary-Layer Meteorology* (101), s. 293-301.

Sørensen, N. N. (1995). *General purpose flow solver applied to flow over hills.* Risø National Lab.

Sørensen, N. N. (1998). *Hypgrid2D - a 2-D mesh generator.* Risø National Lab.

Taylor, P. A., & Teunissen, H. W. (1985). The Askervein Hill Project: Overview and Background Data.

VEA online. Retrieved March 2, 2010, from http://veaonline.risoe.dk/rodeo/ProjectOverview.aspx?&Project=4&Rnd=73430

Versteeg, H. K., & Malalasekera, W. (1995). *An introduction to Computational Fluid Dynamics - The Finite volume Method.* Pearson Prentice Hall.

Walmsley, J. L. (1989). Internal boundary-layer height formulae - A comparison with atmospheric data. *Boundar-Layer Meteorology* (47), pp. 251-262.

Weng, W., Taylor, P. A., & Salmon, J. R. (2009). A 2-D numerical model of boundary-layer flow over single and multiple changes in surface conditions: I Roughness cahnges.

White, F. M. (2006). *Viscous Fluid Flow.* McGraw-Hill.